Coherent and Measurement-based Feedback in Quantum Mechanics

Alfred Harwood

A dissertation submitted in partial fulfillment

of the requirements for the degree of

Doctor of Philosophy

of

University College London.

Department of Physics and Astronomy

University College London

July 19, 2022

I, Alfred Harwood, confirm that the work presented in this thesis is my own. Where information has been derived from other sources, I confirm that this has been indicated in the work.

Abstract

This thesis is about the theory of quantum feedback control. In particular, it focuses on the theory of coherent feedback-a form of quantum feedback in which no measurements are performed- and how it can be compared with measurement-based feedback. After introducing the background concepts and formalisms, the first part of this thesis is concerned with coherent feedback in the regime of Gaussian quantum systems. We derive a general model for describing Gaussian coherent feedback, and use this to derive a compact description of passive, interferometric coherent feedback. The performance of this model is then evaluated for the task of squeezing a bosonic mode and it is shown that no setup of this kind is able to generate steady-state squeezing of a quadrature beyond the '3dB bound'. This performance is compared to the performance of homodyne monitoring which in certain circumstances can outperform the passive coherent feedback setups. After this, we apply our model of Gaussian coherent feedback to optomechanical systems. We investigate the tasks of cooling a mechanical oscillator, generating entanglement between optical and mechanical modes and generating optical and mechanical squeezing. Finally, we develop a unified model of coherent and measurement-based feedback, inspired by collision models and not restricted to Gaussian states. Within this model, we compare the two feedback methods for the tasks of generating low entropy steady-states and simulating unitary evolution on an unknown input state.

Impact Statement

Controlling quantum systems is important for the development of quantum technologies, such as quantum computers and quantum sensors, which have recently enjoyed great interest in both academia and industry. A key theme of this thesis is identifying which kind of quantum feedback is optimal for specific tasks, which is important, both for experimental implementations of the tasks, and further theoretical investigations in quantum feedback. In particular, we detail optimal feedback protocols for key tasks implemented in optomechanical systems. Optomechanical systems have been investigated for the purpose of quantum sensing, particularly gravitational sensing, which has applications in geophysics and astrophysics. They have also been used to test theories of fundamental physics, such as collapse models. Greater understanding of the theory of controlling these systems may have an impact on these applications.

Acknowledgements

First and foremost, thanks to my supervisor Alessio Serafini for making the last three and a half years fun and interesting. Thanks also to Alessio's family for kindly having me to stay in Italy.

Thanks to my examiners Jason Ralph and Marzena Szymanska for reading this thesis and for their helpful comments.

Thanks to Matteo Brunelli for his help and collaboration.

Thanks to everyone I spent time with at UCL for the friendly atmosphere and interesting conversations: Andy Maxwell, Abbie Bray, Matt Flinders, Lia Li and in particular Sofia Qvarfort and Paul Brookes, with whom I shared an office.

Thanks to my friends and housemates throughout my time on the PhD: Laurence, Zoe, Nick, Henry, Jude, Rob and Daniel.

Finally, thanks to my family: Mum, Dad and Martha, for their love and support.

List of Publications

This thesis is based on the following publications:

[1] A. Harwood and A. Serafini, "Ultimate squeezing through coherent quantum feedback," *Physical Review Research*, vol. 2, no. 4, p. 043103, 2020

[2] A. Harwood, M. Brunelli, and A. Serafini, "Cavity optomechanics assisted by optical coherent feedback," *Physical Review A*, vol. 103, no. 2, p. 023509, 2021

[3] A. Harwood, M. Brunelli, and A. Serafini, "Unified collision model of coherent and measurement-based quantum feedback
for optimal state and operator control," *(Unpublished Manuscript, in preparation)*, 2022

Contents

List of Figures

Chapter 1

Introduction

This thesis is concerned with the theory of quantum feedback control in several contexts. The following introductory chapter is divided into four sections which will provide context and background information for the rest of the thesis. To start with, in Section 1.1, we briefly review the field of quantum feedback control and introduce the definitions of coherent and measurement-based feedback control. Then, in Section 1.2, we introduce the covariance matrix formalism of quantum Gaussian states, which is used in Chapters 2 and 3. In Section 1.3, we introduce the theory of optomechanical systems, which are the focus of Chapter 3. Finally, in Section 1.4, we review quantum collision models, which are used heavily in Chapter 4.

1.1 Quantum Feedback

In the classical regime, systems can be controlled through feedback loops. Classical feedback loops are implemented by performing measurements and using the results to inform manipulations on the system. The theory of control through feedback loops in the classical regime has been widely studied [4, 5]. However, classical control theory assumes that performing measurements does not affect the state of a system. This assumption does not hold in the quantum regime, meaning that much of classical control theory is not applicable to quantum systems.

It was therefore necessary to develop a new body of theory to describe

feedback control in the quantum regime. Broadly, the feedback control of quantum systems can be implemented in two different ways. In 'measurement-based feedback' (MF), measurements are performed on a quantum system, yielding results which are and used to inform manipulations on the system for the purpose of control. The process of quantum measurement can often introduce stochasticity in the evolution of a system undergoing measurement. In contrast, 'coherent feedback' (CF) designates a broad class of strategies where the controller is itself a quantum system. Quantum information flows from the system to the controller, is processed by the controller, and fed back into the system without measurements being performed at any stage.

The theory of quantum measurement-based feedback begins with the work of Belavkin, who first extended ideas from classical control theory to the quantum regime [6, 7]. Coherent feedback has its roots in 'all-optical feedback', where an optical beam output from a cavity is used to modulate the cavity's dynamics, without measurements being performed. All-optical feedback was first introduced by Wiseman and Milburn [8, 9], and was based on earlier work on 'cascaded quantum systems' [10].

Later, Lloyd used the term 'coherent feedback' to describe more general setups involving the use of one quantum system to control another without measurements being performed [11]. This definition of coherent feedback does not have an explicit feedback loop structure, and could therefore be considered closer to 'open-loop control' [12]. However, since all coherent feedback can be considered as open-loop control, some authors argue that this distinction is unnecessary [13]. Nonetheless, it is important to bear mind which definition of coherent feedback is being used.

Quantum optics allows this distinction to be disregarded, as the input-output formalism allows for a clear separation between a system, and the environmental continuum of modes which is used as a controller [14]. The input-output formalism describes the system as a set of 'stationary' modes and the environment as a series of travelling modes, known as 'input modes' which

each interact with the system, before being scattered as 'output modes'. This distinction allows CF and MF to both be framed as explicit feedback loops. Coherent feedback can be implemented by feeding the output modes back into the system, after some transformation. Measurement-based feedback can be implemented by monitoring the output modes and using the measurement result to generate a classical continuous signal which can be used to modify the system Hamiltonian or environmental input at another interface.

Another advantage of quantum optical systems is that they are often analytically treatable using Gaussian states which evolve linearly. As a result, CF and MF have been widely studied in the context of quantum optics [8, 9, 12, 15, 16, 17]. Feedback in the linear quantum optical systems, both coherent and measurement-based, can be treated using the SLH formalism [18, 19] which can also be used to describe feed *forward* control, where the controller is assumed to have access to the source of the noise affecting the system [20].

As previously stated, in quantum optics, it is conventional to implement MF by monitoring output fields and using the measurement record to generate a continuous classical signal which is then used to manipulate the feedback process. It can be shown [12] that the signal produced in this kind of MF can always be mimicked using direct manipulation of the output fields. This means one can always find a coherent output of the system which has the same statistics as the classical measurement signal. Since CF also allows for quantum signals, consisting of non-commuting operators, the converse is not always true. As a result, MF controllers (as defined in this way) are a subset of CF controllers. It is in this sense that CF is often described as superior to MF (for example, in [16]).

It has been shown that this difference is relevant when considering the performance of MF and CF in achieving several tasks. For example, [17], showed that CF outperformed MF for cooling quantum oscillators, and [16] showed that CF could achieve three tasks (back-action evading measurement, generation of a quantum non-demolition variable, and generation of a decoherence-

free subspace) which MF could not.

The superiority of CF is also claimed in the different framwork of [11], which considers the task of swapping the system state for a controller state-a process which can be performed coherently, but is disrupted if a measurement is performed. A similar task and framework is considered in [13], and again CF is found to be quantifiably superior.

At this point, it should be stressed that the superiority of CF is derived within in a specific model of quantum feedback, and does not mean that all effects of quantum measurement can be mimicked coherently, which would be a solution to the measurement problem. Since the measurement process cannot always be mimicked using coherent evolution, it is interesting to ask whether there are any cases where measurement is beneficial for quantum control. This question will be a key theme of this thesis and, in different contexts, is the focus of both Chapters 2 and 4.

Experimentally, MF has been implemented in a variety of platforms including: optomechanical systems [21], single neutral atoms [22], ensembles of atoms [23], trapped ions [24], superconducting qubits [25], solid state qubits [26] and cavity QED systems (at microwave and optical frequencies) [27, 28]. Coherent feedback has been implemented in circuit QED setups [29, 30, 31], quantum optical setups [32], solid state qubits in NV centres [33], optical resonators [34], nanomechanics [35], and optomechanical systems [36, 37].

1.2 Quantum Continuous Variables

Since much of the work in this thesis takes place in the regime of Gaussian quantum mechanics, we will take some time reviewing the theory of quantum continuous variables and Gaussian states. We will follow the treatment of this subject presented in [38].

1.2.1 The Canonical Commutation Relations

A system of n bosonic modes can be described using n pairs of self-adjoint operators, labelled $\hat{x}_j$ and $\hat{p}_j$ which obey the Canonical Commutation Relation

(CCR):

$$[\hat{x}_j, \hat{p}_k] = i\delta_{jk}\hbar\hat{\mathbb{1}}\,. \tag{1.1}$$

For convenience, we will often collect these operators into a $2n$-dimensional vector $\hat{\boldsymbol{r}} = (\hat{x}_1, \hat{p}_1 ... \hat{x}_n, \hat{p}_n)^\mathsf{T}$. In this vector form, the CCR can be written by introducing the anti-symmetrized commutator:

$$[\hat{\boldsymbol{r}}, \hat{\boldsymbol{r}}^\mathsf{T}] = \hat{\boldsymbol{r}}\hat{\boldsymbol{r}}^\mathsf{T} - (\hat{\boldsymbol{r}}\hat{\boldsymbol{r}}^\mathsf{T})^\mathsf{T}\,, \tag{1.2}$$

where $\hat{\boldsymbol{r}}\hat{\boldsymbol{r}}^\mathsf{T}$ is taken to be an outer product so that $[\hat{\boldsymbol{r}}, \hat{\boldsymbol{r}}^\mathsf{T}]$ is a $2n$-dimensional matrix of operators. We will also introduce a $2n \times 2n$ real, anti-symmetric matrix, known as the symplectic form, which is defined as follows:

$$\Omega_n = \bigoplus_j^n \Omega_1 \quad \text{where} \quad \Omega_1 = \begin{pmatrix} 0 & 1 \\ -1 & 0 \end{pmatrix}\,. \tag{1.3}$$

Often, we will drop the subscript of Ω, letting the context specify the dimension. We will also use the convention that $\hbar = 1$. The introduction of Ω allows the multimode CCR to be written in the compact form:

$$[\hat{\boldsymbol{r}}, \hat{\boldsymbol{r}}^\mathsf{T}] = i\Omega\,. \tag{1.4}$$

1.2.2 Quadratic Hamiltonians

We will use the terms 'quadratic' or 'second-order' Hamiltonians to refer to Hamiltonians of continuous variable systems which can be expressed as second-order polynomials of the canonical operators $\hat{x}_j$ and $\hat{p}_j$. Such Hamiltonians can be written in the following form:

$$\hat{H} = \frac{1}{2}\hat{\boldsymbol{r}}^\mathsf{T} H \hat{\boldsymbol{r}} + \boldsymbol{d}^\mathsf{T}\Omega\hat{\boldsymbol{r}}, \tag{1.5}$$

where $\hat{H}$ is the Hamiltonian operator, H is a, $2n \times 2n$ matrix known as the Hamiltonian matrix, and $\boldsymbol{d}$ is a $2n$-dimensional real vector sometimes known

as the 'linear drive'. The factor of Ω is included for reasons which will become apparent later. The matrix H must be real to ensure that the Hamiltonian operator is Hermitian. Furthermore, we can assume that H is symmetric, since any asymmetric components will result in commutator terms which are proportional to the identity and therefore can be discarded. In what follows we will also require that the Hamiltonian $\hat{H}$ is bounded from below, which corresponds to the Hamiltonian matrix being positive definite.

1.2.3 The Definition of Gaussian States

Gaussian states are quantum states in continuous variable systems can be defined as the ground and thermal states of quadratic Hamiltonians [38]. Thermal states have density operators which can be written as:

$$\rho = \frac{e^{-\beta\hat{H}}}{\mathrm{Tr}[e^{-\beta\hat{H}}]}\,, \tag{1.6}$$

where β is the inverse temperature. All such states for finite β are mixed, but become pure in the limit of zero temperature, when they correspond to ground states:

$$\rho = \lim_{\beta\to\infty} \frac{e^{-\beta\hat{H}}}{\mathrm{Tr}[e^{-\beta\hat{H}}]}\,. \tag{1.7}$$

When $\hat{H}$ is a quadratic Hamiltonian of the form given in equation (1.5), then equations (1.6) and (1.7) describe the density operators of Gaussian states.

1.2.4 The Covariance Matrix Formalism

Since the operators corresponding to quantum continuous variables live in an infinite dimensional Hilbert space, they are often cumbersome to treat analytically or numerically. However, Gaussian states allow for a convenient parameterisation, as they are completely determined by their first and second statistical moments [38], which we will now define.

For a quantum state ρ, the expectation value of an observable $\hat{x}$ is given by $\langle\hat{x}\rangle = \mathrm{Tr}[\rho\hat{x}]$. We can define the vector of first moments $\bar{\boldsymbol{r}}$ as the vector of the expectation values $\bar{\boldsymbol{r}} = \mathrm{Tr}[\hat{\rho}\hat{\boldsymbol{r}}] = (\langle\hat{x}_1\rangle, \langle\hat{p}_1\rangle \ldots \langle\hat{x}_n\rangle, \langle\hat{p}_n\rangle)^{\mathsf{T}}$.

The second statistical moments of a state can be described by a real, symmetric matrix, $\boldsymbol{\sigma}$, known as the covariance matrix. It is defined by:

$$\boldsymbol{\sigma} = \mathrm{Tr}[\rho\{(\hat{\boldsymbol{r}} - \bar{\boldsymbol{r}}), (\hat{\boldsymbol{r}} - \bar{\boldsymbol{r}})^{\mathsf{T}}\}] \,. \tag{1.8}$$

In this equation, we are implicitly using the convention that each element of $\bar{\boldsymbol{r}}$ is multiplied by the identity operator. It is also worth pointing out that some other work (eg. [39]) uses the convention that the covariance matrix is half of what have defined here. Note that using our convention, as shown in equation (1.8), the diagonal elements of $\boldsymbol{\sigma}$ will in fact be *twice* the variance of field quadratures. To correspond to a physical state, a real $2n \times 2n$ matrix must be positive definite and obey the Robertson-Schrödinger uncertainty relation $\boldsymbol{\sigma} + i\Omega \geq 0$ [38].

Finding the states of subsystems of multimode states in the covariance matrix formalism is straightforward. The first moments of any mode are easily extracted from the total vector of first moments $\bar{\boldsymbol{r}}$. The covariance matrix for the i-th mode is given by the the i-th 2×2 diagonal block of the overall covariance matrix. The diagonal 2×2 blocks of the overall covariance matrix describe each mode, and the off-diagonal blocks describe correlations between different modes.

1.2.5 Evolution Under Quadratic Hamiltonians

We will now investigate the Heisenberg picture evolution of the vector $\hat{\boldsymbol{r}}$ under a quadratic Hamiltonian of the form given in equation (1.5). The evolution due to the linear drive and the quadratic part of the Hamiltonian can be considered separately. Writing the j-th element of the vector $\hat{\boldsymbol{r}}$ as $\hat{r}_j$, the linear drive causes the following evolution:

$$\dot{\hat{r}}_j = i[\boldsymbol{d}^{\mathsf{T}}\Omega\hat{\boldsymbol{r}}, \hat{r}_j] = i\sum_{lm} d_l \Omega_{lm}[\hat{r}_m, \hat{r}_j] = -\sum_{lm} d_l \Omega_{lm}\Omega_{mj} = d_j \,. \tag{1.9}$$

Using the symmetry of H and the anti-symmetry of Ω, the evolution due to the quadratic part of the Hamiltonian can be written:

$$\dot{\hat{r}}_j = i[\frac{1}{2}\hat{\boldsymbol{r}}^{\mathsf{T}} H \hat{\boldsymbol{r}}, \hat{r}_j] = \frac{i}{2}\sum_{lm}[H_{lm}\hat{r}_l\hat{r}_m, \hat{r}_j] \tag{1.10}$$

$$= \frac{i}{2}\sum_{lm} H_{lm}([\hat{r}_l, \hat{r}_j]\hat{r}_m + \hat{r}_l[\hat{r}_m, \hat{r}_j]) = i\sum_{lm}\Omega_{jl}H_{lm}\hat{r}_m\,. \tag{1.11}$$

These equations can be cast in vector form to give the overall evolution

$$\dot{\hat{\boldsymbol{r}}} = \Omega H \hat{\boldsymbol{r}} + \boldsymbol{d}\,. \tag{1.12}$$

For the dimensions of this equation to be correct, we have implicitly assumed that each element of $\boldsymbol{d}$ is multiplied by the identity operator. Such objects (real or complex numbers multiplied by the identity operator) are known as c-numbers. This equation can be re-cast in the covariance matrix formalism to give the evolution of the first and second statistical moments of a Gaussian state. The evolution of the first moments follows straightforwardly, by taking the expectation value of each side of equation (1.12):

$$\dot{\bar{\boldsymbol{r}}} = \langle\dot{\hat{\boldsymbol{r}}}\rangle = \Omega H \bar{\boldsymbol{r}} + \boldsymbol{d}\,. \tag{1.13}$$

The evolution of the covariance matrix can be derived using equation (1.12) and the product rule. Using the shorthand $\hat{\boldsymbol{R}} = \hat{\boldsymbol{r}} - \bar{\boldsymbol{r}}$, we find:

$$\dot{\boldsymbol{\sigma}} = \frac{d}{dt}\langle\{\hat{\boldsymbol{R}}, \hat{\boldsymbol{R}}^{\mathsf{T}}\}\rangle = \langle\{\hat{\boldsymbol{R}}, \dot{\hat{\boldsymbol{R}}}^{\mathsf{T}}\}\rangle + \langle\{\dot{\hat{\boldsymbol{R}}}, \hat{\boldsymbol{R}}^{\mathsf{T}}\}\rangle \tag{1.14}$$

$$= \langle\{\Omega H\hat{\boldsymbol{R}}, \hat{\boldsymbol{R}}^{\mathsf{T}}\}\rangle + \langle\{\hat{\boldsymbol{R}}, \hat{\boldsymbol{R}}^{\mathsf{T}} H\Omega^{\mathsf{T}}\}\rangle = \Omega H\boldsymbol{\sigma} + \boldsymbol{\sigma}H\Omega^{\mathsf{T}}\,. \tag{1.15}$$

Since Gaussian states are entirely characterised by their first and second moments, the equations above fully characterise their evolution under quadratic Hamiltonians. However, these equations will not govern open-system or 'diffusive' dynamics, which can be treated using the input-ouput formalism, which we will discuss shortly.

1.2.6 The Symplectic Group

Let us consider the evolution of the vector $\hat{\boldsymbol{r}}$, given by equation (1.12). The solution to this equation is $\hat{\boldsymbol{r}}(t) = e^{\Omega H t}\hat{\boldsymbol{r}}(0) - (\Omega H)^{-1}\boldsymbol{d}$. Since this characterises unitary evolution of the operators, it will preserve the CCR. The linear drive $\boldsymbol{d}$ is a vector of c-numbers, so will not affect the CCR, meaning that the following holds:

$$i\Omega = [\hat{\boldsymbol{r}}(t), \hat{\boldsymbol{r}}(t)^{\mathsf{T}}] = [e^{\Omega H t}\hat{\boldsymbol{r}}(0), \hat{\boldsymbol{r}}(0)^{\mathsf{T}}(e^{\Omega H t})^{\mathsf{T}}] = e^{\Omega H t}[\hat{\boldsymbol{r}}(0), \hat{\boldsymbol{r}}(0)^{\mathsf{T}}](e^{\Omega H t})^{\mathsf{T}} \tag{1.16}$$

$$= e^{\Omega H t}(i\Omega)(e^{\Omega H t})^{\mathsf{T}}\,. \tag{1.17}$$

From this we can see that the matrix $S = e^{\Omega H t}$ preserves the symplectic form so that $\Omega = S\Omega S^{\mathsf{T}}$. Matrices which preserve the symplectic form in this way are said to belong to the real symplectic group denoted by $Sp_{2n,\mathbb{R}}$ for $2n$-dimensional matrices [40]. If we absorb t into the magnitude of H, we can define the unitary $\hat{U}_H = e^{i\frac{1}{2}\hat{\boldsymbol{r}}^{\mathsf{T}} H \hat{\boldsymbol{r}}}$ generated by a quadratic Hamiltonian and the related symplectic matrix $S_H = e^{\Omega H}$, and use them to write the useful relation

$$\hat{U}_H \hat{\boldsymbol{r}} \hat{U}_H^{\dagger} = S_H \hat{\boldsymbol{r}},\ . \tag{1.18}$$

This can be used to derive the following transformations of the statistical moments under the same Hamiltonian:

$$\bar{\boldsymbol{r}} \to \langle \hat{U}_H \hat{\boldsymbol{r}} \hat{U}_H^{\dagger} \rangle = S_H \bar{\boldsymbol{r}}\,, \tag{1.19}$$

$$\boldsymbol{\sigma} \to S_H \boldsymbol{\sigma} S_H^{\mathsf{T}}\,. \tag{1.20}$$

Since evolution under a quadratic Hamiltonian maintains the Gaussian character of a Gaussian state [41], these transformations will be useful.

Later, we will be concerned with with so-called 'passive' operations [41]. These are Gaussian operations which do not change the energy of the system. The energy of a bosonic mode is proportional to the number of excitations it

carries, which is given by the number operator $\hat{N} = \hat{a}^\dagger \hat{a} = \frac{1}{2}(\hat{x}^2 + \hat{p}^2 - 1)$. Operations which leave the energy unchanged will therefore preserve the quantity $\sum_i \hat{x}_i^2 + \hat{p}_i^2 = \hat{\boldsymbol{r}}^\mathsf{T} \hat{\boldsymbol{r}}$. This occurs when the symplectic matrix representing the operation is orthogonal so that $SS^\mathsf{T} = S^\mathsf{T} S = \mathbb{1}$. This fact will be used later in the context of passive coherent feedback. Some examples of common symplectic transformations, including passive transformations, are given in Appendix A.1.

1.2.7 Entanglement of Gaussian States

At later points in this thesis, we will be concerned with quantifying the entanglement between two modes in a Gaussian state. We will do this using the logarithmic negativity [42], which is an entanglement monotone [43]. A two-mode Gaussian state will have a 4×4 covariance matrix which can be expressed in terms of its 2×2 submatrices:

$$\boldsymbol{\sigma} = \begin{pmatrix} \boldsymbol{\sigma}_A & \boldsymbol{\sigma}_{AB} \\ \boldsymbol{\sigma}_{AB}^\mathsf{T} & \boldsymbol{\sigma}_B \end{pmatrix} . \tag{1.21}$$

Here, we present a simple expression for the logarithmic negativity in terms of these 2×2 submatrices. The logarithmic negativity for a system of two single-mode Gaussian states was first derived in [42], though here we present it using the notation from [38]. The logarthmic negativity E_N is given by:

$$E_N = \max\{0, -\log_2(\tilde{\nu}_-)\} , \tag{1.22}$$

where

$$\tilde{\nu}_- = \sqrt{\frac{\tilde{\Delta} - \sqrt{\tilde{\Delta}^2 - 4\mathrm{Det}\boldsymbol{\sigma}}}{2}} \quad \text{and} \tag{1.23}$$

$$\tilde{\Delta} = \mathrm{Det}\boldsymbol{\sigma}_A + \mathrm{Det}\boldsymbol{\sigma}_B - 2\mathrm{Det}\boldsymbol{\sigma}_{AB} . \tag{1.24}$$

We will use this expression when calculating the entanglement between the optical and mechanical modes of an optomechanical system.

1.2.8 The Input-Output formalism

The input-output formalism is an approach often used in quantum optics to describe the open-system evolution of bosonic modes coupled to environments which consist of a continuum of modes, such as the free electromagnetic field [44]. It can be shown that, under a series of reasonable approximations, the interaction with such a field can be modelled as a series of instantanous interactions with different modes (known as 'input modes') at each time [14]. These hypothetical modes interact once with the system only to be scattered away, never to interact with the system again. If the environment is a heat bath, with a continuum of frequencies, its Hamiltonian will take the form

$$\hat{H}_B = \int_0^\infty d\omega \omega b^\dagger(\omega) b(\omega)\,, \tag{1.25}$$

where $b(\omega)$ is the annihilation operators for the mode of the field with frequency ω. These operators satisfy $[b(\omega), b^\dagger(\omega')] = \delta(\omega - \omega')$. These annihilation operators are can be written in terms of the environmental quadratures by the relation $b(\omega) = \frac{1}{\sqrt{2}}(x(\omega) + ip(\omega))$. To treat multiple environmental fields, we will write $\hat{\boldsymbol{s}}(\omega) = (x_1(\omega), p_1(\omega), ...x_m(\omega), p_m(\omega))^\mathsf{T}$. For such an environment, we can define an input field with annihilation operator $b_{in}(t)$ which interacts with the system at time t and is given by:

$$b_{in}(t) = \frac{1}{\sqrt{2\pi}} \int_{-\infty}^{\infty} d\omega e^{-i\omega t} b(\omega)\,, \tag{1.26}$$

where $b(\omega)$ are taken to be evaluated at time $t = 0$, before they have interacted with the system. The input modes at different times t are completely uncorrelated, as evidenced by the commutation relation:

$$[b_{in}(t), b_{in}^{\dagger}(t')] = \frac{1}{2\pi}\int_{-\infty}^{\infty} d\omega \int_{-\infty}^{\infty} d\omega' e^{i(\omega' t' - \omega t)}[b(\omega), b^{\dagger}(\omega')] \tag{1.27}$$

$$= \frac{1}{2\pi}\int_{-\infty}^{\infty} d\omega \int_{-\infty}^{\infty} d\omega' e^{i(\omega' t' - \omega t)}\delta(\omega - \omega') \tag{1.28}$$

$$= \frac{1}{2\pi}\int_{-\infty}^{\infty} d\omega e^{i\omega(t'-t)} = \delta(t - t')\,. \tag{1.29}$$

The standard quadratures can be defined in relation to the input annihilation operator as $b_{in}(t) = \frac{1}{\sqrt{2}}(x_{in}(t) + ip_{in}(t))$. For m environmental fields, we can define a $2m$-dimensional input vector $\hat{\boldsymbol{r}}_{in}(t) = (x_{in,1}(t), p_{in,1}(t), ...x_{in,m}(t), p_{in,m}(t))^{\mathsf{T}}$. The elements of this vector satisfy the CCR, given by:

$$[\hat{\boldsymbol{r}}_{in}(t), \hat{\boldsymbol{r}}_{in}(t')^{\mathsf{T}}] = i\Omega\delta(t - t')\,. \tag{1.30}$$

We will now find the statistical moments of the input field $\hat{\boldsymbol{r}}_{in}(t)$. To do this, we will need to make the assumption that the moments of each environmental mode are independent of the frequency, which means that the first moments of $\hat{\boldsymbol{r}}_{in}(t)$ can be taken to be the same as the environment, and the second moments are delta-correlated in frequency:

$$\langle\{\hat{\boldsymbol{s}}(\omega), \hat{\boldsymbol{s}}(\omega')^{\mathsf{T}}\}\rangle = \boldsymbol{\sigma}_{in}\delta(\omega - \omega')\,, \tag{1.31}$$

where $\boldsymbol{\sigma}_{in}$ is the covariance matrix of the environmental models. This means that the second moments of $\hat{\boldsymbol{r}}_{in}(t)$ will satisfy:

$$\langle\{\hat{\boldsymbol{r}}_{in}(t), \hat{\boldsymbol{r}}_{in}(t')^{\mathsf{T}}\}\rangle = \boldsymbol{\sigma}_{in}\delta(t - t')\,. \tag{1.32}$$

The conditions (1.30) and (1.32) enforce 'white noise' conditions on the environment and imply that the environment interacting with the system is completely uncorrelated with itself at different times. This means that the evolution of the system under such conditions is Markovian, as we will soon see.

A white noise environment can also be framed using infinitesimal increments known as 'quantum Wiener processes' in analogy with classical Wiener processes. We will briefly review this approach, known as 'quantum stochastic calculus'. The first step is to consider the input signal integrated over a time period Δt, defined as $\Delta\hat{\boldsymbol{r}}_{in} = \int_t^{t+\Delta t} \hat{\boldsymbol{r}}_{in}(t')dt'$. Using equations (1.30) and (1.32), we can find the commutators and anti-commutators of $\Delta\hat{\boldsymbol{r}}_{in}$:

$$[\Delta\hat{\boldsymbol{r}}_{in}(t), \Delta\hat{\boldsymbol{r}}_{in}^{\mathsf{T}}(t)] = i\Omega\Delta t\,, \tag{1.33}$$

$$\langle\{\Delta\hat{\boldsymbol{r}}_{in}(t), \Delta\hat{\boldsymbol{r}}_{in}(t')^{\mathsf{T}}\}\rangle = \boldsymbol{\sigma}_{in}\Delta t\,. \tag{1.34}$$

In the infinitesimal limit $\Delta t \to dt$, we have $\Delta\hat{\boldsymbol{r}}_{in} = \hat{\boldsymbol{r}}_{in}dt$. This allows us to write the following relations:

$$[\hat{\boldsymbol{r}}_{in}(t), \hat{\boldsymbol{r}}_{in}^{\mathsf{T}}(t)](dt)^2 = i\Omega dt\,, \tag{1.35}$$

$$\langle\{\hat{\boldsymbol{r}}_{in}(t), \hat{\boldsymbol{r}}_{in}(t')^{\mathsf{T}}\}\rangle(dt)^2 = \boldsymbol{\sigma}_{in}dt\,. \tag{1.36}$$

The infinitesimal operators $\hat{\boldsymbol{r}}_{in}dt$ are known as quantum Wiener processes. When monitored (continuously measured), the resulting signal is described by a classical Wiener process, [38, 12] as we will see in Section 1.2.11.

1.2.9 Gaussian Diffusive Dynamics

Here, we will present the general evolution equations of a system coupled to a white noise environment through a quadratic Hamiltonian.

Let C be a $2m \times 2n$ real matrix and let $\hat{H}_C = \hat{\boldsymbol{r}}_{in}^{\mathsf{T}} C\hat{\boldsymbol{r}}$ be the quadratic coupling Hamiltonian between m input modes and n system modes. If the system is subject to this Hamiltonian, as well as a Hamiltonian $H_S = \frac{1}{2}\hat{\boldsymbol{r}}^{\mathsf{T}} H_S\hat{\boldsymbol{r}}$ acting purely on the system, its evolution, after the environment is traced out, is given by a modification of equations (1.13) and (1.14). The evolution of the first and second moments of the system is given by [38]:

$$\dot{\bar{\boldsymbol{r}}} = A\bar{\boldsymbol{r}} + \boldsymbol{d} + \Omega C\bar{\boldsymbol{r}}_{in}\,, \tag{1.37}$$

$$\dot{\boldsymbol{\sigma}} = A\boldsymbol{\sigma} + \boldsymbol{\sigma}A^{\mathsf{T}} + D\,, \tag{1.38}$$

where A and D are respectively known as the drift and diffusion matrices and are given by

$$A = \Omega H_S + \frac{1}{2}\Omega C\Omega C^{\mathsf{T}}\,, \qquad D = \Omega C\boldsymbol{\sigma}_{in}C^{\mathsf{T}}\Omega^{\mathsf{T}}\,. \tag{1.39}$$

We will often be concerned about the steady state covariance matrix of a system, that is, the solution when the left hand side of (1.38) is equal to zero. In this case, (1.38), takes the form of the Lyapunov equation [45, 46]. The solution is given by [47]:

$$\boldsymbol{\sigma}_{SS} = \int_0^\infty e^{At}De^{A^{\mathsf{T}}t}dt\,. \tag{1.40}$$

The condition for a system to have a steady state is that the drift matrix A must be 'Hurwitz', meaning that the real part of each of its eigenvalues is negative [45, 47]. This is evident from the integral in equation (1.40), which would diverge otherwise.

An alternative but equivalent way of capturing the diffusive dynamics of equations (1.14) and (1.13) is through stochastic Heisenberg evolution equations known as 'quantum Langevin equations'. The quantum Langevin equation for a setup with drift matrix A and coupling matrix C is given by

$$d\hat{\boldsymbol{r}} = A\hat{\boldsymbol{r}}dt + \boldsymbol{d}dt + \Omega C\hat{\boldsymbol{r}}_{in}dt\,. \tag{1.41}$$

This equation, combined with the white noise conditions (1.35) and (1.36), is fully equivalent to the drift-diffusion equations (1.37) and (1.38) for Gaussian states which are fully characterised by their first and second moments.

The evolution of a system under Gaussian diffusive dynamics can also be captured through a diffusive master equation, which describes the evolution of the system density matrix. This master equation can be expressed in terms of the drift and diffusion matrices. It is derived in [38], but we state it here for

completeness:

$$\dot{\rho} = \sum_{jk} \left[\left(\frac{i}{2} \Omega A - \frac{\Omega D \Omega^{\mathsf{T}}}{4} \right)_{jk} \hat{r}_j \hat{r}_k \rho + H.C \right] + \left[\left(\frac{i}{2} \Omega A + \frac{\Omega D \Omega^{\mathsf{T}}}{4} \right)_{jk} \hat{r}_j \rho \hat{r}_k + H.C \right] \tag{1.42}$$

where '$H.C$' indicates the Hermitian conjugate.

1.2.10 Gaussian Measurements

Measurements performed on Gaussian states do not always yield Gaussian states as outcomes. 'General-dyne' measurements [12] are a class of measurements which do, meaning that their effect can be described using the covariance matrix formalism. The class of general-dyne measurements includes homodyne and heterodyne measurements, which are commonly performed experimentally [39]. A general-dyne measurement is characterised by its covariance matrix $\boldsymbol{\sigma}_m$ which, along with the measurement outcome $\boldsymbol{r}_m$, specifies the post-measurement state of the measured subsystem.

The statistical moments of a general, multimode Gaussian state, with subsystems A and B can be written:

$$\boldsymbol{\sigma} = \begin{pmatrix} \boldsymbol{\sigma}_A & \boldsymbol{\sigma}_{AB} \\ \boldsymbol{\sigma}_{AB}^{\mathsf{T}} & \boldsymbol{\sigma}_B \end{pmatrix}, \quad \bar{\boldsymbol{r}} = \begin{pmatrix} \bar{\boldsymbol{r}}_A \\ \bar{\boldsymbol{r}}_B \end{pmatrix}. \tag{1.43}$$

A measurement performed on subsystem B, with measurement result $\boldsymbol{r}_m$ and covariance matrix $\boldsymbol{\sigma}_m$, leads to the following conditional evolution of subsystem A [48, 49]:

$$\boldsymbol{\sigma}_A \to \boldsymbol{\sigma}_A - \boldsymbol{\sigma}_{AB} \frac{1}{\boldsymbol{\sigma}_A + \boldsymbol{\sigma}_m} \boldsymbol{\sigma}_{AB}^{\mathsf{T}}, \tag{1.44}$$

$$\bar{\boldsymbol{r}}_A \to \bar{\boldsymbol{r}}_A + \boldsymbol{\sigma}_{AB} \frac{1}{\boldsymbol{\sigma}_A + \boldsymbol{\sigma}_m} (\boldsymbol{r}_m - \bar{\boldsymbol{r}}_B). \tag{1.45}$$

Note that the evolution of $\boldsymbol{\sigma}_A$ does not depend on the measurement result. The second moments evolve deterministically, regardless of the measurement outcome. The first moments, however evolve stochastically. They depend on the measurement outcome $\boldsymbol{r}_m$, which follows a Gaussian distribution with

probability density

$$p(\boldsymbol{r}_m) = \frac{e^{(\boldsymbol{r}_m - \bar{\boldsymbol{r}}_B)^{\mathsf{T}}(\boldsymbol{\sigma}_B + \boldsymbol{\sigma}_m)^{-1}(\boldsymbol{r}_m - \bar{\boldsymbol{r}}_B)}}{\pi^{n_B}\sqrt{\mathrm{Det}(\boldsymbol{\sigma}_B + \boldsymbol{\sigma}_m)}}\,, \tag{1.46}$$

where n_B is the number of modes in subsystem B [38].

1.2.11 General-dyne Monitoring

When a system interacts with a white noise environment, through a quadratic Hamiltonian, as described in Sections 1.2.8 and 1.2.9, the interaction can be described as a series of input modes, interacting once with the system, before being scattered away. The resulting scattered modes are known as the output modes, denoted by $\hat{\boldsymbol{r}}_{out}(t)$ and are related to the input modes through the so-called input-output 'boundary condition' [44, 16]:

$$\hat{\boldsymbol{r}}_{out}(t) + \hat{\boldsymbol{r}}_{in}(t) = -\Omega C^{\mathsf{T}}\hat{\boldsymbol{r}}(t)\,, \tag{1.47}$$

which will be derived in the context of Gaussian coherent feedback later, in Section 2.1. These output modes, since they have interacted with the system, become correlated with the system modes. Thus, if these scattered output modes are measured and the measurement outcome recorded, the evolution of the system state will be affected. The process of continuously measuring these scattered modes which have interacted with the system for an infinitesimal amount of time is known as 'monitoring'. Analogously to the case of one-shot measurements described in the previous section, general-dyne monitoring results in stochastic evolution of the first moments and deterministic evolution of the second moments. The evolution of the first moments is found by adding a stochastic term to equation (1.37):

$$d\bar{\boldsymbol{r}} = A\bar{\boldsymbol{r}}dt + \boldsymbol{d}dt + \Omega C\bar{\boldsymbol{r}}_{in}dt + (E - \boldsymbol{\sigma}B)d\boldsymbol{w}\,, \tag{1.48}$$

where $E = \Omega C\boldsymbol{\sigma}_{in}(\boldsymbol{\sigma}_{in} + \boldsymbol{\sigma}_m)^{-1/2}$ and $B = C\Omega(\boldsymbol{\sigma}_{in} + \boldsymbol{\sigma}_m)^{-1/2}$ [38]. The vector $d\boldsymbol{w}$ is a vector of uncorrelated classical Wiener increments which obey the

following statistics:

$$\langle d\boldsymbol{w}\rangle = 0\,, \quad \langle d\boldsymbol{w}, d\boldsymbol{w}^{\mathsf{T}}\rangle = \mathbb{1}dt. \tag{1.49}$$

Note that the averaging process above, denoted by the brackets $\langle\rangle$ indicate a classical averaging process, rather than a quantum expectation value. The evolution of the second moments is given by the following determinstitic Ricatti equation:

$$\dot{\boldsymbol{\sigma}} = \tilde{A}\boldsymbol{\sigma} + \boldsymbol{\sigma}\tilde{A}^{\mathsf{T}} + \tilde{D} - \boldsymbol{\sigma}BB^{\mathsf{T}}\boldsymbol{\sigma}\,, \tag{1.50}$$

where $\tilde{A} = A + EB^{\mathsf{T}}$, $\tilde{D} = D - EE^{\mathsf{T}}$ and E and B are the same as they appear in the evolution of the first moments. In this thesis, we will primarily

1.3 Optomechanics

Optomechanical systems consist of light modes coupled to massive mechanical modes. In what follows we will refer to optomechanics mostly in the context of 'cavity optomechanics' [50, 51] (though we note that other implementations are possible). In this model, the mechanical element acts as a mirror at one end of the cavity which contains the optical mode. Since the optical mode will exert radiation pressure on the mechanical element, it can change the length (and therefore the resonant frequency) of the cavity. The changing frequency of the cavity then leads to a change in radiation pressure, which leads to the optical and mechanical modes becoming coupled. This interaction is, in general, nonlinear. In this section, we will present a linearised version of this Hamiltonian. We will then present some further approximations and useful regimes used in our investigations later.

1.3.1 The Optomechanical Hamiltonian

We will consider a single optical mode whose annihilation operator we will denote $\hat{a}$ and a single mechanical mode denoted by $\hat{b}$. The coupling between the two modes is in general non-linear. However, by assuming that each mode can be approximated as small fluctuations around a large coherent amplitude,

a standard procedure [50, 51, 52] allows this Hamiltonian to be 'linearised' (approximated as a quadratic Hamiltonian which leads to linear evolution). This means the Hamiltonian is quadratic in the system quadratures, leading to linear evolution and allowing the system to be treated using Gaussian states. We will take this Hamiltonian as our starting point. It takes the form [50, 38]:

$$\hat{H}_{OM} = \omega_c \hat{a}^\dagger \hat{a} + \omega_m \hat{b}^\dagger \hat{b} + g(\alpha e^{-i\omega_L t}\hat{a}^\dagger + \alpha^* e^{i\omega_L t}\hat{a})(\hat{b} + \hat{b}^\dagger)\,, \tag{1.51}$$

where ω_c and ω_m are respectively the resonant frequencies of the cavity, and the mechanical oscillator. The optomechanical coupling is denoted by g and we assume that the cavity is being driven by a laser with coherent amplitude α and frequency ω_L. Going into the interaction picture with the the terms $\omega_c \hat{a}^\dagger \hat{a} + \omega_m \hat{b}^\dagger \hat{b}$ yields the following interaction Hamiltonian:

$$\hat{H}_{int} = g(\alpha e^{-i\Delta t}\hat{a}^\dagger + \alpha^* e^{i\Delta t}\hat{a})(e^{-i\omega_m t}\hat{b} + e^{i\omega_m t}\hat{b}^\dagger)\,, \tag{1.52}$$

where $\Delta = \omega_L - \omega_c$ is the detuning between the laser driving frequency and the cavity resonant frequency which can be changed to manipulate the behaviour of the system. Without loss of generality, we will assume that α is real and define the linearised coupling strength as $G = g\alpha$.

1.3.2 The Blue and Red Sideband Regimes

In the investigations presented later, we will be interested in two coupling strength regimes and two sideband driving regimes. The two coupling regimes are the 'weak coupling regime' where $G \ll \omega_m$ and the 'strong coupling regime', where this is not true. The two sideband regimes we are interested in are the 'red-sideband regime' where $\Delta = -\omega_m$ and the blue sideband regime, where $\Delta = \omega_m$.

First, we consider red sideband driving in the weak coupling regime. Setting $\Delta = -\omega_m$ in equation (1.52) yields

$$H = G(\hat{a}^\dagger \hat{b} + \hat{a}\hat{b}^\dagger + e^{-2i\omega_m t}\hat{a}^\dagger \hat{b}^\dagger + e^{2i\omega_m t}\hat{a}\hat{b})\,. \tag{1.53}$$

The weak coupling regime allows us to make the rotating wave approximation and discard the terms rotating with $e^{\pm 2i\omega_m t}$, yielding the time-independent Hamiltonian:

$$\hat{H}_R = G(\hat{a}^\dagger \hat{b} + \hat{b}^\dagger \hat{a})\,. \tag{1.54}$$

Notice that this Hamiltonian corresponds to an exchange of excitations between the optical and mechanical modes. Since the optical mode is higher frequency than the mechanical mode, it typically has a much lower temperature, meaning that driving the red sideband acts to cool the mechanical oscillator. This process is known as 'sideband cooling' [53, 54] and is one of several methods used to cool the mechanical oscillator, along with sympathetic cooling [55, 56, 37] and parametric feedback cooling (a form of measurement-based feedback) [57, 58, 59, 60].

By setting $\Delta = \omega_m$ in equation (1.52) and applying the rotating wave approximation, we find the following time-independent expression for the blue sideband Hamiltonian in the weak coupling regime:

$$\hat{H}_B = G(\hat{a}^\dagger \hat{b}^\dagger + \hat{a}\hat{b})\,. \tag{1.55}$$

This Hamiltonian generates two-mode squeezing which entangles the optical and mechanical modes.

In the strong coupling regime [61, 62, 63], we are unable to perform the rotating wave approximation. Instead, we start from equation (1.51) and 'unwind' the laser driving to obtain:

$$H_{Str} = -\Delta \hat{a}^\dagger \hat{a} + \omega_m \hat{b}^\dagger \hat{b} + G(\hat{a} + \hat{a}^\dagger)(\hat{b} + \hat{b}^\dagger)\,. \tag{1.56}$$

The Hamiltonians for the red and blue sidebands in the strong coupling regime are found respectively by substituting $\Delta = -\omega_m$ and $\Delta = \omega_m$ into equation (1.56).

1.4 Quantum Collision Models

Quantum collision models (CMs) are a class of model for quantum open systems which model system-bath dynmaics as a series of repeated interactions between a system and an environment, which is modelled as a series of ancillas, which interact one at a time [64]. They were first introduced in a study of the relaxation of spins and harmonic oscillators [65] and subsequently, they found use in the modelling of continuous weak measurements [66, 67]. In this work, they proved useful, as a weak measurement on the system could be modelled as a weak interaction with an ancilla, followed by a measurement of that ancilla.

Markovian open system dynamics can easily be modelled using CMs where the environment is 'memoryless' – that is, it interacts once with the system and never again. However, there is also great interest in using CMs to investigate non-Markovian dynamics, which can be obtained from CMs if one allows ancillas which have previously interacted with the system interact again, at a a later time. Such models are known as 'cascaded collsion models', and have been used to derive general non-Markovian master equations [68, 69, 70].

Collision models have found application in studies of quantum optics [71] and quantum thermodynamics [72]. The study [71] is of particular interest to us, as it frames the input-output formalism as a CM. CMs can also be realised experimentally in circuit QED setups [73, 74, 75, 76, 77] and linear optics [78, 79].

We will now briefly introduce Markovian CMs and their links to the input output formaism, mostly following the treatments found in [64, 70].

1.4.1 Discrete Collision Models

First, we will examine CMs with discrete timesteps, before taking the continuous limit. We consider a system S and a series of ancilla systems, all initialised in the state η which model the environment. The ancilla systems are labelled with the index n. At the nth timestep, the system will interact with the nth ancilla before the ancilla is scattered away and does not interact with the system again (see Figure 1.1).

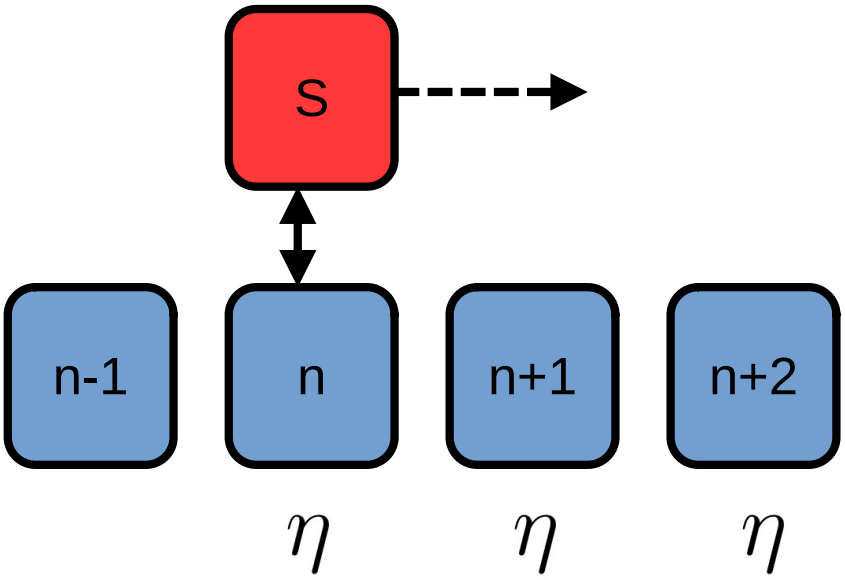

Figure 1.1: A schematic diagram of a quantum collision model. A system S interacts with a series of ancillas, each initialised in state η.

Let the interaction with the nth ancilla be given by the unitary U_n. Apart from interacting with different ancillas, all U_n operators take the same form. If the inital state of the system is given by ρ_0, after one timestep, the system state will be given by:

$$\rho_1 = \mathrm{Tr}_{E_1}[U_1 \rho_0 \otimes \eta U_1^\dagger] \,, \tag{1.57}$$

where the partial trace is taken the Hilbert space of the first environmental ancilla, as denoted by the subscript E_1. A single interaction of this kind is known as a 'collision'. After n such collisions, the system will be in a state given by:

$$\rho_n = \mathrm{Tr}_{E_n}[U_n \rho_{n-1} \otimes \eta U_n^\dagger] \,. \tag{1.58}$$

1.4.2 Continuous-Time Collision Models

Here, we assume that each interaction U_n takes an amount of time Δt. Taking Δt to be small, we can expand U_n as:

$$U_n = e^{-i(H_S + V_n)\frac{\Delta t}{2}} \approx \mathbb{1} - i(H_S + V_n)\frac{\Delta t}{2} - \frac{1}{2}V_n^2(\frac{\Delta t}{2})^2 \,, \tag{1.59}$$

where H_S is the Hamiltonian which generates the internal system dynamics and V_n is the Hamiltonian which generates the system-environment interaction. Note that we have expanded to second-order with respect to V_n, but only first-order in H_S, thus we are implicitly assuming that the characteristic frequency V_n of V_n is much larger than that of H_S. This assumption will be physically justified later in the context of quantum optics and the input-output formalism. The change in the system density operator over each timestep is given by:

$$\Delta\rho = \rho_n - \rho_{n-1} = \mathrm{Tr}_{E_n}[U_n \rho_{n-1} \otimes \eta] - \rho_{n-1}\,. \tag{1.60}$$

Using the expansion (1.59) and again keeping second order Δt terms only if they are also second order in V_n we can write this as:

$$\begin{aligned}\Delta\rho = &-i[H_S, \rho_n]\Delta t - i\mathrm{Tr}_{E_n}\big([V_n, \rho_n \otimes \eta]\big)\Delta t \\ &+ \mathrm{Tr}_{E_n}\big(V_n\rho_n \otimes \eta V_n - \frac{1}{2}\{V_n^2, \rho_n \otimes \eta\}\big)(\Delta t)^2\,.\end{aligned} \tag{1.61}$$

Now, we can define an effective Hamiltonian which acts on the system (also known a the Lamb shift):

$$H_S' = \mathrm{Tr}_{E_n}[V_n \eta]\,. \tag{1.62}$$

We can also recover the Lindblad dissipator:

$$\mathcal{D}[\rho] = \mathrm{Tr}_{E_n}\big(V_n\rho \otimes \eta V_n - \frac{1}{2}\{V_n^2, \rho \otimes \eta\}\big)\Delta t\,. \tag{1.63}$$

By writing the environmental state as $\eta = \sum_j p_j \left|j\right\rangle \left\langle j\right|$ in the basis of its eigenvectors and using this basis to perform the partial trace, we obtain the Lindblad dissipator in its familiar form, written in terms of jump operators:

$$\mathcal{D}[\rho] = \sum_{jk}\left(L_{jk}\rho L_{jk}^\dagger - \frac{1}{2}\{L_{jk}^\dagger L_{jk}, \rho\}\right)\Delta t\,, \tag{1.64}$$

where the jump operators are given by:

$$L_{jk} = \sqrt{p_k} \langle j | V_n | k \rangle \ . \tag{1.65}$$

Using this notation, we can write the discrete evolution of the system as:

$$\frac{\Delta\rho}{\Delta t} = i[H_S + H'_S, \rho] + \mathcal{D}[\rho] \, , \tag{1.66}$$

which is a discrete version of the Lindblad master equation. Taking the continuous limit $\Delta t \to 0$ gives the continuous Lindblad master equation:

$$\frac{d\rho}{dt} = i[H_S + H'_S, \rho] + \mathcal{D}[\rho] \, . \tag{1.67}$$

Since our expresssion for the dissipator (1.63) is proportional to Δt, we might expect it to vanish in the limit $\Delta t \to 0$. However, this can be avoided if we assume that $V_n \propto \frac{1}{\sqrt{\Delta t}}$. As we will see in the next section, this condition is already implicit in the input-output formalism.

1.4.3 The Input-Output Formalism as a Collision Model

We will now show that the collisional evolution of a system is equivalent to the evolution of system of bosonic modes interacting with an environment through an input-output interface. Previously, we have seen that the input-output formalism models interactions with the environment as a series of interactions with 'input modes' which we have labelled $\hat{\boldsymbol{r}}_{in}(t)$, which interact with the system at different times t. It should therefore not be surprising that this is can be captured by a collision model.

Recall that, in the input-output formalism, we assumed that the system was coupled to the environment through a Hamiltonian given by $V(t) = \hat{\boldsymbol{r}}^{\mathsf{T}} C \hat{\boldsymbol{r}}_{in}(t)$. This is equivalent to the CM coupling Hamiltonian V_n, as described in the previous section. The input modes $\hat{\boldsymbol{r}}_{in}$ satisfy the commutation relation

given in (1.35), which we will repeat here for convenience:

$$[\hat{\boldsymbol{r}}_{in}(t), \hat{\boldsymbol{r}}_{in}^{\mathsf{T}}(t)](dt)^2 = i\Omega dt\,. \tag{1.68}$$

Note that this is *not* a standard CCR, due to presence of the dt and $(dt)^2$ on each side. While $\hat{\boldsymbol{r}}_{in}$ are linearly coupled to the system, they are not associated with physical field modes, since they do not obey a CCR. We can define a new vector of operators $\hat{\boldsymbol{r}}'_{in}$ which are related to $\hat{\boldsymbol{r}}_{in}$ through the relation $\hat{\boldsymbol{r}}'_{in}\sqrt{dt} = \hat{\boldsymbol{r}}_{in}dt$. These new operators satisfy the CCR:

$$[\hat{\boldsymbol{r}}'_{in}(t), \hat{\boldsymbol{r}}'^{\mathsf{T}}_{in}(t)] = i\Omega\,. \tag{1.69}$$

Writing the coupling Hamiltonian in terms of $\hat{\boldsymbol{r}}'_{in}$, we get: $V\sqrt{dt} = \hat{\boldsymbol{r}}^{\mathsf{T}} C \hat{\boldsymbol{r}}'_{in}$, which justifies our claim in the previous section that $V \propto \frac{1}{\sqrt{dt}}$.

We will now demonstrate the equivalence of the two formalisms for a simple example; that of a single bosonic mode subject to losses through an exchange of excitations with a vacuum environment, given by a coupling Hamiltonian:

$$\hat{H}_C = \sqrt{\gamma}(\hat{p}\hat{x}_{in} - \hat{x}\hat{p}_{in})\,, \tag{1.70}$$

where γ is the system-environment coupling strength. For simplicity, we will assume that the Hamiltonian acting on the system is the identity.

First, using the input-output formalism in Gaussian diffusive dynamics, we can model this interaction using a coupling matrix $C = \sqrt{\gamma}\Omega^{\mathsf{T}}$. The vacuum environment is captured by $\boldsymbol{\sigma}_{in} = \mathbb{1}$. Using (1.39), we find that this leads to an evolution characterised by drift and diffusion matrices given by:

$$A = -\frac{1}{2}\mathbb{1} \quad \text{and} \quad D = \gamma\mathbb{1}\,. \tag{1.71}$$

By plugging these matrices into equation (1.42), we find that this evolution is

characterised by a master equation given by:

$$\dot{\rho} = \gamma \hat{a}\rho\hat{a}^\dagger - \frac{\gamma}{2}(\rho\hat{a}^\dagger\hat{a} + \hat{a}^\dagger\hat{a}\rho)\,, \tag{1.72}$$

where we have used the annihilation operator as defined by $\hat{a} = \frac{1}{\sqrt{2}}(\hat{x} + i\hat{p})$. Now we will show that the same equation can be derived using the collision model formalism described in Section 1.4.2. First, we will write the coupling Hamiltonian in terms of the physical field modes $\hat{\boldsymbol{r}}'_{in}$, so

$$V_n = \frac{1}{\sqrt{dt}}\sqrt{\gamma}(\hat{p}\hat{x}'_{in} - \hat{x}\hat{p}'_{in}). \tag{1.73}$$

To be completely rigorous, we should write this in terms of a finite increment Δt and only later take the limit $\Delta t \to dt$. However, here, this distinction does not make a difference to the final result and makes the calculations lengthier so for convenience we do not make it here. The reader is referred to [71] for a more rigorous treatment.

Now, we will use expression (1.73) to find the Lamb shift and the Lindblad dissipator which characterise the evolution in the CM, as given by (1.67). First, the Lamb shift Hamiltonian:

$$\begin{aligned} H'_S = \mathrm{Tr}_{E_n}[V_n\eta] &= \frac{\sqrt{\gamma}}{\sqrt{dt}}\mathrm{Tr}_{E_n}\left[(\hat{p}\hat{x}'_{in} - \hat{x}\hat{p}'_{in})\mathbb{1}\otimes\eta\right] \\ &= \frac{\sqrt{\gamma}}{\sqrt{dt}}\left[\hat{p}\mathrm{Tr}[\hat{x}'_{in}\eta] - \hat{x}\mathrm{Tr}[\hat{p}'_{in}\eta]\right] = 0\,, \end{aligned} \tag{1.74}$$

where we have use the fact that, since η is vacuum state, its first moments will be zero, so $\mathrm{Tr}[\hat{x}'_{in}\eta] = \mathrm{Tr}[\hat{p}'_{in}\eta] = 0$. Now, we will use this expression to find the Lindblad dissipator, as given by (1.63). When V_n is given by (1.73), we have:

$$\begin{aligned} \mathrm{Tr}_{E_n}\big(V_n\rho\otimes\eta V_n\big)(dt) = \gamma\big(&\hat{p}\rho\hat{p}\mathrm{Tr}[\hat{x}'^2_{in}\eta] + \hat{x}\rho\hat{x}\mathrm{Tr}[\hat{p}'^2_{in}\eta] \\ &- \hat{x}\rho\hat{p}\mathrm{Tr}[\hat{p}'_{in}\eta\hat{x}'_{in}] - \hat{p}\rho\hat{x}\mathrm{Tr}[\hat{x}'_{in}\eta\hat{p}'_{in}]\big)\,, \end{aligned} \tag{1.75}$$

When η is a vaccuum state $\mathrm{Tr}(\eta x'^2_{in}) = \mathrm{Tr}(\eta p'^2_{in}) = \frac{1}{2}$ and $\mathrm{Tr}(\eta xp) = \frac{i}{2}$. Plugging

these into (1.75), we obtain:

$$\mathrm{Tr}_{E_n}\big(V_n\rho\otimes\eta V_n\big)(dt)=\frac{\gamma}{2}(\hat{x}\rho\hat{x}+\hat{p}\rho\hat{p}-i\hat{x}\rho\hat{p}+i\hat{p}\rho\hat{x})=\gamma\hat{a}\rho\hat{a}^\dagger\,. \tag{1.76}$$

Applying a similar process, we obtain:

$$\mathrm{Tr}_{E_n}\big(V_n^2\rho\otimes\eta\big)(dt)=\frac{\gamma}{2}(\hat{p}^2+\hat{x}^2-i\hat{p}\hat{x}+i\hat{x}\hat{p})\rho=\hat{a}^\dagger\hat{a}\rho\,, \tag{1.77}$$

$$\mathrm{Tr}_{E_n}\big(\rho\otimes\eta V_n^2\big)(dt)=\frac{\gamma}{2}(\hat{p}^2+\hat{x}^2+i\hat{p}\hat{x}-i\hat{x}\hat{p})\rho=\rho\hat{a}^\dagger\hat{a}\,. \tag{1.78}$$

Since the Lamb shift Hamiltonian is equal to zero, plugging these expressions into (1.63) completely characterises the evolution. We obtain the expression:

$$\dot{\rho}=\mathcal{D}[\rho]=\gamma\hat{a}\rho\hat{a}^\dagger-\frac{\gamma}{2}(\rho\hat{a}^\dagger\hat{a}+\hat{a}^\dagger\hat{a}\rho)\,, \tag{1.79}$$

which is identical to the expression we obtained using the input-output formalism.

1.5 A Note on the use of Mathematica

Throughout this thesis, Mathematica 12 [80] was used for both numerical and analytical investigations. When it is used it is explicitly stated. Frequently, it was used to minimise or maximise figures of merit within certain constraints. In these cases, the in-built functions 'FindMinimum', 'FindMaximum', 'NMinimize' and 'NMaximise' were used. 'FindMinimum' and 'FindMaximum' use Interior Point Methods [81] to perform the optimisation under constraints [82]. 'NMinimize' and 'NMaximise' use simplex methods [81] in linear cases, and Nelder-Mead methods [83] in non-linear cases [82].

Chapter 2

A General Model of Gaussian Coherent Feedback

In this chapter, we will derive a general model of coherent feedback in the Gaussian regime and investigate some of its implications. In the first section, we derive an input-output boundary condition for a general quadratic coupling. Then, we investigate what happens when we perform a CP-map on the some of the output modes, before feeding them back into the system through the input-output interfaces, creating a CF loop. We then derive the resulting modifications to the drift and diffusion matrices which govern the evolution of the system. After this, we investigate passive coherent feedback loops coupled to a system through rotating wave couplings. We derive a compact way of describing such loops. Finally, we show such coherent feedback loops do not allow for squeezing of any quadrature below the so-called '3dB limit' [84]. The performance of these loops is compared to the squeezing generated by continuous monitoring and we discuss whether this constitutues a fair comparison between MF and CF. The contents of this chapter along with Figure 2.1 is partially based on work published in [1].

2.1 The General Input-Output Relation

We will now derive the Langevin evolution equation of Gaussian diffusive dynamics (1.41) as well as the input-output boundary condition (1.47). Previ-

ously we have noted that the input-output formalism treats interactions with a continuous environment as series of instantaneous interactions with different input modes at different times. The input mode that interacts at time t is denoted $\hat{\boldsymbol{r}}_{in}(t)$. For reasons that will become apparent later, we will use a slightly modified notation for this derivation. We will denote the vector of operators corresponding to the environmental modes which interact with the system at time x as $\hat{\boldsymbol{s}}_x(t)$. Later, we will identify $\hat{\boldsymbol{s}}_x(t)$ as $\hat{\boldsymbol{r}}_{in}(x)$ for $t < x$, before it has interacted with the system and as $\hat{\boldsymbol{r}}_{out}(x)$ for $t > x$, after it has been scattered from the system.

The Hamiltonian which corresponds to a series of instantaneous interactions through a coupling matrix C is:

$$\hat{H}(t) = \int_{\mathbb{R}} \hat{\boldsymbol{r}}^{\mathsf{T}} C \hat{\boldsymbol{s}}_x \delta(x-t)dx = \int_{\mathbb{R}} \hat{r}_i C_{ij} (\hat{\boldsymbol{s}}_x)_j \delta(x-t)dx\,, \tag{2.1}$$

where we have used Einstein notation for summation over repeated indices. The Heisenberg evolution of the system variables is given by:

$$\dot{\hat{r}}_k(t) = i[\hat{H}(t), \hat{r}_k] = i\int_{\mathbb{R}} C_{ij}(\hat{\boldsymbol{s}}_x)_j [\hat{r}_i, \hat{r}_k]\delta(x-t)dx \tag{2.2}$$

$$= i\int_{\mathbb{R}} C_{ij}(\hat{\boldsymbol{s}}_x)_j i\Omega_{ik}\delta(x-t)dx \tag{2.3}$$

$$= -C_{ij}\Omega_{ik}(\hat{\boldsymbol{s}}_t)_j\,. \tag{2.4}$$

In vector form, this gives us $\frac{d\hat{\boldsymbol{r}}}{dt} = \Omega C \hat{\boldsymbol{s}}_t(t)$. The Heisenberg evolution of the travelling modes is given by:

$$\frac{d(\hat{\boldsymbol{s}}_x)_k}{dt} = i[\hat{H}(t), (\hat{\boldsymbol{s}}_x)_k] = i\int_{\mathbb{R}} \hat{r}_i C_{ij}[(\hat{\boldsymbol{s}}_{x'})_j, (\hat{\boldsymbol{s}}_x)_k]\delta(x'-t)dx' \tag{2.5}$$

$$= i\int_{\mathbb{R}} \hat{r}_i C_{ij} i\Omega_{jk}\delta(x-x')\delta(x'-t)dx' = -\hat{r}_i\Omega_{jk}C_{ij}\,. \tag{2.6}$$

In vector form, this is $\frac{d\hat{\boldsymbol{s}}_x(t)}{dt} = \Omega C^{\mathsf{T}}\hat{\boldsymbol{r}}(t)\delta(x-t)$. This can be integrated to obtain:

$$\hat{\boldsymbol{s}}_x(t) = \hat{\boldsymbol{s}}_x(0) + \Omega C^{\mathsf{T}}\hat{\boldsymbol{r}}\theta(x-t)\,, \tag{2.7}$$

where $\theta(t-x)$ is a step function which takes value 0 when $t < x$, takes values 1 when $t > x$ and, by convention, takes value $\frac{1}{2}$ when $t = x$. Substituting this into the evolution equation for $\hat{\boldsymbol{r}}$ yields the equation:

$$\dot{\hat{\boldsymbol{r}}}(t) = \Omega C \hat{\boldsymbol{s}}_t(0) + \frac{1}{2}\Omega C \Omega C^{\mathsf{T}} \hat{\boldsymbol{r}}\,. \tag{2.8}$$

This recovers the familiar generalised quantum Langevin equation, given in (1.41) if we identify $\hat{\boldsymbol{s}}_t(0) = \hat{\boldsymbol{r}}_{in}(t)$. We can also identify $\hat{\boldsymbol{s}}_{t'}(t) = -\hat{\boldsymbol{r}}_{out}(t)$ for $t > t'$ to yield the generalised input-output relation:

$$\hat{\boldsymbol{r}}_{out}(t) + \hat{\boldsymbol{r}}_{in}(t) = -\Omega C^{\mathsf{T}} \hat{\boldsymbol{r}}(t)\,. \tag{2.9}$$

2.2 A General Model of Gaussian Coherent Feedback

Now that we have derived a general input-output relation we can investigate what happens when we feed some of the output modes back as input modes, leading to a coherent feedback loop. Here, we will present the most general, multimode Gaussian coherent feedback setup and derive the drift and diffusion matrices which govern the evolution of the system in such a setup. A diagram of the scheme considered is shown in Figure 2.1.

We will consider set of system modes $\hat{\boldsymbol{r}}$, which interacts with an arbitrary number of environmental modes. The interactions with theses modes are split into two sets a and b, which interact with the system through coupling matrices matrices C_a and C_b respectively. This corresponds to a coupling Hamiltonian matrix:

$$H_C = \begin{pmatrix} 0 & C_a & C_b \\ C_a^{\mathsf{T}} & 0 & 0 \\ C_b^{\mathsf{T}} & 0 & 0 \end{pmatrix}, \tag{2.10}$$

which leads to a coupling Hamiltonian $\hat{H}_C = \frac{1}{2}\hat{\boldsymbol{r}}_T H_C \hat{\boldsymbol{r}}_T$ where $\hat{\boldsymbol{r}}_T = \hat{\boldsymbol{r}} \oplus \hat{\boldsymbol{r}}_{in,a} \oplus \hat{\boldsymbol{r}}_{in,b}$.

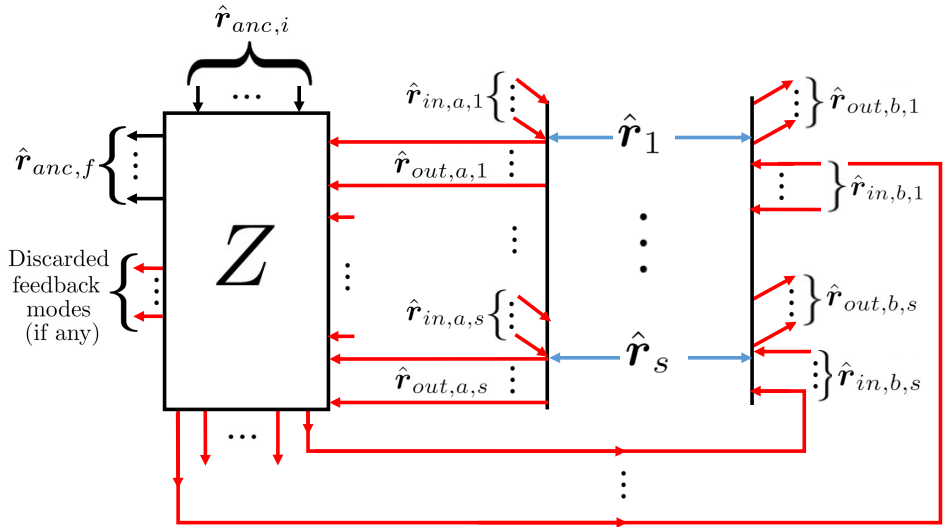

Figure 2.1: The general Gaussian coherent feedback scheme considered in this chapter. The coherent feedback loop is labelled in red, system modes are labelled in blue and ancilla modes are black. The symplectic transformation S_Φ, made on the ancilla and output modes is here denoted Z. Since the dimension of a may not be the same as b, we allow for the possibility that feedback modes need to be discarded before the rest are fed back into the b interface

Coherent feedback corresponds to setting $\hat{\boldsymbol{r}}_{in,b} = \Phi(\hat{\boldsymbol{r}}_{out,a})$. In words: the output modes from the a interfaces are subjected to a CP-map Φ before being fed back into the system through the b interfaces. We note that this treatment is completely general and does not require that the number of modes interacting at a and b are the same, since we can always include non-interacting ancilla modes to ensure the same dimensions on both sides of the equation $\hat{\boldsymbol{r}}_{in,b} = \Phi(\hat{\boldsymbol{r}}_{out,a})$.

A general Gaussian CP-map can be performed on $\hat{\boldsymbol{r}}_{out,a}$ by performing a general symplectic operation on $\hat{\boldsymbol{r}}_{out,a}$, along with ancilla modes which we will label $\hat{\boldsymbol{r}}_{anc}$ and trace out after the interaction. This can be written as $\Phi(\hat{\boldsymbol{r}}_{out,a}) = \mathrm{Tr}_{anc}[S_\Phi \hat{\boldsymbol{r}}_{out,a} \oplus \hat{\boldsymbol{r}}_{anc}]$ where S_Φ is the symplectic matrix which generates the CP-map. We can write:

$$\Phi(\hat{\boldsymbol{r}}_{out,a}) = E\hat{\boldsymbol{r}}_{out,a} + F\hat{\boldsymbol{r}}_{anc} \quad \text{when} \quad S_\Phi = \begin{pmatrix} E & F \\ G & H \end{pmatrix}. \tag{2.11}$$

Since the ancilla modes $\hat{\boldsymbol{r}}_{anc}$ are part of the environment, we assume that they also satisfy the same white noise conditions that $\hat{\boldsymbol{r}}_{in,a}$ do. At this point it is important to clarify a slight change in notation. Until now, we have used the subscript *in* to refer to any white noise environmental modes which also happen to be the modes which are the inputs at each interface. However, coherent feedback involves replacing the environmental input with an input generated by the output of another interface. To clarify this, in what follows, we will use the subscript e to indicate environmental white noise modes and the subscript *in* to describe whatever modes are input at a given interface. In our coherent feedback model, this means that $\hat{\boldsymbol{r}}_{in,a} = \hat{\boldsymbol{r}}_{e,a}$, as the inputs at the a interfaces are white noise environmental modes. However $\hat{\boldsymbol{r}}_{in,a} \neq \hat{\boldsymbol{r}}_{e,b}$, as the inputs through the b interfaces are not environmental modes, but are the result of processing $\hat{\boldsymbol{r}}_{out,a}$.

The effect of setting $\hat{\boldsymbol{r}}_{in,b} = \Phi(\hat{\boldsymbol{r}}_{out,a}))$ can be represented by the transformation:

$$\begin{pmatrix} \hat{\boldsymbol{r}} \\ \hat{\boldsymbol{r}}_{in,a} \\ \hat{\boldsymbol{r}}_{in,b} \end{pmatrix} = \begin{pmatrix} \mathbb{1} & 0 & 0 & 0 \\ 0 & \mathbb{1} & 0 & 0 \\ 0 & 0 & E & F \end{pmatrix} \begin{pmatrix} \hat{\boldsymbol{r}} \\ \hat{\boldsymbol{r}}_{e,a} \\ \hat{\boldsymbol{r}}_{out,a} \\ \hat{\boldsymbol{r}}_{anc} \end{pmatrix} . \tag{2.12}$$

We can use the generalised input-output boundary condition (2.9) to write $\hat{\boldsymbol{r}}_{out,a}$ in terms of $\hat{\boldsymbol{r}}$ and $\hat{\boldsymbol{r}}_{e,a}$. Putting this in matrix form yields:

$$\begin{pmatrix} \hat{\boldsymbol{r}} \\ \hat{\boldsymbol{r}}_{e,a} \\ \hat{\boldsymbol{r}}_{out,a} \\ \hat{\boldsymbol{r}}_{anc} \end{pmatrix} = \begin{pmatrix} \mathbb{1} & 0 & 0 \\ 0 & \mathbb{1} & 0 \\ -\Omega C_a^{\mathsf{T}} & -\mathbb{1} & 0 \\ 0 & 0 & \mathbb{1} \end{pmatrix} \begin{pmatrix} \hat{\boldsymbol{r}} \\ \hat{\boldsymbol{r}}_{e,a} \\ \hat{\boldsymbol{r}}_{anc} \end{pmatrix} . \tag{2.13}$$

We can combine equations (2.12) and (2.13) to write the inputs at each interface as a transformation of the white noise environmental modes $\hat{\boldsymbol{r}}_{e,a}$ and $\hat{\boldsymbol{r}}_{anc}$,

along with the system modes $\hat{\boldsymbol{r}}$.

$$\begin{pmatrix} \hat{\boldsymbol{r}} \\ \hat{\boldsymbol{r}}_{in,a} \\ \hat{\boldsymbol{r}}_{in,b} \end{pmatrix} = \begin{pmatrix} \mathbb{1} & 0 & 0 & 0 \\ 0 & \mathbb{1} & 0 & 0 \\ 0 & 0 & E & F \end{pmatrix} \begin{pmatrix} \mathbb{1} & 0 & 0 \\ 0 & \mathbb{1} & 0 \\ -\Omega C_a^{\mathsf{T}} & -\mathbb{1} & 0 \\ 0 & 0 & \mathbb{1} \end{pmatrix} \begin{pmatrix} \hat{\boldsymbol{r}} \\ \hat{\boldsymbol{r}}_{e,a} \\ \hat{\boldsymbol{r}}_{anc} \end{pmatrix} = R \begin{pmatrix} \hat{\boldsymbol{r}} \\ \hat{\boldsymbol{r}}_{e,a} \\ \hat{\boldsymbol{r}}_{anc} \end{pmatrix} \tag{2.14}$$

Since the coupling Hamiltonian couples the system to the environment $\hat{\boldsymbol{r}}_{in,a} \oplus \hat{\boldsymbol{r}}_{in,b}$, the effect of coherent feedback is to couple the system to the environment $\hat{\boldsymbol{r}}_{e,a} \oplus \hat{\boldsymbol{r}}_{anc}$ through a modified coupling Hamilontian matrix $H_C^{cf} = R^{\mathsf{T}} H_C R$ which has the form

$$H_C^{cf} = \begin{pmatrix} -C_a \Omega^{\mathsf{T}} E^{\mathsf{T}} C_b^{\mathsf{T}} - C_b E \Omega C_a^{\mathsf{T}} & C_a - C_b E & C_b F \\ C_a^{\mathsf{T}} - E^{\mathsf{T}} C_b^{\mathsf{T}} & 0 & 0 \\ F^{\mathsf{T}} C_b^{\mathsf{T}} & 0 & 0 \end{pmatrix}. \tag{2.15}$$

From this, it is clear that, under coherent feedback the system is coupled to the environment $\hat{\boldsymbol{r}}_{e,a} \oplus \hat{\boldsymbol{r}}_{anc}$ through an effective coupling matrix $(C_a - C_b E, C_b F)$. Additionally, the term $-C_a \Omega^{\mathsf{T}} E^{\mathsf{T}} C_b^{\mathsf{T}} - C_b E \Omega C_a^{\mathsf{T}}$ appears in the block of Hamiltonian matrix corresponding to purely system operators. Depending on the nature of the couplings involved, coherent feedback can induce interactions between different system modes (or cause system modes to interact with themselves). The effect of this is that the effective system Hamiltonian matrix H_S is modified by the addition of this term.

To summarise this model, we can say that Gaussian coherent feedback for an arbitrary number of system modes and environmental interactions is fully characterised by a coupling matrix $(C_a - C_b E, C_b F)$, a system Hamiltonian matrix $H_S - C_a \Omega^{\mathsf{T}} E^{\mathsf{T}} C_b^{\mathsf{T}} - C_b E \Omega C_a^{\mathsf{T}}$ and the state of the white noise environment $\hat{\boldsymbol{r}}_{in,a} \oplus \hat{\boldsymbol{r}}_{anc}$.

Note that here, we have assumed that the feedback is instantaneous, so that $\hat{\boldsymbol{r}}_{in,b}(t) = \Phi(\hat{\boldsymbol{r}}_{out,a}(t))$. This means that evolution is Markovian, meaning

that it can be expressed using a drift-diffusion equation of the form (1.38). In practice, there will be a small delay in between a mode being output from one interface and fed back into another, meaning that $\hat{\boldsymbol{r}}_{in,b}(t) = \Phi(\hat{\boldsymbol{r}}_{out,a}(t-\tau))$ for some $\tau > 0$. The assumption that feedback is instantaneous is valid provided that τ is small compared to the timescale of the system. We will investigate feedback with non-negligible delays the next chapter, in the context of optomechanics, but in general its non-Markovianity makes it difficult to treat analytically.

2.3 Passive Gaussian Coherent Feedback

We will now apply this general model in a more specific setting. In particular, we will consider a setup with an arbitrary number of system modes, along with an arbitrary number of input, outputs and ancillas, coupled to a white noise environment in a thermal state through rotating wave couplings. Furthermore, we will assume that the in-loop CP-map is passive, meaning that it does not add any energy to the system. In practice, passive CP-maps are generated through interferometric components such as beam splitters and phase shifters, making them amenable to experimental implementation.

Firstly, the assumption that the white noise environment is thermal means that the covariance matrix takes the form $\boldsymbol{\sigma}_{in} = N\mathbb{1}$ where $N = 2\bar{N}+1$ and $\bar{N}$ is the mean number of environmental thermal excitations. At zero temperature $N = 1$. Furthermore, the environmental thermal state will have first moments equal to zero so that $\bar{\boldsymbol{r}}_{in} = 0$.

'Rotating-wave' system-environment couplings are commonly used to describe optical leakage from a cavity. These couplings are described by a Hamiltonian which corresponds to an exchange of excitations between system and environment. For one system mode and one environmental mode, this Hamiltonian is:

$$\hat{H}_C = \sqrt{\gamma}(\hat{p}\hat{x}_{in} - \hat{x}\hat{p}_{in})\,, \tag{2.16}$$

which corresponds to a coupling matrix $C = \sqrt{\gamma}\Omega^{\mathsf{T}}$ where γ is the frequency

which specifies the strength of the coupling.

We will consider a setup with s system modes. The jth system mode is coupled to $l_j + m_j$ interfaces, each described by a Hamiltonian of the form (2.16). The interfaces whose outputs are used for coherent feedback are labelled l_j and the interfaces into which we will feed these outputs are labelled m_j. Using the notation from the previous section, we can write:

$$C_a = \begin{pmatrix} K_{l_1} & 0 & 0 & \dots & 0 \\ 0 & K_{l_2} & 0 & \dots & 0 \\ \vdots & & \ddots & & \vdots \\ 0 & \dots & 0 & \dots & K_{l_s} \end{pmatrix}, \tag{2.17}$$

$$C_b = \begin{pmatrix} K_{m_1} & 0 & 0 & \dots & 0 \\ 0 & K_{m_2} & 0 & \dots & 0 \\ \vdots & & \ddots & & \vdots \\ 0 & \dots & 0 & \dots & K_{m_s} \end{pmatrix}, \tag{2.18}$$

where K_i indicates a $2 \times 2i$ dimension matrix of the form $\sqrt{\gamma}(\Omega^{\mathsf{T}} \dots \Omega^{\mathsf{T}})$.

The condition that the in-loop CP-map must be passive means that the matrix S_Φ must be orthogonal. This enforces the following conditions on its submatrices:

$$S_\Phi S_\Phi^{\mathsf{T}} = \begin{pmatrix} EE^{\mathsf{T}} + FF^{\mathsf{T}} & EG^{\mathsf{T}} + FH^{\mathsf{T}} \\ GE^{\mathsf{T}} + HF^{\mathsf{T}} & GG^{\mathsf{T}} + HH^{\mathsf{T}} \end{pmatrix} = \begin{pmatrix} \mathbb{1} & 0 \\ 0 & \mathbb{1} \end{pmatrix}. \tag{2.19}$$

In particular, we will make use of the relation $EE^{\mathsf{T}} + FF^{\mathsf{T}} = \mathbb{1}$. We can use the symplecticity of S_Φ to obtain another condition on its submatrices.

$$S_\Phi \Omega S_\Phi^{\mathsf{T}} = \begin{pmatrix} E\Omega E^{\mathsf{T}} + F\Omega F^{\mathsf{T}} & E\Omega G^{\mathsf{T}} + F\Omega H^{\mathsf{T}} \\ G\Omega E^{\mathsf{T}} + H\Omega F^{\mathsf{T}} & G\Omega G^{\mathsf{T}} + H\Omega H^{\mathsf{T}} \end{pmatrix} = \begin{pmatrix} \Omega & 0 \\ 0 & \Omega \end{pmatrix}. \tag{2.20}$$

Recall that we are using the convention that the dimensions of Ω are specified by the context. Again, we will be particularly interested in the equation

concerning E and F: $E\Omega E^{\mathsf{T}} + F\Omega F^{\mathsf{T}} = \Omega$.

We will now state another feature of orthogonal symplectic matrices which will be useful. If we label the 2×2 blocks of S_Φ as S_{jk}, then they will all take the form [38]:

$$S_\Phi = \begin{pmatrix} S_{11} & \dots & S_{1n} \\ \vdots & \ddots & \vdots \\ S_{n1} & \dots & S_{nn} \end{pmatrix} \quad S_{jk} = \begin{pmatrix} x_{jk} & y_{jk} \\ -y_{jk} & x_{jk} \end{pmatrix} , \tag{2.21}$$

which is a fact we will use later.

2.3.1 The Diffusion Matrix for Passive Coherent Feedback

Now we have described the setup, we will derive the diffusion matrix D of the system. We will derive D_0, the diffusion matrix for a zero temperature environment with $\boldsymbol{\sigma}_{in} = \mathbb{1}$, but the results can be easily modified to reflect a non-zero temperature by multiplying the zero temperature diffusion matrix by an appropriate value of N. The diffusion matrix is given by:

$$D = \Omega C \boldsymbol{\sigma}_{in} \Omega C^{\mathsf{T}} . \tag{2.22}$$

Under coherent feedback, we have $C = C_{cf} = (C_a - C_b E, C_b F)$. Plugging this in to (2.22), we obtain:

$$D_0 = (\Omega C_a - \Omega C_b E)(C_a^{\mathsf{T}} \Omega^{\mathsf{T}} - E^{\mathsf{T}} C_b^{\mathsf{T}} \Omega^{\mathsf{T}}) + \Omega C_b F F^{\mathsf{T}} C_b^{\mathsf{T}} \Omega^{\mathsf{T}} . \tag{2.23}$$

Expanding this equation, and using the previously derived condition $EE^{\mathsf{T}} + FF^{\mathsf{T}} = \mathbb{1}$ gives:

$$D_0 = \Omega(C_a C_a^{\mathsf{T}} + C_b C_b^{\mathsf{T}})\Omega^{\mathsf{T}} - \Omega C_a E^{\mathsf{T}} C_b^{\mathsf{T}} \Omega^{\mathsf{T}} - \Omega C_b E C_a^{\mathsf{T}} \Omega^{\mathsf{T}} . \tag{2.24}$$

We now note that $C_a C_a^\mathsf{T} = \gamma\,\mathrm{diag}(l_1, l_1 \ldots l_s, l_s)$ and $C_b C_b^\mathsf{T} = \gamma\,\mathrm{diag}(m_1, m_1 \ldots m_s, m_s)$, which allows us to write:

$$\Omega(C_a C_a^\mathsf{T} + C_b C_b^\mathsf{T})\Omega^\mathsf{T} = \gamma\,\mathrm{diag}(l_1+m_1, l_1+m_1 \ldots l_s+m_s, l_s+m_s) = \Delta\,. \quad (2.25)$$

After doing this, our expression for the zero-temperature diffusion matrix becomes:

$$D_0 = \Delta - \Omega C_a E^\mathsf{T} C_b^\mathsf{T} \Omega^\mathsf{T} - \Omega C_b E C_a^\mathsf{T} \Omega^\mathsf{T}\,. \quad (2.26)$$

We will call $J = \Omega C_b E C_a^\mathsf{T} \Omega^\mathsf{T}$, allowing us to write:

$$D_0 = \Delta - J^\mathsf{T} - J\,. \quad (2.27)$$

Now, we note the form of ΩC_a and ΩC_b, which are given by:

$$\Omega C_a = \begin{pmatrix} \Gamma_{l_1}^\mathsf{T} & \ldots & 0 \\ \vdots & \ddots & \vdots \\ 0 & \ldots & \Gamma_{l_s}^\mathsf{T} \end{pmatrix} = G_l \text{ and } \Omega C_b = \begin{pmatrix} \Gamma_{m_1}^\mathsf{T} & \ldots & 0 \\ \vdots & \ddots & \vdots \\ 0 & \ldots & \Gamma_{m_s}^\mathsf{T} \end{pmatrix} = G_m\,. \quad (2.28)$$

where Γ_j is a real $2j \times 2$ matrix of the form $\Gamma_j = \sqrt{\gamma}(\mathbb{1}_2, \ldots, \mathbb{1}_2)^\mathsf{T}$. This notation can be used to write $J = G_m E G_l^\mathsf{T}$. We also note the following easily verified relationships which we will use later:

$$\Omega C_b^\mathsf{T} = -G_m^\mathsf{T} \quad \Omega C_a^\mathsf{T} = -G_l^\mathsf{T} \quad \Omega G_m \Omega^\mathsf{T} = G_m \quad \Omega G_l \Omega^\mathsf{T} = G_l\,. \quad (2.29)$$

2.3.2 The Drift matrix for Passive Coherent Feedback

Recall that the drift matrix of a system takes form:

$$A = \Omega H_S + \frac{1}{2}\Omega C \Omega C^\mathsf{T}\,. \quad (2.30)$$

We will take H_S to be completely general and will examine the form of the diffusive part of the drift matrix under passive coherent feedback. We will do

this by plugging $C = C_{cf} = (C_a - C_b E, C_b F)$ into $\Omega C \Omega C^\mathsf{T}$:

$$\Omega C \Omega C^\mathsf{T} = (\Omega K_l - \Omega K_m E)(\Omega K_l^\mathsf{T} - \Omega E^\mathsf{T} K_m^\mathsf{T}) + \Omega K_m F \Omega F^\mathsf{T} K_m^\mathsf{T} . \tag{2.31}$$

Expanding this and using the symplectic condition $E\Omega E^\mathsf{T} + F\Omega F^\mathsf{T} = \Omega$, we obtain:

$$\Omega C \Omega C^\mathsf{T} = \Omega K_l \Omega K_l^\mathsf{T} + \Omega K_m \Omega K_m^\mathsf{T} - \Omega K_l \Omega E^\mathsf{T} K_m^\mathsf{T} - \Omega K_m E \Omega K_l^\mathsf{T} . \tag{2.32}$$

Now, we note that $\Omega K_l \Omega K_l^\mathsf{T} + \Omega K_m \Omega K_m^\mathsf{T} = -G_l G_l^\mathsf{T} - G_m G_m^\mathsf{T} = -\Delta$ where Δ is defined by (2.25) in the previous section. Using the properties of G_m, we observe that $\Omega K_m E \Omega K_l^\mathsf{T} = -G_m E G_l^\mathsf{T} = -J$. We can also manipulate $\Omega K_l \Omega E^\mathsf{T} K_m^\mathsf{T}$ by inserting $\mathbb{1} = \Omega\Omega^\mathsf{T}$:

$$\Omega K_l \Omega E^\mathsf{T} K_m^\mathsf{T} = G_l \Omega E^\mathsf{T} K_m = G_l \Omega E^\mathsf{T} \Omega \Omega^\mathsf{T} K_m^\mathsf{T} = G_l \Omega E^\mathsf{T} \Omega G_m^\mathsf{T} . \tag{2.33}$$

Now we use (2.21) to write E in terms of its 2×2 submatrices:

$$E = \begin{pmatrix} E_{11} & \dots & E_{1p} \\ \vdots & \ddots & \vdots \\ E_{q1} & \dots & E_{qp} \end{pmatrix} \quad \text{where } E_{jk} = \begin{pmatrix} e_{11}^{jk} & e_{12}^{jk} \\ -e_{12}^{jk} & e_{11}^{jk} \end{pmatrix} . \tag{2.34}$$

The submatrices of E clearly satisfy $\Omega E_{jk} \Omega^\mathsf{T} = E_{jk}$, meaning that:

$$\Omega E \Omega^\mathsf{T} = \begin{pmatrix} \Omega E_{11} \Omega^\mathsf{T} & \dots & \Omega E_{1p} \Omega^\mathsf{T} \\ \vdots & \ddots & \vdots \\ \Omega E_{q1} \Omega^\mathsf{T} & \dots & \Omega E_{qp} \Omega^\mathsf{T} \end{pmatrix} = E . \tag{2.35}$$

Using this information, we have that $\Omega E^\mathsf{T} \Omega = -E^\mathsf{T}$, which means that we can write:

$$\Omega K_l \Omega E^\mathsf{T} K_m^\mathsf{T} = G_l \Omega E^\mathsf{T} \Omega G_m^\mathsf{T} = -G_l E^\mathsf{T} G_m^\mathsf{T} = -J^\mathsf{T} . \tag{2.36}$$

Combining this with our previous results means that we can write:

$$\Omega C \Omega C^{\mathsf{T}} = -\Delta + J + J^{\mathsf{T}} = -D_0 \,. \tag{2.37}$$

This means that the drift matrix for any passive coherent feedback protocol can be written as:

$$A = \Omega H_S - \frac{1}{2} D_0 \,. \tag{2.38}$$

2.4 The 3dB Limit

We will now investigate the efficacy of passive coherent feedback for the purposes of stabilising the squeezing of a system quadrature. Recall that squeezing is the process of reducing noise on one quadrature, and causing a corresponding increase in another. In this section, we will derive a bound on the steady-state squeezing achievable for a system mode subject to passive coherent feedback. We will then demonstrate a simple setup which achieves this bound. Finally, we will show that this bound can be beaten by performing homodyne monitoring on the output quadratures.

The noise on each quadrature is given by the diagonal elements of the covariance matrix and is therefore lower-bounded by the smallest eigenvalue of the $\boldsymbol{\sigma}$. We will use this fact to find the optimal passive coherent feedback setup for the production of steady-state squeezing in a single mode system.

Since we are concerned only with properties of the covariance matrix, we will assume that all first moments and linear terms of the Hamiltonian are equal to zero. Apart from this, the system Hamiltonian is taken to be a completely general quadratic Hamiltonian, which takes into account any 'bare' system Hamiltonian, as well as any modifications that come from coherent feedback, which we observed in equation (2.15).

2.4.1 Deriving the bound

First, we will show that, for passive coherent feedback, $\Omega D_0 \Omega^{\mathsf{T}} = D_0$. This result will be useful later. First we notice that, due to the diagonal form of Δ,

we have $\Omega^{\mathsf{T}}\Delta\Omega = \Delta$. Next, using the relationships in (2.29) and inserting the identity $\Omega^{\mathsf{T}}\Omega = \mathbb{1}$, we find that:

$$\Omega J\Omega^{\mathsf{T}} = \Omega G_m E G_l^{\mathsf{T}}\Omega^{\mathsf{T}} = \Omega G_m\Omega^{\mathsf{T}}\Omega E\Omega^{\mathsf{T}}\Omega G_l^{\mathsf{T}}\Omega^{\mathsf{T}} = G_m\Omega E\Omega^{\mathsf{T}}G_l^{\mathsf{T}}\,. \tag{2.39}$$

Next, we plug equation (2.35) into (2.39) which gives us $\Omega J\Omega^{\mathsf{T}} = J$. Combining this with $\Omega\Delta\Omega^{\mathsf{T}} = \Delta$ yields $\Omega D_0\Omega^{\mathsf{T}} = D_0$ which is the desired result. This relation holds for any number of system modes. We will now use this fact to derive a bound on the steady state squeezing for a single mode subject to passive coherent feedback.

The steady state covariance matrix must satisfy the Lyapunov equation

$$A\boldsymbol{\sigma}_\infty + \boldsymbol{\sigma}_\infty A^{\mathsf{T}} + D = 0 \tag{2.40}$$

Let $\boldsymbol{v}$ be the eigenvector corresponding to the largest eigenvalue of $\boldsymbol{\sigma}_\infty$, which we will label σ_1. We have:

$$\sigma_1 = \frac{-\boldsymbol{v}^\dagger D\boldsymbol{v}}{\boldsymbol{v}^\dagger(A + A^{\mathsf{T}})\boldsymbol{v}}\,. \tag{2.41}$$

Plugging in $A = \Omega H - \frac{1}{2}D_0$ and $D = ND_0$ for passive coherent feedback, we obtain:

$$\sigma_1 = \frac{N\boldsymbol{v}^\dagger D_0\boldsymbol{v}}{\boldsymbol{v}^\dagger D_0\boldsymbol{v} - \boldsymbol{v}^\dagger(\Omega H + H\Omega^{\mathsf{T}})\boldsymbol{v}} = \frac{N\delta}{\delta - \alpha}\,, \tag{2.42}$$

where we have labelled $\delta = \boldsymbol{v}^\dagger D_0\boldsymbol{v} > 0$ and $\alpha = \boldsymbol{v}^\dagger(\Omega H + H\Omega^{\mathsf{T}})\boldsymbol{v}$. Now, we define the vector $\boldsymbol{w} = \Omega\boldsymbol{v}$ which is orthogonal to $\boldsymbol{v}$, due to the skew-symmetry of Ω. Since $\boldsymbol{\sigma}_\infty$ is a 2×2 symmetric matrix, $\boldsymbol{w}$ must also be an eigenvector of $\boldsymbol{\sigma}_\infty$ with eigenvalue σ_2. Applying $\boldsymbol{w}$ to both sides of the Lyapunov equation, and noting the result we proved earlier that $D_0 = \Omega D_0\Omega^{\mathsf{T}}$ gives:

$$\sigma_2 = \frac{-\boldsymbol{v}^\dagger\Omega^{\mathsf{T}} D\Omega\boldsymbol{v}}{\boldsymbol{v}^\dagger\Omega^{\mathsf{T}}(A + A^{\mathsf{T}})\Omega\boldsymbol{v}} = \frac{N\boldsymbol{v}^\dagger D_0\boldsymbol{v}}{\boldsymbol{v}^\dagger D_0\boldsymbol{v} + \boldsymbol{v}^\dagger(\Omega H + H\Omega^{\mathsf{T}})\boldsymbol{v}} = \frac{N\delta}{\delta + \alpha} \tag{2.43}$$

Since $\boldsymbol{\sigma}_\infty$ is a positive definite matrix, $\sigma_2 > 0$, meaning that $\alpha > -\delta$. This

yields the following bound on σ_1:

$$\sigma_1 = \frac{N\delta}{\delta - \alpha} > \frac{N}{2} > \frac{1}{2}\,. \tag{2.44}$$

Since the diagonal elements of the covariance matrix are twice the variance of the quadratures, this means that the variance of the most squeezed quadrature cannot be reduced below $\frac{1}{4}$. The bound is known as the 3dB limit (since, in Decibels $10\log_{10}\sigma_1 = 10\log_{10}1/2 \approx 3.01$) and is known to affect phase-insensitive amplifiers [84]. This bound applies to a single mode system subject to any quadratic Hamiltonian and any passive coherent feedback setup. We will now give an example of a simple setup, with passive coherent feedback, originally presented in [38] which reaches this bound.

2.4.2 Simple Coherent Feedback

Consider a single mode system, subject to a squeezing Hamiltonian $\hat{H} = \hat{H}_S + \hat{H}_C$, where $\hat{H}_S = -\frac{\chi}{4}\{\hat{x}, \hat{p}\}$ with $\chi > 0$, corresponding to a Hamiltonian matrix $H_S = -\frac{\chi}{2}\sigma_x$ (where σ_x is the Pauli x-matrix). The mode is coupled to an environment through two input-ouput interfaces and a coupling matrix given by $C = \sqrt{\gamma}(\Omega^{\mathsf{T}}, \Omega^{\mathsf{T}})$. We now apply a simple coherent feedback loop to this setup. The output modes at the first interface are mixed at a beam splitter with thermal white noise modes with the same temperature as the other environmental modes. This corresponds to matrices $E = \eta\mathbb{1}$ and $F = \sqrt{1-\eta}\mathbb{1}$, where $0 < \eta < 1$ is the degree of mixing. The resulting mode is then fed back into the second interface. This results in a modified coupling matrix $C_{cf} = \sqrt{\gamma}((1-\sqrt{\eta})\Omega^{\mathsf{T}}, \sqrt{1-\eta}\Omega^{\mathsf{T}})$. For this setup, the coherent feedback does not induce any modifications to the system Hamiltonian.

The drift matrix for this setup is $A = \frac{\chi}{2}\Omega\sigma_x - \gamma(1-\sqrt{\eta})\mathbb{1}$ and the diffusion matrix is $D = 2N\gamma(1-\sqrt{\eta})\mathbb{1}$, where we have assumed that $\boldsymbol{\sigma}_{in} = N\mathbb{1}$. The steady state covariance matrix of this setup has eigenvalues given by

$$\sigma_{1,2} = \frac{2\gamma(1-\sqrt{\eta})N}{2\gamma(1-\sqrt{\eta}) \pm \chi}\,. \tag{2.45}$$

The smallest eigenvalue, σ_1, is minimised by letting $\sqrt{\eta} \to 1 - \frac{\chi}{2\gamma}$, which results in a squeezing of $\sigma_1 \to \frac{N}{2}$. Since $0 \leq \eta \leq 1$, this optimal setup can be achieved for any system parameters satisfying $0 \leq \frac{\chi}{2\gamma} \leq 1$.As we have seen in the previous section, this is the limit which bounds any passive coherent feedback setup, so we can conclude that this loop is optimal.

2.4.3 Comparison with Homodyne Monitoring

Now, we will compare this optimal passive coherent feedback loop with homodyne monitoring of the output fields. We consider a single mode, system subject to the same Hamiltonian $\hat{H}_S = -\frac{\chi}{4}\{\hat{x}, \hat{p}\}$ with $\chi > 0$ and a single input-output interface with the same system-environment coupling, given by a coupling matrix $C = \sqrt{\gamma}\Omega^{\mathsf{T}}$. If the output modes from this interface are monitored, then the system covariance matrix will evolve according to the Riccati equation (1.50).

Homodyne monitoring of $\hat{x}_{out}$ with efficiency ζ corresponds to $\boldsymbol{\sigma}_m$ given by (see Appendix A.2):

$$\boldsymbol{\sigma}_m = \lim_{z \to 0} \begin{pmatrix} \frac{z+1-\zeta}{\zeta} & 0 \\ 0 & \frac{\frac{1}{z}+1-\zeta}{\zeta} \end{pmatrix} . \tag{2.46}$$

We plug this into equation (1.50), along with $H_S = -\frac{\chi}{2}\sigma_x$, $C = \sqrt{\gamma}\Omega^{\mathsf{T}}$ and $\boldsymbol{\sigma}_{in} = N\mathbb{1}$ and set the steady state condition that $\dot{\boldsymbol{\sigma}} = 0$. This yields quadratic equations for σ_{11} and σ_{22}, the diagonal elements of the steady state $\boldsymbol{\sigma}_\infty$. These are:

$$\frac{\gamma\zeta}{\zeta(N-1)+1}{\sigma_{11}^m}^2 + \left(\gamma + \chi - 2\frac{\gamma\zeta N}{\zeta(N-1)+1}\right)\sigma_{11}^m + \frac{\gamma\zeta N^2}{\zeta(N-1)+1} - \gamma N = 0\,, \tag{2.47}$$

$$(\gamma - \chi)\sigma_{22}^m - \gamma N = 0\,. \tag{2.48}$$

Equation (2.47) has two solutions, but only one corresponds to physical state, as the other is zero or negative, which is forbidden since $\boldsymbol{\sigma}$ must be positive

definite. The solutions are:

$$\sigma_{11}^m = \frac{a + \sqrt{a^2 + b}}{2\zeta}\,, \quad \sigma_{22}^m = \frac{N}{1 - \frac{\chi}{\gamma}}\,. \tag{2.49}$$

for $a = [2N\zeta - (1 + (N-1)\zeta)(1 + \frac{\chi}{\gamma})]$ and $b = 4N\zeta(1-\zeta)$. For this homodyne monitoring scheme to achieve greater steady state squeezing than the optimal passive coherent feedback scheme, we require $\boldsymbol{\sigma}_{11} < N/2$, which can be achieved when the detector efficiency satisfies:

$$\zeta \geq \frac{2\,(\gamma - \chi)}{2\,(\gamma - \chi) + N\,(2\chi - \gamma)}\,. \tag{2.50}$$

However when $\chi < \gamma/2$, the right hand side of this inequality is greater than 1. This means that, when the squeezing strength is weak compared to γ, homodyne monitoring does not outperform coherent feedback

2.5 Conclusions

In this chapter, we have presented a general model which completely characterises Gaussian coherent feedback. We then derived a compact way of describing passive Gaussian coherent feedback. After this, we showed that the squeezing of a single system mode, coupled to any number of passive CF loops through rotating-wave couplings could not go below the 3dB limit. We presented a simple CF protocol which achieves squeezing up to the 3dB limit and then showed that, for certain regimes and efficiencies, homodyne monitoring of the output fields can generate steady-state system squeezing which outperforms the passive CF setups. It is shown in [85] that homodyne monitoring generates greater steady-state squeezing than any other general-dyne detections at zero temperature (when $N = 1$) and is thus optimal. At non-zero temperatures, homodyne monitoring is still beneficial, but full optimisation of the measurement-based control protocol requires access to purifications of the white noise environment, which is unrealistic and we do not consider it here [86]. However, for a weak squeezing Hamiltonian, homodyne monitoring does

not outperform the optimal passive CF protocol.

It is reasonable to ask whether the 3dB bound for passive CF derived here extends to the multimode system case. Optimising the squeezing in a single mode system is relatively straightforward, since it is just given by the smallest eigenvalue of the covariance matrix. This will always correspond to a physical quadrature, since the 2×2 covariance matrix will be diagonalised by an orthogonal matrix, and all 2×2 orthogonal matrices are symplectic. However, this is not the case when the system has more than one mode. The matrix which diagonalises the multimode covariance matrix may not be symplectic and thus the eigenvalues may not correspond to physical quadratures. In Appendix B, we give an example of a two-mode passive CF setup whose eigenvalues can beat the 3dB bound. However, we conjecture that the 3dB bound may still hold on diagonal elements of the covariance matrix, which correspond to physical quadratures.

Another question one may ask is whether or not this represents a fair comparison between MF and CF, since we have restricted CF to only include passive elements. If CF was allowed access to active in-loop elements, it would be able to stabilise squeezing below the 3dB bound. We will investigate such loops in the context of optomechanics in the next chapter. A simple, single-mode example of such a loop is given in Appendix B as well. It can be argued that, since coherent feedback should encompass all coherent operations (including arbitrary amounts of squeezing) it should always outperform MF, and indeed the investigations contained within [87, 15] consider in-loop squeezing and find it beneficial for some tasks. This is a reasonable criticism to make, but we can also make the comparison on practical grounds. Interferometric schemes are fairly straightforward to implement experimentally, as is homodyne monitoring at high efficiencies (over 0.98), while squeezing is more difficult to generate [88]. Furthermore, since squeezing is the resource which we are seeking to optimise, it seems unfair to assume that we already have a separate source which can generate it. Therefore we believe that, at least in

practical terms, it is fair to say that in this context MF can outperform CF.

Chapter 3

Optical Coherent Feedback in Cavity Optomechanics

In this chapter, we will apply our model of Gaussian coherent feedback to an optomechanical setup. We will consider an optical coherent feedback loop where the output of the cavity is processed coherently before being fed back into the cavity. In particular, we will consider three tasks which are of interest in the context of using optomechanical systems for investigations of fundamental physics and implementations of quantum technologies. These are: cooling the mechanical oscillator [89, 90, 91, 92, 93], generating entanglement between optical and mechanical modes [94, 95, 96], and generating optical and mechanical squeezing [97, 98].

Sideband cooling has itself been considered a form of coherent feedback [99], though without considering the addition of CF loops. The optomechanical setup considered here, with explicit loops constructed though input-output interfaces is similar to (though more general than) the setup investigated in [100]. Coherent feedback has also been considered in conjunction with measurement-based feedback for the task of generating mechanical squeezing [101]. However, in contrast to our study, [101] assumes direct manipulation of the mechanical oscillator. Alternative CF approaches not involving optical feedback loops have been considered using optomechanical arrays [102, 103] and to enhance optomechanical nonlinearity [104].

The contents and figures in this chapter are based on work previously published in [2]. All analytic and numerical work presented in this chapter is my own. The investigations within this project were suggested by Alessio Serafini and Matteo Brunelli who also advised regarding parameter regimes and optomechanical Hamiltonians.

3.1 The Setup

We will model the optomechanical system using Gaussian diffusive dynamics. In order to do this, we use the linearised Hamiltonian given by (1.52). The system quadratures are captured in the vector $\hat{\boldsymbol{r}} = (\hat{x}_l, \hat{p}_l, \hat{x}_m, \hat{p}_m)^\mathsf{T}$ where the subscript l indicates the optical quadratures and m indicates the mechanical quadratures. Since we are working in Gaussian regime, the state of the system will be entirely characterised by the first and second statistical moments of the quadratures. The first moments are given by the vector $\bar{\boldsymbol{r}} = (\bar{x}_l, \bar{p}_l, \bar{x}_m, \bar{p}_m)^\mathsf{T}$. The second moments are captured in the 4×4 covariance matrix $\boldsymbol{\sigma}$:

$$\boldsymbol{\sigma} = \begin{pmatrix} \boldsymbol{\sigma}_l & \boldsymbol{\sigma}_{lm} \\ \boldsymbol{\sigma}_{lm}^\mathsf{T} & \boldsymbol{\sigma}_m \end{pmatrix}, \tag{3.1}$$

where $\boldsymbol{\sigma}_l$ and $\boldsymbol{\sigma}_m$ are respectively the 2×2 covariance matrices of the optical and mechanical modes. The correlations between the two modes are captured by $\boldsymbol{\sigma}_{lm}$. Note that, in this chapter $\boldsymbol{\sigma}_m$ is used to denote the mechanical covariance matrix, unlike in the previous chapter, where it denoted the covariance matrix due to monitoring. In our investigations, the properties we are concerned with (cooling, squeezing and entanglement) are soley functions of the covariance matrix $\boldsymbol{\sigma}$. Therefore, from now on, we will disregard the first moments, assuming $\bar{\boldsymbol{r}} = 0$.

The optical and mechanical modes will interact with a white noise environment, through a quadratic Hamiltonian $H_C = \hat{\boldsymbol{r}}^\mathsf{T} C \hat{\boldsymbol{r}}_{in}$, where the white noise environment is characterised by the vector of operators $\hat{\boldsymbol{r}}_{in}(t) = \hat{\boldsymbol{r}}_{in,l1}(t) \oplus \hat{\boldsymbol{r}}_{in,l2}(t) \oplus \hat{\boldsymbol{r}}_{in,m}(t)$ and C is the 4×6 coupling matrix. We assume that the

mechanical mode interacts with one environmental mode $\hat{\boldsymbol{r}}_{in,m}$ and the optical mode interacts with two environmental modes $\hat{\boldsymbol{r}}_{in,l1}$ and $\hat{\boldsymbol{r}}_{in,l2}$, which is required to form a coherent feedback loop. All input fields are assumed to be thermal, meaning that their covariance matrices will be proportional to the identity. The two optical fields will be taken to be at the same temperature, and the mechanical input field will be at a different, much higher temptera-ture. The input covariance therefore takes the form $\boldsymbol{\sigma}_{in} = N_l \mathbb{1}_4 \oplus N_m \mathbb{1}_2$, where N_l is the noise on the optical input modes, and $N_m \gg N_l$ is the noise on the mechanical input mode.

The 'bare' system-environment interactions, before coherent feedback is added, are modelled using a Hamiltonian corresponding to an exchange of excitations between the system and environment. This corresponds to a coupling matrix given by:

$$C = \begin{pmatrix} \sqrt{\kappa}\Omega^{\mathsf{T}} & \sqrt{\kappa}\Omega^{\mathsf{T}} & 0 \\ 0 & 0 & \sqrt{\Gamma_m}\Omega^{\mathsf{T}}, \end{pmatrix} \tag{3.2}$$

where Ω is the 2×2 symplectic form, κ is the optical loss rate and Γ_m is the mechanical loss rate.

Now, we add a coherent feedback loop, by subjecting the outputs from $\hat{\boldsymbol{r}}_{out,l1}$ to a CP-map, before feeding then back into the cavity as $\hat{\boldsymbol{r}}_{in,l2}$. Using the result in equation (2.15), the system-environment effective coupling matrix under coherent feedback becomes:

$$C_{cf} = \begin{pmatrix} \sqrt{\kappa}\Omega^{\mathsf{T}} - \sqrt{\kappa}\Omega^{\mathsf{T}}E & \sqrt{\kappa}\Omega^{\mathsf{T}}F & 0 \\ 0 & 0 & \sqrt{\Gamma_m}\Omega^{\mathsf{T}} \end{pmatrix}, \tag{3.3}$$

where E and F characterised the in-loop CP-map, as described in Section 2.2. Coherent feedback also leads to the modification of the system Hamiltonian, as characterised by equation (2.15). Since the loop only involves the optical modes, only optical terms will be added to the Hamiltonian. Under coherent

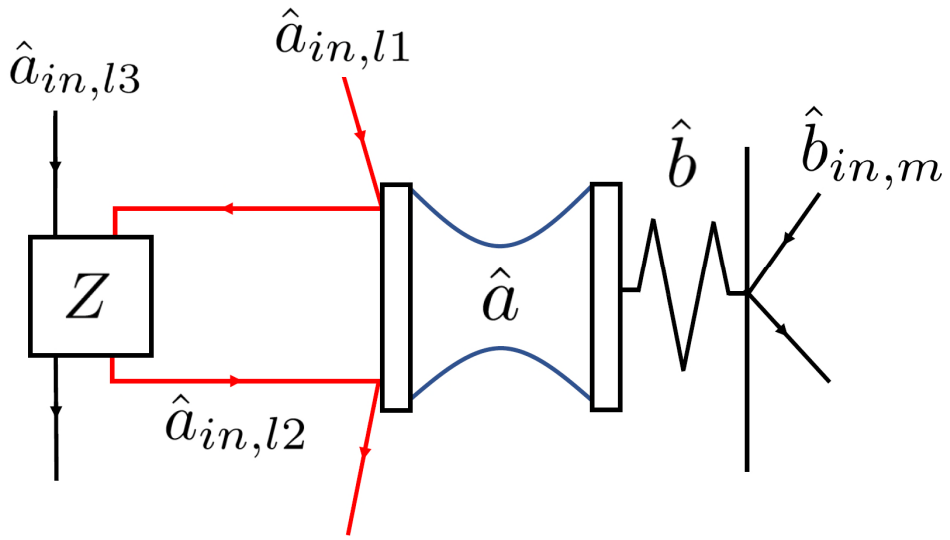

Figure 3.1: A schematic diagram of the coherent feedback setup considered in this section. The optical and mechanical modes are labelled $\hat{a}$ and $\hat{b}$ respectively. Their respective environmental noise modes are labelled $\hat{a}_{in,l1}$ and $\hat{b}_{inm}$ The coherent feedback loop is shown in red. The in-loop operation is labelled Z and the ancilla optical modes are labelled $\hat{a}_{in,l3}$.

feedback, the system Hamiltonian undergoes the transformation:

$$\hat{H}_S \to \hat{H}_S + \frac{1}{2}\hat{\boldsymbol{r}}_l^{\mathsf{T}} H_{cf} \hat{\boldsymbol{r}}_l \,, \tag{3.4}$$

where $H_{cf} = \kappa(\Omega^{\mathsf{T}} E + E^{\mathsf{T}}\Omega)$ and $\hat{\boldsymbol{r}}_l = (\hat{x}_l, \hat{p}_l)^{\mathsf{T}}$. A schematic diagram of the optical coherent feedback loop is shown in Figure 3.1.

3.1.1 A Note on Parameter Values and Experimental Realisation

In this chapter, we will frequently use examples and perform numerical investigations which require giving specific values to the optomechanical parameters. Reasonable ranges for these parameter values were taken from [50, 105]. These works surveyed experimental optomechanical systems that were both historical and state-of-the art. In this sense, the numerical simulations provided here are plausible; where we find CF to be advantageous, it is plausible that it will also

be advantageous in practice. However, the parameters from these sources are from standard cavity optomechanical setups and there have not yet been any experimental realisations of the kind of CF loops investigated in this chapter. As a result, there are certain features that may be important in experimental implementation have not been taken into account here. For example, in some cases we have assumed that the in-loop losses are completely tunable experimentally and that adding a CF loop does not change any other parameters of the system. In practice, there may be some unavoidable losses introduced in the feedback loop and the extra apparatus required to add a CF loop may have other effects on the system which are not taken into account here.

In units where the mechanical frequency is equal to 1, the parameter ranges used are:

$$10^{-2} < \kappa < 10; \qquad 10^{-8} < \Gamma_m < 10^{-3}; \qquad 10^{-3} < G < 1\,.$$

We also take $N_l \approx 1$ and $N_m \approx 100$.

3.2 Three Coherent Feedback loops

Different coherent feedback loops correspond to different choices of in-loop CP-map which result in modifications to the coupling matrix and system Hamiltonian. In turn, these changes result in different drift and diffusion matrices which govern the evolution of the system. We will now characterise three different types of coherent feedback loops by finding their diffusion matrices, the Hamiltonian modifications induced by coherent feedback, and the diffusive parts of their drift matrices. For simplicity, we consider cases which can be implemented with one feedback mode and one ancilla mode, so that E and F are 2×2 real matrices.

3.2.1 Passive Coherent Feedback

First, we will consider passive coherent feedback, as described in Section 2.3. Recall that passive Gaussian in-loop CP-maps do not add energy to the feed-

back mode and, from equations (2.19) and (2.20), are characterised by E and F matrices which must satisfy $EE^{\mathsf{T}} + FF^{\mathsf{T}} = \mathbb{1}$ and $E\Omega E^{\mathsf{T}} + F\Omega F^{\mathsf{T}} = \Omega$. Thus, E and F take the form:

$$E = \begin{pmatrix} a & b \\ -b & a \end{pmatrix}, \quad F = \begin{pmatrix} c & d \\ -d & c \end{pmatrix}, \tag{3.5}$$

where $a^2 + b^2 + c^2 + d^2 = 1$. The effective coupling matrix under passive coherent feedback can be obtained by plugging these expressions for E and F into (3.3). We will call the resulting matrix C_p. This modified coupling matrix can be used to find the drift and diffusion matrices. The diffusion matrix for a passive CF setup is given by:

$$D_p = \Omega C_p \boldsymbol{\sigma}_{in} C_p^{\mathsf{T}} \Omega^{\mathsf{T}} = \begin{pmatrix} \kappa_{\text{eff}} N_l \mathbb{1}_2 & 0 \\ 0 & \Gamma_m N_m \mathbb{1}_2 \end{pmatrix}, \tag{3.6}$$

where $\kappa_{\text{eff}} = 2\kappa(1-a)$. We will denote the drift matrix of the system under passive coherent feedback as $A_p = \Omega H_S + \Omega H_p + \frac{1}{2}\Omega C_p \Omega C_p^{\mathsf{T}}$ where H_S is the system Hamiltonian matrix and H_p is the Hamiltonian matrix corresponding to additional Hamiltonian terms induced by coherent feedback. Keeping the system Hamiltonian general, the drift matrix for passive coherent feedback is characterised by:

$$H_p = \begin{pmatrix} 2\kappa b \mathbb{1}_2 & 0 \\ 0 & 0 \end{pmatrix}, \quad \frac{1}{2}\Omega C_p \Omega C_p^{\mathsf{T}} = \begin{pmatrix} -\frac{\kappa_{\text{eff}}}{2}\mathbb{1}_2 & 0 \\ 0 & -\frac{\Gamma_m}{2}\mathbb{1}_2 \end{pmatrix}. \tag{3.7}$$

From these modifications, we can see that there are two effects of passive CF: a modification of the optical cavity frequency (evidenced in the expression for H_p), and a change in the effective cavity loss rate. Since cavity loss is usually a fixed parameter of an experimental setup, the fact that CF provides a way of tuning it is a promising result. By changing the parameter a (which would correspond to changing a passive element inside the CF loop), we can change the effective cavity loss rate κ_{eff}. A high value of a (close to 1) corresponds to

feeding most of the light output at the first interface back into the cavity, which results in a lower effective loss rate from the cavity. On the other hand, setting a close to -1 corresponds to the input at the second interface constructively interfering with the input at the first interface, increasing the cavity loss rate, up to a maximum of $\kappa_{\text{eff}} = 4\kappa$ (when $a = -1$). We note the magnitude of a is limited by the inherent in-loop losses present in the setup. Setting $a = \pm 1$ requires a perfect channel with no losses which is not experimentally feasible. Nonetheless, imperfect CF can still be implemented within the range allowed and none of our results rely on the case where $a = 1$.

3.2.2 Loops Containing Squeezing and Losses

Now we consider a loop where the feedback mode is subject to losses, followed by squeezing. The E and F matrices for these loops are derived in the Appendix Section A.1.5. They are given by:

$$E_z = \begin{pmatrix} \eta z & 0 \\ 0 & \frac{\eta}{z} \end{pmatrix} \quad \text{and} \quad F_z = \begin{pmatrix} \sqrt{1-\eta^2}z & 0 \\ 0 & \frac{\sqrt{1-\eta^2}}{z} \end{pmatrix}, \tag{3.8}$$

where $z > 0$ is the squeezing parameter (note that $z = 1$ corresponds to no in-loop squeezing). The in-loop losses are parameterised by $0 < \eta < 1$. When $\eta = 0$, the feedback mode is entirely replaced by the noise mode before being squeezed. Values of η close to 1 mean that the in-loop losses are low. Note that, since squeezing adds energy to the loop, $EE^{\mathsf{T}} + FF^{\mathsf{T}} \neq \mathbb{1}$ and the setup is not passive (unless $z = 1$ and there is no in-loop squeezing).

We can obtain the effective coupling matrix C_z for this setup by plugging these matrices into (3.3). The drift matrix for this setup will take the form $A_z = \Omega H_S + \Omega H_z + \frac{1}{2}\Omega C_z \Omega C_z^{\mathsf{T}}$ where H_z captures the system Hamiltonian modifications and $\frac{1}{2}\Omega C_z \Omega C_z^{\mathsf{T}}$ captures the effect of diffusive dynamics. These matrices take the form:

$$H_z = \begin{pmatrix} \sigma_x \kappa \eta (z - \frac{1}{z}) & 0 \\ 0 & 0 \end{pmatrix}, \tag{3.9}$$

$$\frac{1}{2}\Omega C_z \Omega C_z^{\mathsf{T}} = \begin{pmatrix} \frac{1}{2}\kappa(\frac{\eta}{z} + \eta z - 2)\mathbb{1}_2 & 0 \\ 0 & -\frac{\Gamma_m}{2}\mathbb{1}_2 \end{pmatrix}, \tag{3.10}$$

where σ_x is the Pauli x-matrix. The resulting diffusion matrix for this setup is given by $D_z = \Omega C_z \boldsymbol{\sigma}_{in} C_z^{\mathsf{T}} \Omega^{\mathsf{T}}$.

$$D_z = \begin{pmatrix} \kappa N_l(1 - 2\eta z + z^2) & 0 & 0 \\ 0 & \kappa N_l(1 - \frac{2\eta}{z} + \frac{1}{z^2}) & 0 \\ 0 & 0 & \Gamma_m N_m \mathbb{1}_2 \end{pmatrix}. \tag{3.11}$$

Thus, adding this kind of feedback changes the diffusive dynamics of the optical mode, as well as adding a squeezing Hamiltonian $\sigma_x \kappa\eta(z - \frac{1}{z})$ to the optical mode, which squeezes either the $\hat{x}_l$ or $\hat{p}_l$ quadrature, depending on the magnitude of the in-loop squeezing z. The addition of squeezing is worth investigating, as, in several contexts, squeezed light has been shown to improve performance in optomechanical systems [106, 107, 108, 109, 110, 111].

3.2.3 Loops Containing two-mode squeezing

The third type of loop we consider is one where the feedback mode, along with the ancilla, is subject to a two-mode squeezing operation before the ancilla is traced out. This setup without is modelled using E and F matrices given by (see Section A.1.4 for details)

$$E_T = \cosh r \mathbb{1}_2 \quad F_T = \sinh r \sigma_z \,, \tag{3.12}$$

where r is the parameter which determines the strength of the two-mode squeezing operation, and σ_z is the Pauli z-matrix. We obtain the effective coupling matrix for this system, by plugging these matrices into (3.3):

$$C_T = \begin{pmatrix} \sqrt{\kappa}(1 - \cosh r)\Omega^{\mathsf{T}} & \sqrt{\kappa}\sinh r \sigma_x & 0 \\ 0 & 0 & \sqrt{\Gamma_m}\Omega^{\mathsf{T}} \end{pmatrix}. \tag{3.13}$$

This leads to diffusion matrix given by:

$$D_T = \begin{pmatrix} \kappa N_l(2\cosh^2 r - 2\cosh r)\mathbb{1}_2 & 0 \\ 0 & \Gamma_m N_m \mathbb{1}_2 \end{pmatrix} . \tag{3.14}$$

For this setup, CF does not induce modifications to the system Hamiltonian, since $\Omega^\mathsf{T} E_T + E_T^\mathsf{T}\Omega = 0$. This means that we can write the drift matrix as $A_T = \Omega H_S + \frac{1}{2}\Omega C_T \Omega C_T^\mathsf{T}$ with

$$\frac{1}{2}\Omega C_T \Omega C_T^\mathsf{T} = \begin{pmatrix} \kappa(\cosh r - 1)\mathbb{1}_2 & 0 \\ 0 & -\frac{\Gamma_m}{2}\mathbb{1}_2 \end{pmatrix} . \tag{3.15}$$

Note that, since $\cosh r - 1 \geq 0$, this setup will increase the eigenvalues of the drift matrix and destabilise the system. This is often undesirable as we are interested in steady states, which require all eigenvalues of the drift matrix to have negative real parts. To overcome this problem, we can introduce phase shifters into the CF loop and define the new E and F matrices given by $E_S = -E_T$ and $F_S = -F_T$ (see Appendices, Section A.1.4). This new setup leads to drift and diffusion matrices given by:

$$D_S = \begin{pmatrix} \kappa_S N_S \mathbb{1}_2 & 0 \\ 0 & \Gamma_m N_m \mathbb{1}_2 \end{pmatrix} , \quad \frac{1}{2}\Omega C_S \Omega C_S^\mathsf{T} = \begin{pmatrix} -\frac{\kappa_S}{2}\mathbb{1}_2 & 0 \\ 0 & -\frac{\Gamma_m}{2}\mathbb{1}_2 \end{pmatrix} . \tag{3.16}$$

where $\kappa_S = 2\kappa(1 + \cosh r)$ and $N_S = N_l \cosh r$. Thus, these CF loops can be entirely characterised as increasing the effective cavity loss rate, given by κ_S and increasing the noise on the optical mode, as given by N_l.

3.3 Coherent Feedback Enhanced Sideband Cooling

We now look at the efficacy of these feedback loops for enhancing the cooling of the mechanical oscillator. As we have previously stated, sideband cooling is achieved when the cavity is driven with a detuning $\Delta = -\omega_m$.

We will quantify the efficacy of a cooling protocol using the steady-state entropy of the mechanical mode. Using the normal mode decomposition first introduced by Williamson [112] and later re-derived more compactly by Simon et al. [113], we can always write the covariance matrix for a single mode Gaussian state in the form $\boldsymbol{\sigma} = \nu S S^{\mathsf{T}}$ where S is a symplectic matrix which satisfies $S\Omega S^{\mathsf{T}} = \Omega$ and ν is known as the symplectic eigenvalue of $\boldsymbol{\sigma}$ [41, 40]. All entropies of single-mode Gaussian states are increasing functions of ν [38]. Since $\mathrm{Det}S = 1$, we can write $\nu = \sqrt{\mathrm{Det}\boldsymbol{\sigma}}$. Often in our investigations, it will turn out that the steady states involved are thermal states, with $\boldsymbol{\sigma} \propto \mathbb{1}_2$. In this case, the symplectic eigenvalue and the regular eigenvalue of the state coincide. The symplectic eigenvalue can be converted to the average number of mechanical excitations using the formula $\bar{N} = \frac{\nu-1}{2}$ [41].

3.3.1 Passive Coherent Feedback in the Weak coupling Regime

In the weak coupling regime, sideband cooling is characterised by a Hamiltonian given by (1.54). Combining this Hamiltonian with the passive coherent feedback loop described in Section 3.2.1 yields a diffusion matrix given by (3.6) and a drift matrix given by:

$$A = \begin{pmatrix} -\frac{\kappa_{\mathrm{eff}}}{2} & 2\kappa b & 0 & G \\ -2\kappa b & -\frac{\kappa_{\mathrm{eff}}}{2} & -G & 0 \\ 0 & G & -\frac{\Gamma_m}{2} & 0 \\ -G & 0 & 0 & -\frac{\Gamma_m}{2} \end{pmatrix}. \tag{3.17}$$

As detailed in Section 1.2.9, the steady state covariance matrix for the optomechanical system can be found by solving the Lyapunov equation $A\boldsymbol{\sigma} + \boldsymbol{\sigma}A^{\mathsf{T}} + D = 0$, with A given by (3.17) and D given by (3.6). This was done using the LyapunovSolve function in Mathematica 12 [80], which solves the Lyapunov equation symbolically. From the steady-state optomechanical covariance matrix, the mechanical covariance matrix was extracted, by taking

the bottom 2×2 submatrix of the 4×4 optomechanical matrix (see equation (3.1)). This method yields a steady state mechanical covariance matrix of the form $\boldsymbol{\sigma}_m = \sigma_m \mathbb{1}$ where

$$\sigma_m = \frac{\Gamma_m \kappa_{\text{eff}}(16b^2\kappa^2 + (\Gamma_m + \kappa_{\text{eff}})^2)N_m + 4G^2(\Gamma_m + \kappa_{\text{eff}})(\kappa_{\text{eff}} N_l + \Gamma_m N_m)}{4G^2(\Gamma_m + \kappa_{\text{eff}})^2 + \Gamma_m \kappa_{\text{eff}}(16b^2\kappa^2 + (\Gamma_m + \kappa_{\text{eff}})^2)}\,, \tag{3.18}$$

(to reduce the risk of typos in this long equation, it was exported to this document using Mathematica's TeXForm function. The parameters of the coherent feedback loop are b and κ_{eff}. Since we wish to optimise cooling, we analytically minimise this equation using Mathematica's FindMinimum function, yielding the optimal values of $b = 0$ and $\kappa_{\text{eff}} = 2G$. Recall from Section 3.2.1 that $\kappa_{\text{eff}} = 2\kappa(1 - a)$ and the feedback parameter a satisfies $a^2 < 1$, meaning that κ_{eff} can take values in the range $0 < \kappa_{\text{eff}} < 4\kappa$. Therefore, the optimal cooling setup with $\kappa_{\text{eff}} = 2G$ can be achieved for any $G < 2\kappa$ by setting $a = 1 - \frac{G}{\kappa}$. Since we are working in the weak coupling regime, we have already assumed that $G < \kappa$, therefore we can say that the optimal cooling is achievable for all weak couplings $G < \kappa$. If the optimal feedback parameters are used, the steady-state mechanical covariance matrix has the single eigenvalue:

$$\sigma_m^{opt} = \frac{4G^2 N_l + \Gamma_m(4G + \Gamma_m)N_m}{(2G + \Gamma_m)^2}\,. \tag{3.19}$$

At this point we note that, although $\kappa_{\text{eff}} = 2G$ results in the optimal cooling, this optimal value is at a global minimium, meaning that any feedback loop which brings κ_{eff} closer to the optimal value of $2G$ will improve the performance of the cooling. This can be seen by differentiating (3.18) with respect to κ_{eff} in the case where $b = 0$. Figure 3.2a shows a plot of mechanical excitations against κ_{eff} with the minimum at $\kappa_{\text{eff}} = 2G$ (recall that mechanical excitations are obtained from the mechanical eigenvalue through $\bar{N} = (\sigma_m - 1)/2$). It is easy to see in this Figure that any changes to the feedback loop bringing κ_{eff} closer to $2G$ improve the cooling performance.

We also investigate the effect of passive CF on the time taken for the system to relax. This was done by solving the differential equation (1.38) discretely to find the system covariance matrix at each timestep (see Appendix Section C.1 for details). We find that, as well as decreasing steady state temperature, CF also decreases the relaxation time, leading to the steady state being achieved faster. This is demonstrated in Figure 3.2b where the mechanical exitations are plotted against time for systems with different CF setups. It shows that as the effective cavity loss rate is brought closer to the optimal value of $\kappa_{\text{eff}} = 2G$, the rate of relaxation dramatically increases. This numerical investigation of the transient dynamics also provided a way of verifying equation (3.18) for the steady state mechanical excitations under coherent feedback. Figure 3.2c shows the mechanical excitations over time for the same systems considered in 3.2b, but with a dashed line indicating the steady state excitations, as predicted by equation (3.18) which was derived analytically. It is clear from this figure that both the numerical and analytic methods give the same result.

3.3.2 Passive Coherent Feedback in the Strong coupling Regime

Now, we look at cooling with passive feedback in the strong coupling regime. Recall from (1.39) that the drift matrix for any system is the sum of two components: ΩH which characterises the evolution due to the system Hamiltonian, and $\frac{1}{2}\Omega C \Omega C^{\mathsf{T}}$, which characterises the diffusive evolution. The diffusive component of the drift matrix for an optomechanical system subject to passive CF is given by (3.17). The system Hamiltonian matrix H is found by expressing the system Hamiltonian operator, as given by (1.56) in terms of the system quadratures and writing it in the form $\hat{H} = \frac{1}{2}\hat{\boldsymbol{r}}^{\mathsf{T}} H \hat{\boldsymbol{r}}$. This is then used to find ΩH and summed with the diffusive component to give the following drift

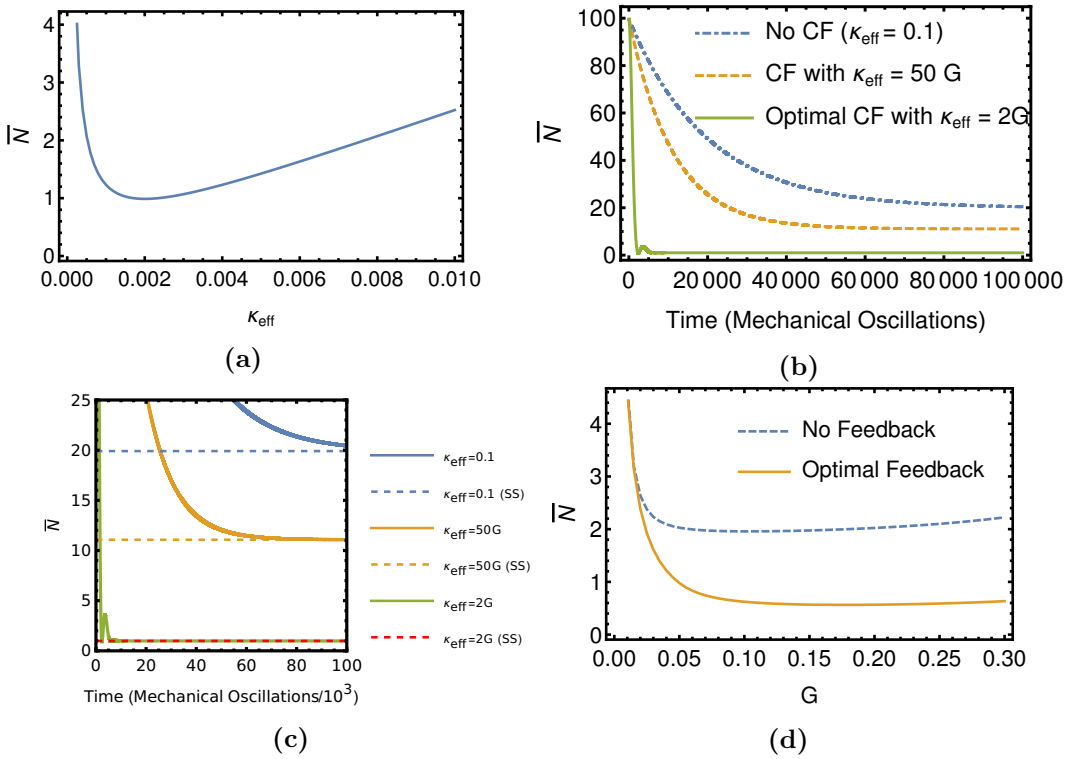

Figure 3.2: (a) Shows the average steady state mechanical excitations against κ_{eff} (in units of mechanical frequency) for a system operating in the weak coupling, red-sideband regime. The parameters used are $\kappa = 0.1$, $\Gamma_m = 10^{-5}$, $G = 10^{-3}$, $N_l = 1$, $N_m = 200$ (where we have set $\omega_m = 1$). The mechanical temperature is minimized at $\kappa_{\text{eff}} = 2G = 2\times10^{-3}$, but any modification which moves κ_{eff} towards this optimal value improves the steady state cooling. (b) Shows average mechanical excitations against time for the setups where $\kappa_{\text{eff}} = 0.1$ (no feedback), $\kappa_{\text{eff}} = 50G = 5\times10^{-2}$ and $\kappa_{\text{eff}} = 2\times10^{-3} = 2G$ with $\Gamma_m = 10^{-5}$, $G = 10^{-3}$, $N_l = 1$, $N_m = 200$. (c) Shows a close-up of Figure 3.2b, with dotted lines (labelled 'SS') showing the steady state mechanical excitations, as predicted by equation (3.18). (d) Shows steady-state mechanical excitations $\overline{N}$ against coupling strength G for a system in the strong coupling red sideband regime with $\kappa = 0.025$, $\Gamma_m = 10^{-3}$, $N_l = 1$, $N_m = 100$. The blue dashed line indicates the steady state cooling when no feedback is used and the orange solid indicates the steady state cooling achievable when passive coherent feedback is numerically optimized for the coupling strength.

matrix:

$$A = \begin{pmatrix} -\frac{\kappa_{\text{eff}}}{2} & -\Delta + 2\kappa b & 0 & 0 \\ \Delta - 2\kappa b & -\frac{\kappa_{\text{eff}}}{2} & -2G & 0 \\ 0 & 0 & -\frac{\Gamma_m}{2} & \omega_m \\ -2G & 0 & -\omega_m & -\frac{\Gamma_m}{2} \end{pmatrix}. \tag{3.20}$$

The diffusion matrix is unnaffected by the Hamiltonian and will take the form given in (3.6). For sideband cooling, we set $\Delta = -\omega_m$. In the strong coupling regime, it is no longer possible to find a simple description of the optimal coherent feedback protocol analytically, and we will investigate numerically, though first, we will make a few observations about this setup.

First, recall that, in order for sideband driving to be effective, the finesse of the cavity must be high enough that the sidebands can be resolved. This means that the cavity loss rate must be much smaller than the mechanical frequency. Since we are manipulating the cavity loss rate through coherent feedback, we will take this to mean that $\kappa_{\text{eff}} < 0.1\omega_m$. By using CF to lower κ_{eff}, coherent feedback can be used to bring a cavity with an otherwise low finesse into the sideband resolved regime. Alternatively, since the matrix (3.20) is not always Hurwitz in the red sideband regime, with large values of G, CF could be used to *increase* κ_{eff} in order to decrease the eigenvalues of A and stabilise otherwise unstable setups.

Numerically optimising the passive CF setup, we find that cooling is improved most when $b = 0$ and κ_{eff} lies in the range $G \lessapprox \kappa_{\text{eff}} \lessapprox 2G$. For couplings $G \gtrapprox 0.05\omega_m$, making κ_{eff} this high brings the system out of the resolved sideband regime, so this protocol cannot be used. Thus, the numerically optimised protocols end up being a compromise between making κ_{eff} high enough to improve performance, but low enough to stay within the resolved sideband regime.

Figure 3.2d shows the minimum steady state mechanical excitations achievable by optimising the passive coherent feedback protocol for a setup in the strong coupling regime, with the extra condition that $\kappa_{\text{eff}} < 0.1$. We

find that in the strong coupling regime, passive feedback can still improve the performance of cooling, though the improvements brought about by CF decrease as G decreases.

3.3.3 Active Coherent Feedback

We now consider the two types of 'active' coherent feedback: coherent feedback with squeezing and losses and coherent feedback with two-mode squeezing as described in Sections 3.2.2 and 3.2.3 respectively. These types of CF are considered to be 'active' (as opposed to passive) since they involve some form of in-loop squeezing. We will investigate whether they can improve the performance of a sideband-cooled optomechanical setup.

First, we note that CF with in-loop two mode squeezing will always be inferior to passive CF, since both allow for the effective cavity loss rate to be altered, but the two-mode squeezing loop does so with the extra cost of increasing the noise on the optical mode. Therefore, we will not consider this type of loop and instead focus on CF loops involving single-mode squeezing and losses.

The evolution of this kind of setup, in the weak coupling regime will be governed by a diffusion matrix given by (3.11). The drift matrix is found by first expressing the system Hamiltonian (1.54) in terms of the system quadratures to obtain the Hamiltonian matrix, then adding the Hamiltonian modifications given by (3.9). This is used to find ΩH which is then added the diffusive component, given by (3.10), to give the full drift matrix:

$$A = \begin{pmatrix} \kappa(\frac{3}{2}\eta z - \frac{1}{2}\frac{\eta}{z} - 1) & 0 & 0 & G \\ 0 & \kappa(\frac{3}{2}\frac{\eta}{z} - \frac{1}{2}\eta z - 1) & -G & 0 \\ 0 & G & -\frac{\Gamma_m}{2} & 0 \\ -G & 0 & 0 & -\frac{\Gamma_m}{2} \end{pmatrix}. \tag{3.21}$$

The steady state optomechanical covariance matrix was again found using Mathematica. It can be found in Appendix C, along with an expression for the resulting sympletic eigenvalue. The entropy of the steady state of such

a setup was numerically minimised with respect to the CF parameters η and z. We find that, for any setup of this kind in the weak coupling regime, the entropy of the steady state is minimised when $z = 1$ and $\eta = 1 - \frac{G}{\kappa}$ which corresponds to the optimal passive setup described in the previous section. In other words, adding squeezing in this way does not lead to better cooling of the mechanical oscillator than the passive CF loop. Thus, the addition of squeezing, which is known to be resource in several other contexts, does not improve the performance of the setup in this context.

3.3.4 Delayed Coherent Feedback

In the previous sections, we have assumed that all feedback occurs instantaneously, meaning that it would lead to Markovian evolution and be treatable with our general model. Here, we look at the effect of introducing delays into the feedback loop. Specifically, we will look at the effect of delays on the performance of our optimal passive coherent feedback loop with sideband cooling in the weak coupling regime. A method for treating CF delays in the Schrödinger picture, by deriving a time-dependent propagator, is presented in [114], but here we will make use of a method in the Heisenberg picture, presented in [32], which involves Fourier transforming the Langevin equation.

We will consider the case where the output of interface 1 is mixed at a beam splitter with an environmental mode $\hat{\boldsymbol{r}}_{in,l3}$ after a delay of τ before being immediately fed back into the cavity through interface 2. This means that we set:

$$\hat{\boldsymbol{r}}_{in,l2}(t) = a\hat{\boldsymbol{r}}_{out,l1}(t-\tau) + c\hat{\boldsymbol{r}}_{in,l3}(t) \tag{3.22}$$

$$= a(\sqrt{\kappa}\hat{\boldsymbol{r}}_{l}(t-\tau) - \hat{\boldsymbol{r}}_{in,l1}(t-\tau)) + c\hat{\boldsymbol{r}}_{in,l3}(t)\,. \tag{3.23}$$

This results in the following delayed (non-Markovian) Langevin equation for

the system variables $\hat{\boldsymbol{r}}$:

$$\begin{aligned}\dot{\hat{\boldsymbol{r}}}(t) =& A\hat{\boldsymbol{r}}(t) + a\kappa \begin{pmatrix} \hat{\boldsymbol{r}}_c(t-\tau) \\ 0 \end{pmatrix} \\ &+ \begin{pmatrix} \sqrt{\kappa}(\hat{\boldsymbol{r}}_{in,l1}(t) - a\hat{\boldsymbol{r}}_{in,l1}(t-\tau) + c\hat{\boldsymbol{r}}_{in,l3}(t)) \\ \sqrt{\Gamma_m}\hat{\boldsymbol{r}}_{in,m}(t) \end{pmatrix},\end{aligned} \tag{3.24}$$

where a and c are the beam splitter paramters, as defined in Section 3.2.1 which satisfy $a^2 + c^2 = 1$ (implicitly assuming that $b = d = 0$) and A is the drift matrix when no CF is present:

$$A = \begin{pmatrix} -\kappa\mathbb{1} & G\mathbb{1} \\ G\mathbb{1} & -\frac{\Gamma_m}{2}\mathbb{1} \end{pmatrix}. \tag{3.25}$$

In order to solve non-Markovian dynamics like these, we will work in the frequency domain. We define the Fourier transform of an operator $\hat{o}$ as

$$\mathcal{F}[\hat{o}(t)] = \hat{o}(\omega) = \frac{1}{\sqrt{2\pi}} \int_{-\infty}^{+\infty} \hat{o}(t) e^{i\omega t} dt\,. \tag{3.26}$$

This allows delays to be treated as complex phases since and $\mathcal{F}[\hat{o}(t-\tau)] = e^{i\omega\tau}\hat{o}(\omega)$. We also note that $\mathcal{F}[\dot{\hat{\boldsymbol{r}}}] = -i\omega\hat{\boldsymbol{r}}(\omega)$. Applying the Fourier transform to both sides of equation (3.24) yields

$$-i\omega\hat{\boldsymbol{r}}(\omega) = \tilde{A}(\omega)\hat{\boldsymbol{r}}(\omega) + B(\omega)\hat{\boldsymbol{r}}_{in}(\omega)\,, \tag{3.27}$$

where:

$$\tilde{A}(\omega) = (A + (\mathbb{1}_2 \oplus 0_2)a\kappa e^{i\omega\tau})\,, \tag{3.28}$$

$$B(\omega) = \begin{pmatrix} \sqrt{\kappa}(1 - ae^{i\omega\tau})\mathbb{1}_2 & \sqrt{\kappa}c\mathbb{1}_2 & 0 \\ 0 & 0 & \sqrt{\Gamma_m}\mathbb{1}_2 \end{pmatrix}, \tag{3.29}$$

$$\hat{\boldsymbol{r}}_{in}(\omega) = \begin{pmatrix} \hat{\boldsymbol{r}}_{in,l1}(\omega) \\ \hat{\boldsymbol{r}}_{in,l3}(\omega) \\ \hat{\boldsymbol{r}}_{in,m}(\omega) \end{pmatrix}. \tag{3.30}$$

Note that, as we have defined it, the Fourier transform of a Hermitian operator is not Hermitian, so in order to investigate physical observables, we must transform back into the time domain. This is done by re-arranging (3.27) to get

$$\hat{\boldsymbol{r}}(\omega) = [-i\omega\mathbb{1} - \tilde{A}(\omega)]^{-1}B\hat{\boldsymbol{r}}_{in}(\omega) = R(\omega)\hat{\boldsymbol{r}}_{in}(\omega)\,. \tag{3.31}$$

The function $R(\omega) = [-i\omega\mathbb{1} - \tilde{A}(\omega)]^{-1}B$ is known as the transfer function of the system and captures the relationship between the system variables and the input modes. In some contexts (eg. [16]) it can be used to derive control-theoretic results. However, here we will just use it for the purpose of finding the time-domain covariance matrix. Applying the Fourier transform to the standard definition of the covariance matrix, given in equation (1.8), we find:

$$\boldsymbol{\sigma}(t) = \frac{1}{2\pi}\int_{-\infty}^{+\infty} d\omega d\omega' \langle\{\hat{\boldsymbol{r}}(\omega), \hat{\boldsymbol{r}}(\omega')^{\mathsf{T}}\}\rangle e^{-i(\omega+\omega')t}\,. \tag{3.32}$$

This equation can be solved by Fourier transforming the input-output relations (1.35) and (1.36) to obtain their frequency-domain forms:

$$[\hat{\boldsymbol{r}}_{in}(\omega), \hat{\boldsymbol{r}}_{in}(\omega')^{\mathsf{T}}] = i\Omega\delta(\omega+\omega')\ , \tag{3.33}$$

$$\langle\{\hat{\boldsymbol{r}}_{in}(\omega), \hat{\boldsymbol{r}}_{in}(\omega')^{\mathsf{T}}\}\rangle = \boldsymbol{\sigma}_{in}\delta(\omega+\omega')\ . \tag{3.34}$$

Plugging these relations into (3.32) leads to an expression with delta functions which can be integrated over, yielding the following expression for the steady-state covariance matrix of the system

$$\boldsymbol{\sigma}(t) = \frac{1}{4\pi}\int_{-\infty}^{+\infty} d\omega \Big[R(\omega)(\boldsymbol{\sigma}_{in} + i\Omega)R(-\omega)^{\mathsf{T}} + R(-\omega)(\boldsymbol{\sigma}_{in} - i\Omega)R(\omega)^{\mathsf{T}}\Big]\,. \tag{3.35}$$

The resulting expression will not depend on t. The reason for this is that the Fourier transform only exists for the time-independent solution to the delayed equation, and will not capture transient dynamics. Though this expression

is not solvable analytically, we can treat it numerically. As an example, we use the setup described previously, where $\kappa = 0.1$, $\Gamma_m = 10^{-5}$, $G = 10^{-3}$, $N_l = 1$, $N_m = 200$ and apply the optimal coherent feedback protocol by setting $a = 1 - \frac{G}{\kappa} = 0.99$. When $\tau = 0$ (no delays) the average steady-state mechanical excitation number is $\bar{N}^0 = 0.988$. Delays of $\tau = 1$, $\tau = 2$, and $\tau = 20$ result in steady state mechanical excitation numbers of 1.036, 1.084 and 1.939 respectively. Thus in-loop delays do reduce the performance of the coherent feedback loops, but only by a small amount when the delays are on the order of the mechanical oscillation time period. We note that, if the limit $\tau \to \infty$, any output modes take an infinite amount of time to pass through the feedback loop and return to the system. In this limiting case, the system behaves in the same manner as if no feedback loop was present, and both interfaces were interacting directly with the white-noise environment.

3.4 Coherent Feedback Enhanced Optomechanical Entanglement

Now, we will investigate the ability of CF to enhance the steady-state entanglement of the optical and mechanical modes, which can be induced by driving the blue sideband with detuning $\Delta = \omega_m$. We will confine our investigation to the weak coupling regime since the blue sideband in the strong coupling regime is almost always unstable.

Even in the weak coupling regime, the blue sideband is often unstable (ie. has negative eigenvalues of the drift matrix) and as a result does not reach a steady state. This suggests two possible applications of CF. The first is enhancing steady state entanglement of stable blue sideband setups and the second is stabilising setups that would otherwise be unstable. Our figure of merit for this section will be the logarithmic negativity, which will be determined using equation (1.22), with system A representing the optical mode and system B representing the mechanical mode.

3.4.1 Passive Coherent Feedback

Passive CF has the ability to tune the effective cavity loss rate κ_{eff} and manipulate the optical cavity frequency. In a preliminary investigation, we found that tuning the optical cavity frequency had no beneficial effect on optomechanical entanglement, so for the remainder of this section, we focus on the effect of tuning of κ_{eff}.

Blue sideband driving in the weak coupling regime with passive coherent feedback is characterised by the drift matrix:

$$A_{blue} = \begin{pmatrix} -\frac{\kappa_{\text{eff}}}{2}\mathbb{1}_2 & -G\sigma_x \\ -G\sigma_x & -\frac{\Gamma_m}{2}\mathbb{1}_2 \end{pmatrix}, \tag{3.36}$$

which comes from combining the diffusive elements found in Section 3.2.1 and writing the blue sideband Hamiltonian (1.55) in terms of a Hamiltonian matrix. The diffusion matrix for this setup will be given by (3.6). Recall that, for the system to be stable, (3.36) must have negative real parts for all eigenvalues. The eigenvalues of (3.36) are given by:

$$\lambda = \frac{1}{4}\big(-\Gamma_m - \kappa_{\text{eff}} \pm \sqrt{16G^2 + \Gamma_m^2 - 2\Gamma_m\kappa_{\text{eff}} + \kappa_{\text{eff}}^2}\big)\,. \tag{3.37}$$

In order for the setup to be stable, the cavity loss rate must satisfy the condition $\kappa_{\text{eff}} > 4G^2/\Gamma_m$. Through the use of CF, we can tune the effective cavity loss rate within the range $0 < \kappa_{\text{eff}} < 4\kappa$. This means that we can use CF to stabilise unstable blue sideband systems by increasing κ_{eff}. However, for systems with $\kappa_{\text{eff}} < G^2/\Gamma_m$, the cavity loss rate is too low for the system to be stabilised using this method.

Now, we look at the ability of CF to increase the entanglement generated by a stable setup. We investigated this problem numerically and found that entanglement was often maximised when κ_{eff} was as small as it could be without violating the stability criterion. This is done by setting $\kappa_{\text{eff}} = 4G^2/\Gamma_m + \epsilon$ where $\epsilon > 0$ is a small real number. As an example, take the system charac-

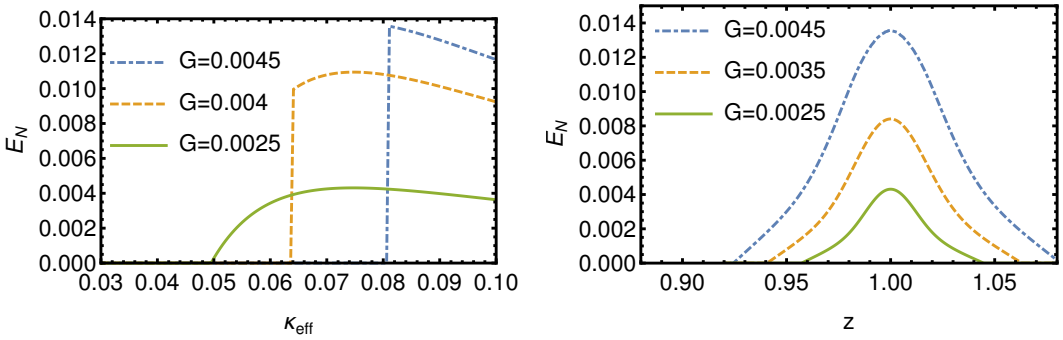

Figure 3.3: (a) Shows the maximum steady state logarithmic negativity achievable for three setups at different values of κ_{eff} in a blue-sideband driven setup in the weak coupling regime. The plot is shown for three different setups, each with $\Gamma_m = 10^{-3}$, $N_l = 1$, $N_m = 100$, but with different values of the coupling G. (b) Shows the maximum achievable steady state logarithmic negativity against in-loop squeezing z for three setups, each with $\kappa = 0.1$, $\Gamma_m = 10^{-3}$, $N_l = 1$, $N_m = 100$ and different values of G.

terised by $G = 4.5 \times 10^{-3}$, $\Gamma_m = 10^{-3}$ and $\kappa = 0.1$. This setup is stable and, at steady state, the system has a logarithmic negativity of $E_N = 0.01166$. Applying the optimal passive CF protcol yields a steady state logarithmic negativity of $E_N = 0.0138$. This increase small in absolute terms, and both logarithmic negativities are too small to be of practical use. However, in relative terms, it does represent a modest increase.

A plot of stable logarithmic negativity against κ_{eff} for three setups (including the one described above) is shown in Figure 3.3a. If the system is not stable for a particular value of κ_{eff}, then E_N is recorded as 0. We find that, for the weaker couplings ($G = 4 \times 10^{-3}$ and $G = 2.5 \times 10^{-3}$), the optimal protocol does not involve setting κ_{eff} to the minimum stable value. Instead, it is optimal for κ_{eff} to be higher than $4G^2/\Gamma_m$. Nonetheless, we find that for all three setups, tuning κ_{eff} can have some small but positive effect on E_N. The sudden vertical jumps in E_N exhibited by the setups with $G = 0.004$ and $G = 0.0045$ occur at the points when κ_{eff} becomes large enough to stabilise the system.

3.4.2 Coherent Feedback with Squeezing and Losses

Now, we investigate the effect of CF with squeezing and losses (as described in Section 3.2.2) on steady-state entanglement. The presence of in-loop squeezing adds energy to the system and increases the eigenvalues, destabilising the system. Thus, such feedback loops will be worse at stabilising unstable setups than passive CF. We will therefore restrict our investigation to look at the enhancement of entanglement, rather than stabilisation.

A blue-sideband driven system subject to such a CF loop is governed by a drift matrix given by:

$$A = \begin{pmatrix} \kappa(\frac{3}{2}\eta z - \frac{1}{2}\frac{\eta}{z} - 1) & 0 & 0 & -G \\ 0 & \kappa(\frac{3}{2}\frac{\eta}{z} - \frac{1}{2}\eta z - 1) & -G & 0 \\ 0 & -G & -\frac{\Gamma_m}{2} & 0 \\ -G & 0 & 0 & -\frac{\Gamma_m}{2} \end{pmatrix}, \tag{3.38}$$

which is obtained by combining the diffusive elements from active CF given (3.10), the Hamiltonian modifications given by (3.9) and the blue sideband Hamiltonian given by (1.55).The diffusion matrix is given by (3.11). We can optimise the steady-state entanglement of this setup numerically with respect to the feedback parameters η and z. We find that the logarithmic negativity of the system peaks when $z = 1$, i.e., when there is no in-loop squeezing. In this case, the feedback loop simply reduces to a passive loop, as considered in the previous section. A plot of optimal steady state logarithmic negativity against in-loop squeezing is shown in Figure 3.3b for three setups. Note that, in each case, E_N peaks when $z = 1$ and there is no in-loop squeezing. Thus, we can conclude that in-loop squeezing for the purpose of entanglement does not add any additional benefits beyond what is achievable through passive CF.

3.5 Coherent Feedback for Optical and Mechanical Squeezing

In this section, we will investigate whether adding squeezing in the CF loop can be used to generate steady state optical and mechanical squeezing. Mechanical squeezing, in particular is of interest for using optomechanical systems for sensing and metrology. Since active CF of the kind described in Section 3.2.2 adds squeezing inside the loop, we will consider this kind of CF, combined with red sideband driving.

First, we note that this kind of setup can stabilise optical squeezing. Figure 3.4a shows the smallest eigenvalue of the steady state of the optical mode against the in-loop losses parameter η. This is considered for two setups, one with squeezing parameter z equal to one (which generates no in-loop squeezing and is therefore passive) and the other with in-loop squeezing characterised by $z = 1.3$. The passive loop, with $z = 1$ generates steady states with optical eigenvalues $\sigma_l \geq 1$, which are thermal, not squeezed. The active loop on the other hand can stabilise squeezing for all values of the beam splitter parameter below $\eta = 0.59$. Above $\eta = 0.59$, the system becomes unstable and no steady state exists. We note that adding in-loop squeezing allows for the optical eigenvalue to squeezed below the 3dB limit. We now ask whether the steady states for these setups also have *mechanical* squeezing. Figure 3.4b shows the smallest steady-state mechanical eigenvalues for both of the feedback loops discussed previously. First, we note that *neither* passive nor active feedback loops generate any steady-state mechanical squeezing, as all mechanical eigenvalues are greater than the vaccuum noise characterised by $\sigma_m = 1$. We find that the presence of in-loop squeezing can reduce the noise on the mechanical quadratures, compared to the case where there is no feedback. Furthermore, the active loop with squeezing can outperform the passive loop for equivalent values of the beam splitter parameter η (note that the beam splitter parameter η is equivalent to the passive CF parameter a). However, since the active setup is unstable for $\eta > 0.59$, the passive loop is superior in this regime. This

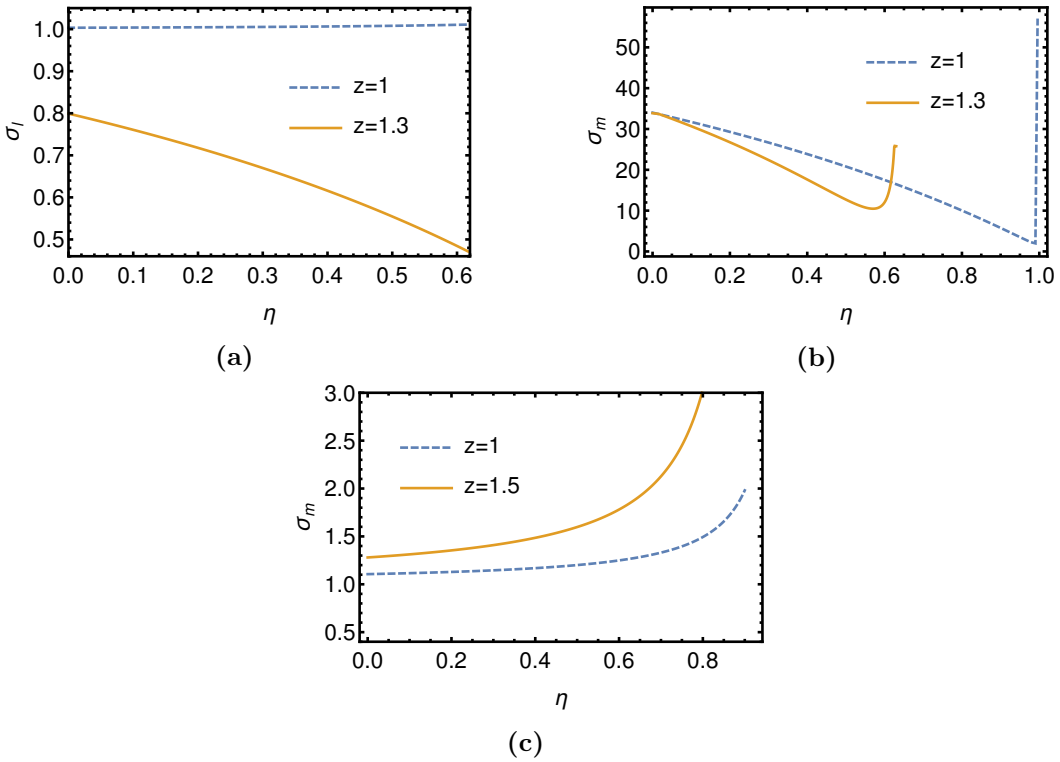

Figure 3.4: (a) Shows the smallest steady state optical eigenvalue against beam splitter parameter η for a passive loop (with $z = 1$) and active feeback loop (with $z = 1.3$). The setup considered is in the weak coupling, red sideband regime an has $\kappa = 0.1$, $G = 10^{-3}$, $\Gamma_m = 10^{-5}$, $N_l = 1$, $N_m = 100$ in units where $\omega_m = 1$. (b) Shows the smallest steady state mechanical eigenvalue against beam splitter parameter η for two different in-loop squeezings. The setup considered is in the red sideband, weak coupling regime and has $\kappa = 0.1$, $G = 10^{-3}$, $\Gamma_m = 10^{-5}$, $N_l = 1$, $N_m = 100$. The values for $z = 1.3$ are only shown in the range $0 < \eta < 0.6388$ where the setup is stable. (c) Shows the smallest steady state mechanical eigenvalue against beam splitter parameter η for a passive loop (with $z = 1$) and an active loop with $z = 1.5$. The setup is in the strong coupling, red sideband regime and has $\kappa = 0.05$, $G = 0.2$, $\Gamma_m = 10^{-4}$, $N_l = 1$, $N_m = 100$. The setup with $z = 1.5$ is stable for $\eta < 0.924$.

regime is important, since it contains the optimal passive loop, achieved by setting $\eta = 1 - \frac{G}{\kappa}$ when $z = 1$. It turns out that this optimal passive loop results in lower steady state noise on a quadrature than any active feedback loop.

In further numerical investigation, we could identify no CF loop that would push the noise of a mechanical quadrature below the vacuum level. Thus, we tentatively conclude that CF is not useful for generating mechanical squeezing.

3.6 Conclusions

We have investigated the effect of optical coherent feedback for the purpose of enhancing several figures of merit in the setting of cavity optomechanics.To do this, we choose three types of optical coherent feedback loops: passive, interferometric coherent feedback, along with feedback involving squeezing and losses and feedback involving two-mode squeezing. The effect of these loops was characterised by drift and diffusion matrices of governing the Gaussian evolution of the system.

We found that the steady-state cooling of the mechanical oscillator in the red sideband regime was greatly enhanced by passive CF in both the weak and strong coupling regimes, both in terms of lowering the number of steady state mechanical excitations and decreasing the time taken for the system to relax to the steady state. We also analytically derived the optimal passive CF protocol in the weak coupling regime. Furthermore, we found that the active CF loops could not outperform the optimal passive loop. Additionally, we quantified the performance of the optimal passive CF protocol in the presence of non-zero in-loop delays and found that the resulting reduction in cooling power was small.

In the blue sideband regime, we found that passive CF is capable of increasing the steady state optomechanical entanglement, and stabilising setups that would otherwise be unstable. We numerically optimised these setups and

found that CF could give modest increases in performance, but the steady-state logarithmic negativity was small in absolute terms. Again, the active feedback loops were found to be unhelpful in this context.

Adding in-loop squeezing was found to generate steady-state squeezing of the *optical* mode, but we could not identify any CF loop which would generate steady-state squeezing of the mechanical mode. This can be contrasted to measurement-based protocols for generating mechanical squeezing such as those found in [115, 116, 117, 105, 118]. With the exception of generating optical squeezing, the addition of active elements into the feedback loop was detrimental to the performance for all the tasks we considered. Since active elements add energy to the system, they also increase the noise and destabilise the setup. This drawback repeatedly outweighed any benefits that might have otherwise been gained from active feedback. This is surprising, since, in other contexts, squeezed light has been found to be beneficial for optomechanical systems [106, 107, 108, 109, 110, 111].

Most of the benefits of CF came from the passive case. In particular, the ability of passive CF to adjust the cavity loss rate proved useful in several contexts. This feature is interesting, since the cavity loss rate, along with the cavity frequency, is normally assumed to be a fixed parameter of the setup, but passive CF allows these features to be modified by changing interferometric elements in the feedback loop.

Chapter 4

A Unified Collision Model of Quantum Feedback

In the previous chapters, we have described coherent feedback in the regime of Gaussian continuous variables. We restricted our investigations to setups where the system was a set of bosonic modes and the environment could be treated using the input-output formalism. In this chapter, we will relax these restrictions to obtain a more general framework for describing coherent feedback, inspired by collision models (CMs). By analogy, we will derive a similar, general model to describe measurement-based feedback and compare for several archetypal tasks. Control tasks can be broadly split into two groups. The first group, known as 'state control' tasks, are concerned with preparing the system into a state with particular properties. The second group are known as 'operator control' tasks, and are concerned with simulating unitary evolution, without advance knowledge of the input state. As an example of state control, we will consider the task of minimising the steady state entropy of a system subject to noise. For operator control, we consider first the task of implementing a bit-flip on an unknown, pure qubit input state. We also investigate whether our setups can achieve 'complete operator controllability' (that is, being able to generate any unitary evolution) in the limit of weak system-controller coupling.

We will do this first in the discrete regime, before taking the continuous-

time limit. The contents of this chapter are based on the work in an unpublished manuscript [3], which is currently in preparation for publication.

4.1 A Discrete Collision Model of Quantum Feedback

Our Gaussian CF model consists of the following three stages. First, the system interacts with the noise environment through a quadratic Hamiltonian. Next, the scattered output modes, and any ancillas are subject to another quadratic Hamiltonian which generates a symplectic transformation (such as squeezing, beam splitting, etc.). Finally, the transformed environmental modes interact once again with the system through another quadratic Hamiltonian. After the second interaction, the scattered modes do not interact again, and a new set of modes are incident at the system interfaces. Note that not all white noise inputs to the system will have outputs which are available for CF, generated by inacessable dynamics (such as the noise on the mechanical mode in the previous section).

This process can be generalised to describe a CF loop for quantum systems and controllers of arbitrary dimension. This general model is described by the following steps:

1. The controller is initialised to the default environmental state η.

2. A CP-map, representing the noise generated by inaccessible dynamics, is applied to the system.

3. The system and controller interact through a fixed unitary U_1

4. A unitary is applied to the controller only. The unitary is chosen from the set $\{V_j\}$ which, in practice, will be determined by experimental specifications.

5. The system and controller then interact again through unitary U_2.

This model, we argue, fits the specification of coherent quantum feedback. In step 3, quantum information is exchanged between system and controller. In step 4, the information extracted from the system is processed coherently. In step 5, the result of this coherent processesing is fed back into the system.

Some treatments, such as [11] and [13], will combine steps 3-5 as one step and characterise any unitary interaction between system and controller as coherent feedback. While this approach is valid, we believe that the extra restrictions we place on the form of the unitary interaction give the model an explicit 'feedback loop' structure, which is lacking in the alternative definition. This structure also fits the way that coherent feedback is implemented in quantum optics: in practice, the interactions between a controller and system and limited by the form of the coupling at the input-output interfaces. This is mimicked in our model by the fixed interaction unitaries U_1 and U_2.

By describing the CF loop in terms of a flow of quantum information, as we have just done, an equivalent model of MF suggests itself. In this model, instead of being processed coherently, the quantum information extracted coherently is measured and then processed, using the in-loop unitaries. Thus, measurement-based feedback can be described by replacing step 3 in the above protocol with the following modified step:

3′ The controller is measured using a non-demolition measurement. In practice, the type of measurement will be determined by experimental specifications. Then, depending on the measurement outcome, a unitary from the set $\{V_j\}$ is applied to the controller.

An important feature of our model of MF is that it involves non-demolition measurements (also known as 'non-destructive measurements'). This means that we assume that the purified, post-measurement state is available for further processing and is not destroyed by the measurement. Non-demolition measurements are assumed in some models of MF (such as [11]), but most of the quantum-optical investigations assume that measurements are destructive, which is the case in practice for most setups involving the monitoring of

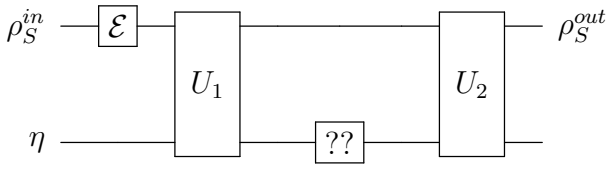

Figure 4.1: A schematic circuit diagram for our model of quantum feedback. Note that the model can apply to any type of system, not just qubits.

output fields [12, 16]. When measurements are destructive, it means that the post-measurement state is not available for further processing–the process of measurement assumed to have 'destroyed' the state. When destructive measurements are involved, MF is implemented by using the measurement signal to inform manipulations on the system, rather than the post-measurement state itself.

A schematic quantum circuit for this model of feedback is shown in Figure 4.1. In this figure, the in-loop process is marked by a box labelled '??'. To model CF, this can be replaced by a unitary, and to model MF, this box can be replaced by a measurement, followed by a unitary.

Note that, we only allow for unitary operations inside the CF loop, and do not allow for more general non-unitary operations, as represented by CP-maps. However, when we restrict to in-loop unitary operations in CF and measurement plus unitary operations in MF, we are not ruling out the possibility of more complex in-loop CP-maps since all CP-maps can represented as unitary operations on a larger Hilbert space [119]. However, a key feature of this model is that the in-loop *unitary* operations available to MF and CF are the same. This allows us to isolate the effect of performing a measurement and determine whether or not that measurement is useful for a particular task.

For most MF setups, the output will depend on the measurement result, which is stochastic. This presents us with two approaches to MF. The first, which we will call 'filtered' or 'conditional' MF, is to keep track of the measurement record [12]. This will result in stochastic dynamics. For a POVM characterised by Kraus operators $\{K_j\}$, a single iteration of the filtered MF

protocol will result in an ouput which depends on the particular measurement outcome, which we will label μ. This output will be given by:

$$\rho_S^{out,\mu} = \frac{1}{N_\mu}\mathrm{Tr}[U_2 V_\mu K_\mu U_1 \mathcal{E}(\rho_S^{in}) \otimes \eta U_1^\dagger K_\mu^\dagger V_\mu^\dagger U_2^\dagger]\,, \tag{4.1}$$

where N_μ is a normalisation factor and V_μ is the feedback unitary applied to the controller as a result of measurement outcome μ. Note that equation (4.1) can be thought of as a discrete version of the stochastic master equation [12], albeit with specific restrictions on the form of the system-environment interaction. Alternatively, we can consider 'unfiltered' MF, which we will also refer to as 'unconditional' or 'averaged' MF. In this approach, we average over the measurement results. The advantage of averaged feedback is that it can be treated as a CP-map, whose outcome is deterministic, since we have averaged over the stochasticity. The output of a single iteration of averaged MF does not depend on the measurement outcome, and is given by:

$$\rho_S^{out} = \sum_i \mathrm{Tr}[U_2 V_i K_i U_1 \mathcal{E}(\rho_S^{in}) \otimes \eta U_1^\dagger K_i^\dagger V_i^\dagger U_2^\dagger]\,. \tag{4.2}$$

4.1.1 The Limit of Weak Measurement

A nice feature of this model is that coherent feedback can be framed as measurement feedback in the limit of weak measurements, and in this sense, the two feedback methods can be viewed as different ends of a spectrum.

To demonstrate this, we use the observation, noted in [13], that the Kraus operators defining a POVM $\{K_j\}$, can be written using the polar decomposition as $K_j = U_j P_j$, where U_j is a unitary matrix, and P_j is a positive semidefinite matrix. Notice that, since $\sum_j K_j^\dagger K_j = \mathbb{1}$, then we must have $\sum_j P_j^\dagger P_j = \mathbb{1}$ as well. This means that we can view P_j a POVM as well. Thus, any POVM can be characterised as a 'bare' measurement, (characterised by $\{P_j\}$) followed by a unitary transformation U_j, which depends on the measurement outcome.

The properties of P_j determine the strength of the measurement. For example, if all P_j are rank-one projectors, then the POVM has equivalent

strength to a projective measurement and has the power to reduce the entropy of a mixed state to a pure state. On the other hand, if P_j are all proportional to the identity, the POVM will have no power of entropy reduction and will reduce to a unitary channel. In-between cases of weak but non-negligible measurement are captured by other types of P_j matrices. In this sense, CF can be viewed as a case of MF for a POVM where all P_j are proportional to the identity. We will explore this idea more concretely in a later section.

4.1.2 A Toy Model

In this chapter, we will investigate several control tasks within this framework, and use them to compare the performance of CF and MF. To do this, we will present a simple toy model within this framework, which includes all important features of the model while still being analytically tractable in most cases.

In this toy model, the system and environment are both taken to be d-dimensional systems. The noise on the system is taken to be the depolarising map, whose action is characterised by:

$$\mathcal{E}(\rho) = \lambda\rho + (1-\lambda)\frac{1}{d}\mathbb{1}\,, \tag{4.3}$$

where $0 < \lambda < 1$ is the parameter which characterises the strength of the noise. Both U_1 and U_2 will be taken to be the partial swap, which takes the form:

$$U_s = \cos\theta\mathbb{1} - i\sin\theta\hat{S}\,, \tag{4.4}$$

where $\hat{S}$ is the full swap unitary and θ is the parameter which determines the strength of the interaction. For compactness, we will often write $c = \cos\theta$ and $s = \sin\theta$. The in-loop unitaries $\{V_j\}$ which are allowed for CF and MF will be any single qudit unitaries. In addition, MF will be allowed rank-one projective measurements to be performed in-loop (though we will explore weaker measurements as a proof of concept in Section 4.3.3).

Finally, we will consider a wide range of initial controller states. We will refer to the case when $\eta = \frac{1}{d}\mathbb{1}$ as the 'high temperature' or 'noisy controller'

case, and the case when η is a pure state will be referred to as the 'low temperature' or 'clean' controller.

4.2 Quantum Feedback for Cooling

In this section, we will compare CF and MF for the task of cooling the system. Our figure of merit will be the steady-state entropy of the system. The steady state is a system state ρ_{ss} which, when put through one iteration of the protocol, is unchanged. The steady state will be reached by repeated application of the protocol to any state.

4.2.1 Coherent Feedback Cooling at High Temperature

In this section, we consider the efficacy of the toy model of CF, presented in the previous section, for the task of minimising the steady state entropy. We will look at the 'high temperature' case, where the controller is initialised in the maximally mixed state $\eta = \frac{1}{d}\mathbb{1}$. It is fairly straightforward to show that the only possible steady state for CF, regardless of the in-loop unitary chosen, is the maximally mixed state. We will do this by showing that a single iteration of the CF protocol cannot reduce the entropy of the system input.

In what follows, the subscript T will be used to denote the system and controller, jointly considered as a whole, and the subscript S will be used to denote the system on its own. We will use η^{in} to denote the initial state of the controller. For a generic system input ρ_S^{in}, the von Neumann entropy of the total input state $\rho_S^{in} \otimes \eta^{in}$ is given by [119]:

$$S_T^{in} = S(\rho_S^{in} \otimes \eta) = S(\rho_S^{in}) + S(\eta^{in})\,. \tag{4.5}$$

After the application of the depolarising map, the system is still in a separable state and the total entropy is:

$$S_T = S(\mathcal{E}(\rho_S^{in})) + S(\eta^{in})\,. \tag{4.6}$$

Now, we note the important fact that, for CF, the rest of the protocol is entirely

described by unitary operations, which leave the total entropy unchanged, meaning that we can write:

$$S_T^{out} = S_T = S(\mathcal{E}(\rho_S^{in})) + S(\eta^{in})\,. \tag{4.7}$$

If we call the system output state ρ_S^{out}, and the controller output state η^{out}, we can use the subadditivy of entropy [119] to obtain the following bound:

$$S(\rho_S^{out}) \geq S_T^{out} - S(\eta^{out}) = S(\mathcal{E}(\rho_S^{in})) - \Delta S(\eta)\,. \tag{4.8}$$

where $\Delta S(\eta) = S(\eta^{out}) - S(\eta^{in})$ is the change in entropy of the controller. However, in the high-temperature case we are considering here, η^{in} is maximally mixed so the maximum value of $\Delta S(\eta^{in})$ is 0. This gives us the bound on the entropy of the output:

$$S(\rho_S^{out}) \geq S(\mathcal{E}(\rho_S^{in})) \geq S(\rho_S^{in})\,. \tag{4.9}$$

The entropy of the system output state can never be lower than the entropy of the input. Furthermore, the input and output entropies are only equal when $S(\mathcal{E}(\rho_S^{in})) = S(\rho_S^{in})$ which is only true when ρ_S^{in} is maximally mixed. This means that the only steady state that can be achieved by coherent feedback is the maximally mixed state.

4.2.2 Conditional Measurement-based Feedback at High Temperature

Here, we will consider a MF protocol in our toy model where the measurement outcome is recorded and the system evolves stochastically. In general, the stochastitcity of such 'filtered' protocols means that they do not have a steady state. Nonetheless, we can investigate their ability to reduce entropy. In what follows, we will denote the action of the initial depolarising map using the notation $\rho_N = \mathcal{E}(\rho_{in}) = \lambda\rho_{in} + \frac{1-\lambda}{d}\mathbb{1}$. After the interaction through the first partial swap, the controller will be measured in the basis $\{|i\rangle\}$ and a unitary

V_i will be applied to the controller, depending on the measurement outcome. At this point in the protocol, after a measurement outcome labelled by j, the system and controller will be in the product state $\rho_j \otimes |\psi_j\rangle\langle\psi_j|$, where $|\psi_j\rangle = V_j |j\rangle$ and the system density matrix ρ_j takes the form:

$$\rho_j = \frac{1}{p_j}\big(\frac{1}{d}c^2\rho_N + s^2\eta(\rho_N)_{jj} - isc[|j\rangle\langle j|, \rho_N]\big), \tag{4.10}$$

where $p_j = \frac{1}{d}c^2 + s^2(\rho_N)_{jj}$ and $(\rho_N)_{jj} = \langle j|\rho_N|j\rangle$. To derive this, we have used the fact that $\mathrm{Tr}_B[\hat{S}, A\otimes B] = [B, A]$. The final system output state is found by applying a partial swap once more to this state, and tracing out the controller. This leads to an output state:

$$\rho_{out,j} = \mathrm{Tr}_C[U_s\rho_j \otimes |\psi_j\rangle\langle\psi_j| U_s^\dagger]. \tag{4.11}$$

We will now derive the conditional MF protocol which minimises the entropy of $\rho_{out,j}$ for an input state which is diagonal in the measurement basis $\{|j\rangle\}$ (as the maximally mixed state would be). First, we note that, if ρ_{in} is diagonal in the measurement basis, then so is ρ_N, and the commutator term in equation (4.10) will be equal to zero. In this case, ρ_j will have the same eigenvectors and eigenvector ordering as ρ_{in} (ie. they both have the same vector corresponding to the largest eigenvalue, the same vector corresponding to the second largest eigenvalue, etc.). Entropy Power Inequalities (EPIs) have been studied specifically for expressions of the form (4.11) [120, 121]. Using a majorisation relation found in [120], we can write the following:

$$\lambda(\rho_{out,j}) \prec c^2\lambda(\rho_j) + (1-c^2)\lambda(|\psi_j\rangle\langle\psi_j|), \tag{4.12}$$

where $\lambda(\rho)$ indicates the ordered spectrum of ρ. The right hand side of this relation is majorised when $|\psi_j\rangle$ points along the direction of the eigenvector of ρ_j which correpsonds to the largest eigenvalue. The largest eigenvector of ρ_j is the same for all j and is equal to the largest eigenvector of ρ_{in}. Thus, to

minimise the output entropy for an input state diagonal in the measurement basis, $|\psi_j\rangle$ must be set to the largest eigenvector of ρ_{in}, regardless of the measurement outcome.

4.2.3 Unconditional Measurement-based Feedback at High Temperatures

Now, we will investigate the performance of unconditional MF, first generally, then specifically for the optimal conditional protocol identified in the previous section. After the first system-environment interaction, the system and controller are prepared in an entangled state given by:

$$\rho_T = c^2\rho_N \otimes \eta + s^2\eta \otimes \rho_N - isc[S, \rho_N \otimes \eta]\,. \tag{4.13}$$

Then, a measurement is performed and the unitary V_j is applied to the controller. This process, performed unconditionally, can be viewed as a CP-map with Kraus operators given by $\{|\psi_j\rangle\langle j|\}$, where $\{|j\rangle\}$ is the measurement basis, and $|\psi_j\rangle = V_j|j\rangle$, as before. This prepares the system and contoller in the separable state:

$$\rho_T = \sum_j p_j\rho_j \otimes |\psi_j\rangle\langle\psi_j|\,, \tag{4.14}$$

where ρ_j and p_j are defined as in equation (4.10). Finally, the system and controller interact again through the partial swap unitary. After the controller is traced out, the system output state is:

$$\rho_{out} = \sum_i p_i\Big(c^2\rho_i + s^2|\psi_i\rangle\langle\psi_i| - isc[|\psi_i\rangle\langle\psi_i|, \rho_i]\Big)\,. \tag{4.15}$$

The optimal conditional protocol from the previous section involves applying an in-loop unitary to set each measurement result to the same state, which here we will call $|0\rangle$. This involves setting $|\psi_j\rangle = |0\rangle$ for all j. Applying this to equation (4.15) and simplifying yields the following output state:

$$\rho_{out} = c^4\rho_N + s^2c^2\eta + s^2|0\rangle\langle 0| - isc^3[|0\rangle\langle 0|, \rho_N]\,. \tag{4.16}$$

This equation shows the relationship between the output and input states for a single iteration of our MF protocol. To find the steady state, we will set $\rho_{in} = \rho_{out} = \rho_{ss}$ and solve the equation for ρ_{ss}. The fact that $\eta = \frac{1}{d}\mathbb{1}$ allows us to write $\rho_N = \lambda\rho_{in} + (1-\lambda)\eta$. Plugging these expressions into (4.16) and solving for ρ_{ss} yields:

$$\rho_{ss} = \frac{1}{1-c^4\lambda}\left((c^4(1-\lambda)+s^2c^2)\eta + s^2\left|0\right\rangle\left\langle 0\right| - \lambda isc^3[\left|0\right\rangle\left\langle 0\right|, \rho_{ss}]\right). \quad (4.17)$$

The only solution to this equation is diagonal in the $|j\rangle$ basis, containing $|0\rangle$. This is evident if we act with $\langle j|$ and $|k\rangle$ from the left and right (for $j \neq k$) and obtain:

$$\langle j|\,\rho_{ss}\,|k\rangle = \frac{1}{1-c^4\lambda}(-\lambda isc^3(\delta_{j0}\,\langle 0|\,\rho_{ss}\,|k\rangle - \langle j|\,\rho_{ss}\,|0\rangle\,\delta_{0k})\,. \quad (4.18)$$

Due to the delta functions, the right hand side of this equation is only nonzero when either j or k is equal to zero. For $j = 0$, $k \neq 0$, we obtain:

$$\langle 0|\,\rho_{ss}\,|k\rangle = \frac{1}{1-c^4\lambda}(-\lambda isc^3(\langle 0|\,\rho_{ss}\,|k\rangle)\,, \quad (4.19)$$

whose only solution is when $\langle 0|\,\rho_{ss}\,|k\rangle = 0$. Thus, we can conclude that ρ_{ss} is diagonal in the basis $\{|j\rangle\}$, and its eigenvalues are obtained by acting on (4.17) from the left and right with $\langle j|$ and $|j\rangle$. The largest eigenvalue of ρ_{ss} is associated with the eigevector $|0\rangle$ and has the value:

$$\alpha_0 = \frac{1}{1-c^4\lambda}\left(\frac{c^4(1-\lambda)+s^2c^2}{d} + s^2\right). \quad (4.20)$$

The remaining $d-1$ eigenvalues are degenerate, each with value:

$$\alpha_j = \frac{1}{1-c^4\lambda}\left(\frac{c^4(1-\lambda)+s^2c^2}{d}\right). \quad (4.21)$$

This means that we can write the steady state for this unconditional MF

protocol as:

$$\rho_{ss} = \frac{1}{d}\frac{d(1-c^2)+c^2-\lambda c^4}{1-\lambda c^4}\left|0\right\rangle\left\langle 0\right| + \sum_{j=1}^{d-1}\frac{1}{d}\frac{c^2-\lambda c^4}{1-\lambda c^4}\left|j\right\rangle\left\langle j\right| . \tag{4.22}$$

The linear entropy for this state is:

$$S_L = 1-\sum_j \alpha_j^2 = (1-\frac{1}{d}) - \frac{\left(c^2-1\right)^2(d-1)}{d\left(c^4\lambda-1\right)^2}. \tag{4.23}$$

Since this steady state always has lower entropy than the maximally mixed state (for non-trivial values of c), we can say that unconditional MF outperforms all CF protocols in this setup for the task of minimising steady state entropy.

4.2.4 Coherent Feedback Cooling at Low Temperature

We will consider a setup identical to CF protocol considered in Section 4.2.1, except that the environment is initialised to a pure state $\left|0\right\rangle\left\langle 0\right|$, instead of a maximally mixed state. We will restrict to the case where $d = 2$ and both system and controller are qubits. For this setup, we will find the lowest entropy steady state achievable through CF which is diagonal in the $\{\left|0\right\rangle, \left|1\right\rangle\}$ basis. This will not amount to a total optimisation over all possible CF protocols, but gives a heuristic reason to believe that the protocol we find is optimal (or close to it). We express the in-loop unitary as using the general decomposition:

$$U = \begin{pmatrix} e^{i\varphi_1}\cos\chi & e^{i\varphi_2}\sin\chi \\ -e^{-i\varphi_2}\sin\chi & e^{-i\varphi_1}\cos\chi \end{pmatrix} . \tag{4.24}$$

The steady state of this setup will be unchanged by a single iteration of the feedback loop. This can be expressed as:

$$\rho_{ss} = \mathrm{Tr}_C\left[U_s(\mathbb{1}\otimes U)U_s\mathcal{E}(\rho_{ss})\otimes\eta U_s^\dagger(\mathbb{1}\otimes U\dagger)U_s^\dagger\right] . \tag{4.25}$$

This was written as a 2×2 matrix equation in Mathematica, expressing all operators in the $\{|0\rangle, |1\rangle\}$ basis. To simplify the search for solutions, we searched for the steady state diagonal in the $\{|0\rangle, |1\rangle\}$ basis. This was done by setting $\rho_{01} = \rho_{10} = 0$. This meant that equation (4.25) could be expressed as simultaneous equations for ρ_{00} and ρ_{11} which were then solved using Mathematica's 'Solve' function, yielding the following solution:

$$\rho_{ss} = \mathrm{diag}(e_1, 1 - e_1) \tag{4.26}$$

with

$$e_1 = \frac{-2c^4(\lambda+1)p^2(q+1) + 2c^2\left(p^2(\lambda(q+2)+q+1) - \lambda\right) + \lambda - 2\lambda p^2 + 1}{\lambda\left(4c^2\left(p^2\left(\left(c^2-1\right)q + c^2 - 2\right) + 1\right) + 4p^2 - 2\right) - 2}, \tag{4.27}$$

where $p = \cos\chi$ and $q = \cos 2\varphi_1$. The entropy of this state was analytically minimised using Mathematica's 'FindMinimum' function. The protocol which minimises the entropy is one in which χ and φ_1 are both integer multiples of π. This is satisfied when the in-loop unitary U is equal to the identity. In this case the steady state has linear entropy:

$$S_L = \frac{1}{2} - \frac{8c^4\left(c^2-1\right)^2}{\left(\left(1-2c^2\right)^2\lambda - 1\right)^2}. \tag{4.28}$$

If this CF protocol (applying the identity in-loop) is applied to a setup with a system and environment of dimension d, and the environment prepared in the pure state $|0\rangle$, the system steady state will have its largest eigenvalue (with eigenvector $|0\rangle$) equal to:

$$\beta_0 = \frac{4\left(c^2-1\right)c^2(d+\lambda-1) + \lambda - 1}{d\left(\left(1-2c^2\right)^2\lambda - 1\right)}. \tag{4.29}$$

The other $(d-1)$ eigenvalues will be degenerate, and take the value:

$$\beta_j = \frac{\left(1-2c^2\right)^2(\lambda-1)}{d\left(\left(1-2c^2\right)^2\lambda - 1\right)}. \tag{4.30}$$

For dimension d, this steady state will have linear entropy:

$$S_L = (1 - \frac{1}{d}) - \frac{16c^4 \left(c^2 - 1\right)^2 (d-1)}{d\left(\left(1-2c^2\right)^2 \lambda - 1\right)^2}\,. \tag{4.31}$$

which is always less than the linear entropy of the maximally mixed state. Note that when $c = \frac{1}{\sqrt{2}}$, $\beta_0 = 1$ and $\beta_{j\neq 0} = 0$ and the steady state is pure. This is because, when $c = s = \frac{1}{\sqrt{2}}$, the partial swap is the square root of the full swap, so applying it twice enacts a full swap, replacing the system mode with the pure environmental mode. This can be seen since:

$$U_s U_s = \frac{1}{\sqrt{2}}(\mathbb{1} - i\hat{S})\frac{1}{\sqrt{2}}(\mathbb{1} - i\hat{S}) = \frac{1}{2}(\mathbb{1} - 2i\hat{S} - \hat{S}^2) = -i\hat{S}\,. \tag{4.32}$$

For certain couplings, the coherent nature of the CF protocol allows low-entropy controller states to be swapped with the system state. As we will see in the next section, this process can be disturbed by the process of measurement.

Before moving on to MF, we will investigate the effect of this CF protocol when the environment is initialised in an state of arbitrary temperature. Restricting to qubits, we will write the environmental state as $\eta = \eta_0 \left|0\right\rangle \left\langle 0\right| + (1-\eta_0)\left|1\right\rangle \left\langle 1\right|$. Applying the CF protocol where the in-loop unitary is the identity, we obtain a steady state which is diagonal in the $\{\left|0\right\rangle, \left|1\right\rangle\}$ basis, with the eigenvector $\left|0\right\rangle$ corresponding to the eigenvalue:

$$\beta_0 = \frac{4\left(c^2-1\right)c^2(2\eta_0 + \lambda - 1) + \lambda - 1}{2\left(1-2c^2\right)^2\lambda - 2}\,. \tag{4.33}$$

This qubit steady state has a linear entropy:

$$S_{CF} = \frac{1}{2} - \frac{8c^4\left(c^2-1\right)^2(1-2\eta_0)^2}{\left(\left(1-2c^2\right)^2\lambda - 1\right)^2}\,. \tag{4.34}$$

4.2.5 Measurement-based Feedback at Intermediate Temperatures

We will now look at the effect of our averaged MF protocol when the environment is of an arbitrary temperature. We will consider a qubit system with a generic environmental input state η which will have an arbitrary temperature and apply the same MF protocol presented in Section 4.2.3, where the controller is measured in the $\{|j\rangle\}$ basis, then all measurement outcomes are mapped to the $|0\rangle$ state. After one iteration of this MF protocol, the output state is:

$$\rho_{out} = c^4\rho_N + s^2c^2\eta + s^2 |0\rangle \langle 0| - isc^3[|0\rangle \langle 0| , \rho_N] . \tag{4.35}$$

Previously, we assumed that η was maximally mixed, but it need not be. We will restrict to qubits and choose $|0\rangle$ to point along the direction of the dominant eigenvector of η, so we can write the controller state of arbitrary temperature as $\eta = \eta_0 |0\rangle \langle 0| + (1-\eta_0) |1\rangle \langle 1|$. Solving for steady state gives:

$$\begin{aligned}\rho_{ss} =& \frac{1}{1-c^4\lambda}(c^4(1-\lambda)\frac{1}{d}\mathbb{1} + (s^2c^2\eta_0 + s^2) |0\rangle \langle 0| + s^2c^2(1-\eta_0) |1\rangle \langle 1| \\ & - i\lambda sc^3[|0\rangle \langle 0| , \rho_{ss}]) .\end{aligned}$$

As before, this state is diagonal in the basis $\{|j\rangle\}$. It has eigenvalues

$$\alpha_0 = \frac{1}{1-c^4\lambda}\left(c^4(1-\lambda)\frac{1}{2} + s^2c^2\eta_0 + s^2\right) , \tag{4.36}$$

$$\alpha_1 = \frac{1}{1-c^4\lambda}\left(c^4(1-\lambda)\frac{1}{2} + s^2c^2(1-\eta_0)\right) , \tag{4.37}$$

corresponding to the eigenvectors $|0\rangle$ and $|1\rangle$ respectively. The linear entropy of this state is:

$$S_{MF} = \frac{1}{2} - \frac{(c^2-1)^2\left(c^2(2\eta_0-1)+1\right)^2}{2\left(c^4\lambda-1\right)^2} . \tag{4.38}$$

A maximally mixed environment corresponds to $\eta_0 = 1/2$, which recovers the expression from earlier. For a pure environment, we set $\eta_0 = 1$ and we obtain the following expression:

$$S_{MF} = \frac{1}{2} - \frac{(c^4 - 1)^2}{2(c^4\lambda - 1)^2}\,. \tag{4.39}$$

We will now prove that, even when $\eta_0 = 1$, and the environment is pure no unconditional MF protocol of any form can prepare a pure system steady state when $c = \frac{1}{\sqrt{2}}$. Recall that, for $c = \frac{1}{\sqrt{2}}$ and a pure environment CF produces a pure steady state, so this is an interesting point of comparison. We will restrict the investigation to qubits. As we have seen before, after projective measurement in the basis $|j\rangle$ and the action of an in-loop unitary, the system and controller are prepared in a joint state:

$$\rho_T = \sum_j p_j \rho_j \otimes |\psi_j\rangle \langle\psi_j| \,, \tag{4.40}$$

where

$$\rho_j = \frac{1}{p_j}\big(\frac{1}{2}c^2\rho_N + s^2\eta(\rho_N)_{jj} - isc[|j\rangle\langle j|\,, \rho_N]\big)\,. \tag{4.41}$$

The first step of this proof is to show that ρ_j cannot be pure. This is done by writing ρ_j in the basis containing $|j\rangle$ and restricting to the case of interest, when $c = s = \frac{1}{\sqrt{2}}$. This gives us:

$$\rho_S^{(1)} = \frac{1}{2}\begin{pmatrix} 1 + \rho_{00} & \rho_{01}(1+i) \\ \rho_{10}(1-i) & 1 - \rho_{00} \end{pmatrix}\,, \tag{4.42}$$

where ρ_{ij} are the matrix elements of ρ_N. This matrix has eigenvalues:

$$\lambda_{+/-} = \frac{1}{2}\big(1 \pm \sqrt{\rho_{00}^2 + 2\rho_{01}\rho_{10}}\big) \geq 0\,. \tag{4.43}$$

If this state is pure, its determinant will be equal to 0, which requires $\sqrt{\rho_{00}^2 + 2\rho_{01}\rho_{10}} = 1$. Since both eigenvalues must be greater than or equal

zero, $\rho_{00}^2 + 2\rho_{01}\rho_{10} \leq 1$. The equality is reached only in the case where $\rho_{00} = 1$, which could only be the case if ρ_N was pure. However, $\rho_N = \mathcal{E}(\rho_{in})$ where $\mathcal{E}$ is the depolarising map. For any non-trival value of the noise parameter λ (ie. any case with $\lambda \neq 1$), the depolarising map monotonically increases the entropy. This means that, regardless of input state, ρ_N will not be pure. This fact, combined with the fact we have just shown that ρ_j cannot be pure unless ρ_N is also pure means that we can conclude that ρ_j are not pure.

After the second system-controller interaction, the controller is traced out and the output state is given by:

$$\rho_{out} = \sum_i p_i \Big(c^2 \rho_i + s^2 \left|\psi_i\right\rangle \left\langle\psi_i\right| - isc[\left|\psi_i\right\rangle \left\langle\psi_i\right|, \rho_i] \Big) = \sum_i p_i \sigma_i \,. \tag{4.44}$$

Applying the same argument that we used to prove that ρ_j could not be pure, we can prove that σ_j cannot be pure. Therefore, since ρ_{out} is a classical mixture of mixed states, it cannot be pure. This means that, in contrast to CF, no unconditional MF protocol can stabilise a pure steady state in the case where $s = c = \frac{1}{\sqrt{2}}$.

4.2.6 Comparison at Intermediate Temperature

We will now compare the CF protocol used in Section 4.2.4 (where the in-loop unitary is the identity) and the MF protocol used in Section 4.2.5 (where measurement is used to prepare the controller in the $|0\rangle$ state) in the case where the environment is at an arbitrary temperature. This will be done by comparing equations (4.38) and (4.34) which give the steady state linear entropies for these protocols when applied to qubits.

In the MF protocol, the in-loop measurement process results in the controller being prepared in the $|0\rangle$ state. It is optimal to use MF to prepare the controller in the state corresponding to the largest eigenvalue of the environmental input. For $\eta_0 < 1/2$, this corresponds to $|0\rangle\langle 0|$ and for $\eta > 1/2$, this corresponds to $|1\rangle\langle 1|$. For our comparison, we assume that the optimal MF protocol is used. The steady state entropy for this protocol, along with

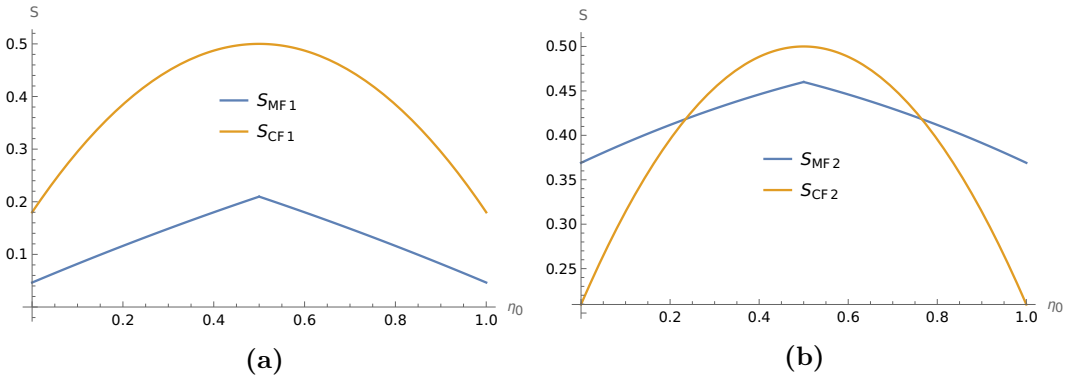

Figure 4.2: (a) Shows the steady-state linear entropy against the largest eigenvalue of the environmental stae for MF and CF setups, as given by equations (4.38) and (4.34) where $c = 0.5$ and $\lambda = 0.25$. (b) Shows the same expressions for setups with stronger noise and weaker coupling, where $c = 0.9$ and $\lambda = 0.5$.

steady state CF entropy given by equation (4.34) is plotted in Fig. 4.2 for different environmental states, as parameterised by η_0 and different setups, parameterised by different values of c and λ.

We find that for the setup with $c = 0.5$, MF outperforms CF for all environmental temperatures. For a weaker system-environment interaction, characterised by $c = 0.9$ and noise parameter $\lambda = 0.5$, we find that MF outperforms CF for high temperature environments with $0.357 < \eta_0 < 0.764$, but CF outperforms MF at low temperatures characterised by $\eta_0 < 0.357$ and $\eta_0 > 0.764$. Broadly, we can make the following observation: for low temperature environments and weak couplings, the act of measurement disturbs the coherent process which allows for low entropy environmental states to be transferred to the system, meaning that MF is inferior to CF. However, with strong couplings and noisy environments, the purification from the act of measurement compensates for this and leads MF to be superior to CF.

4.3 Quantum Feedback For Operator Control

We will now investigate CF and MF within our toy model for the purpose of operator control. Recall that 'operator control' refers to tasks aimed at simulating a particular unitary evolution, without knowledge of the input state.

As as archetypal example, we will consider the task of implementing a bit-flip on a generic qubit input. We will then investigate the efficacy of MF and CF for the task of simulating any unitary dynamics in the limit of infinitesimally weak system-controller coupling. For simplicity, we assume that the system is not subject to any noise is either case and the controller is initialised to a generic input state of the form $\eta = \eta_0 |0\rangle \langle 0| + (1 - \eta_0) |1\rangle \langle 1|$.

4.3.1 Performing a bit-flip using Coherent Feedback

Here, we consider the performance of an intuitive CF protocol for performing a bit-flip on the system input state. In this protocol, after the first system-controller partial swap interaction, the in-loop unitary performed is the Pauli x-matrix σ_x. The system and controller then interact again through a partial swap interaction. For a generic input state of the form:

$$|\psi\rangle = \cos\frac{\chi}{2}|0\rangle + e^{i\phi}\sin\frac{\chi}{2}|1\rangle \ , \tag{4.45}$$

the output density matrix of this protocol is:

$$\rho_{out} = \frac{1}{2}\begin{pmatrix} (c^4 - s^4)\cos(\chi) + 1 & e^{-i\phi}\sin(\chi)\left(c^2 + s^2 e^{2i\phi}\right) \\ e^{-i\phi}\sin(\chi)\left(s^2 + c^2 e^{2i\phi}\right) & (s^4 - c^4)\cos(\chi) + 1 \end{pmatrix} . \tag{4.46}$$

This result was obtained by expressing the problem in terms of 2×2 matrices, and multiplying them in Mathematica. For implementing a bit-flip, the desired output state is:

$$|\psi_X\rangle = \sigma_x |\psi\rangle = \cos\frac{\chi}{2}|1\rangle + e^{i\phi}\sin\frac{\chi}{2}|0\rangle \ . \tag{4.47}$$

The fidelity of the output state to the desired state is given by:

$$F_{CF}(\chi,\phi) = \langle\psi_X|\,\rho_S^{out}\,|\psi_X\rangle = \frac{1}{4}(c^2\left(\cos(2\phi) - 2\cos(2\chi)\cos^2(\phi)\right) - 3c^2 + 4)\,. \tag{4.48}$$

Note that this fidelity depends on the input state, as parameterised by χ and ϕ. Since we wish to evaluate the performance of this protocol on any input, we will average over the Haar-measure for the input states to obtain a figure of merit which is independent of χ or ϕ (see eg. [122] for details of the Haar measure in $SU(2)$ which is used here). This Haar-measure averaged fidelity is given by:

$$A_{CF} = \frac{1}{4\pi}\int_0^{\pi} d\chi \int_0^{2\pi} d\phi F_{CF}(\chi,\phi)\sin(\chi) = 1 - \frac{2}{3}c^2\,. \tag{4.49}$$

We note that the fidelity is an increasing function of the interaction strength. As $c^2 \to 0$, the partial swap becomes a full swap, and the fidelity of the bit-flip becomes perfect. Weaker interactions lead to lower fidelities, to a minimum of 1/3, when $c^2 = 1$. We will now show that no projective MF protocol can outperform this CF protocol.

4.3.2 Performing a bit-flip using Projective Measurement-based Feedback

We will now consider unconditional MF protocols for the same setup as the previous section: both system and controller are qubits, coupled through partial swap gates and the controller is initialised in a generic state $\eta = \eta_0 |0\rangle\langle 0| + (1-\eta_0)|1\rangle\langle 1|$. After the first partial swap, a projective measurement is made on the controller in the $\{|0\rangle, |1\rangle\}$ basis (we will consider more general POVMs in the next section). After the measurement, if the result is $|0\rangle$, the unitary U is applied to the controller, and if the result is $|1\rangle$, the unitary V is applied instead. This process, applied unconditionally, is equivalent to a CP-map acting on the controller with Kraus operators given by $\{U|0\rangle\langle 0|, V|1\rangle\langle 1|\}$. After this CP-map is applied, the system and controller interact again through the partial swap.

We will now find the Haar-measure averaged output fidelity in the same way as in the previous section. The in-loop unitaries U will be taken to be completely general two-qubit unitaries. We will aim to find the optimal values

of U and V. For a general input given by equation (4.45), the fidelity of the output to the desired state is $F_{MF} = \langle\psi_X| \rho^{out}_{S,MF} |\psi_X\rangle$. For the sake of space, this expression is printed in the Appendix Section D.1. This expression was calculated by expressing the problem in terms of 2×2 matrices in Mathematica. The Haar measure average was taken using Mathematica's inbuilt 'Integrate' function. After the Haar measure average is taken, we obtain the following managable expression:

$$\begin{aligned} A_{MF} &= \frac{1}{4\pi}\int F_{MF}(\chi,\phi)\sin(\chi)d\chi d\phi \\ &= \frac{1}{12}(6 - 2c^4 - s^4\cos 2\theta_u - s^4\cos 2\theta_v)\,, \end{aligned} \tag{4.50}$$

where we have used the decomposition of 2×2 unitary matrices to write magnitudes of the matrix elements u_{jk} and v_{jk} as

$$|u_{00}| = \cos\theta_u\,, \quad |u_{10}| = \sin\theta_u\,, \quad |v_{11}| = \cos\theta_v\,, \quad |v_{01}| = \sin\theta_v\,. \tag{4.51}$$

The equation (4.50) can be analytically optimised with respect to the in-loop unitary parameters θ_u and θ_v. The Haar-measure averaged fidelity (4.50) is maximised when $\theta_u = \theta_v = \frac{\pi}{2}$. This means that the optimal projective MF performance is achieved when $U = V = \sigma_x$ (up to a phase which does not affect the output fidelity). Plugging these optimal values into (4.50) and simplifying yields the maximum averaged output fidelity for projective MF:

$$A_{MF} = \frac{1}{3}(1 + s^2) = \frac{2}{3} - \frac{1}{3}c^2\,. \tag{4.52}$$

This fidelity increases as the system-environment interaction increases. However, for all values of c, this fidelity is lower than the fidelity achieved in an equivalent setup using coherent feedback, as given by equation (4.49). Therefore, we can say that CF outperforms all MF protocols involving projective measurements. We will now investigate whether any POVM, not limited to projective measurements, can outperform CF for this task.

4.3.3 Measurement-based Feedback with General POVMs

We will now investigate what happens when we relax the restriction that the in-loop measurement must be projective, and consider more general in-loop POVMs. Recall that in Section 4.1.1, we showed that all POVMs can be represented as a 'bare' measurement, characterised by positive semidefinite Kraus operators P_j, followed by a unitary U_j depending on the measurement outcome. Since, in MF, we already allow for the action of a unitary depending on the measurement result, we can absorb U_j into the feedback unitaries. Additionally, since our final figure of merit is averaged over the Haar measure, it is therefore unitarily invariant and we can assume that P_j are diagonal in the $\{|0\rangle, |1\rangle\}$ basis.

Restricting to projective measurements in the previous section is equivalent to requiring that P_j are rank-one projectors. Relaxing this condition allows us to write the general qubit POVM Kraus operators as:

$$P_0 = a\,|0\rangle\langle 0| + b\,|1\rangle\langle 1| \quad , \quad P_1 = \sqrt{1-a^2}\,|0\rangle\langle 0| + \sqrt{1-b^2}\,|1\rangle\langle 1| \ , \quad (4.53)$$

for $0 \leq a \leq 1$ and $0 \leq b \leq 1$. We can recover the case of projective measurement as a limit, when $a = 1$ and $b = 0$. Also, note that when $a = b$, both elements of the POVM are proportional to the identity. This case corresponds to no measurements being performed, and it is in this limit that MF becomes equivalent to CF. Since we will absorb the action of U_j into U and V, the in-loop process will be captured by a CP-map with elements $\{UP_0, VP_1\}$. The fidelity of the output of this setup to the desired state can be optimised with respect to U and V in a similar way to the previous section. Details of this optimisation, including full expressions for the fidelity can be found in Appendix D.2. The optimisation was performed numerically for different values of c. For every value we investigated, we found that the optimal protocol was achieved when $U = V = \sigma_x$ and $a = b$. Since the case where $a = b$ corresponds to the case of coherent feedback, for the values of c we surveyed, we conclude that CF outperforms all possible MF protocols.

Applying the protocol where $U = V = \sigma_x$ (which is optimal in both CF and projective MF) to MF characterised by a general POVM leads to the following output fidelity:

$$A_{MF} = \frac{1}{3}\left(\sqrt{1-a^2}\sqrt{1-b^2}s^2 + abs^2 + 2 - c^2\right). \tag{4.54}$$

This expression can be analytically optimised with respect to a and b and is maximised when $a = b$. When a=b, P_0 and P_1 are proportional to the identity, so no measurement is performed and the protocol is equivalent to the optimal CF protocol. We note that any changes which bring the value of a closer to b (and accordingly weaken the measurement) will also improve the performance of MF.

To conclude, we conjecture that there is no MF protocol involving non-trivial measurement which can outperform the optimal CF protocol for this task. However, the performance of the MF protocol can be improved by using weaker measurements.

4.3.4 Operator Control in the Limit of Weak Interactions

Now we investigate the more general task of simulating *any* unitary evolution on a generic system input. We consider this task in our toy model setup with arbitrary dimension system and controller and no noise present. We will also take the limit of weak interactions. For the partial swap coupling $U_s^\theta = \cos\theta\mathbb{1} - i\sin\theta\hat{S}$, weak interactions are characterised by taking the infinitesimal limit $\theta \to d\theta$. Expanding U_s and taking this limit yields the expression:

$$\lim_{\theta \longrightarrow d\theta} U_s^\theta = \mathbb{1} - id\theta\hat{S} + o((d\theta)^2). \tag{4.55}$$

Then, for an generic operator U_T, to first order in $d\theta$ we have:

$$U_s U_T U_s = U_T - id\theta\{S, U_T\}. \tag{4.56}$$

The effect of one iteration of the CF protocol on the system input state is

$$\rho_S \to \mathrm{Tr}_C[U_s U_T U_s \rho_S \otimes \eta U_s^\dagger U_T^\dagger U_s^\dagger] \,, \tag{4.57}$$

where $U_T = \mathbb{1} \otimes V_j$ is a unitary which acts only on the controller. Taking the limit $\theta \to d\theta$ and keeping only first-order terms:

$$\rho_S \to \mathrm{Tr}_C\big[U_T \rho_S \otimes \eta U_T^\dagger - id\theta\{S, U_T\}\rho_S \otimes \eta U_T^\dagger + id\theta U_T \rho_S \otimes \eta\{S^\dagger, U_T^\dagger\}\big] \,. \tag{4.58}$$

Using the fact that $\mathrm{Tr}_C\big(SA \otimes B\big) = BA$ and the fact that the partial trace is cyclically invariant over the subspace which is being traced over, we obtain:

$$\mathrm{Tr}_C[\{S, U_T\}\rho_S \otimes \eta U_T^\dagger] = V_j \eta V_j^\dagger \rho_S + \eta \rho_S \,, \tag{4.59}$$

$$\mathrm{Tr}_C[U_T \rho_S \otimes \eta\{S^\dagger, U_T^\dagger\}] = \rho_S V_j \eta V_j^\dagger + \rho_S \eta \,. \tag{4.60}$$

Thus, we can write the transformation of the system state after one iteration of the CF protocol in the weak limit as:

$$\rho_S \to \rho_S + i[\rho_S, V_j \eta V_j^\dagger] d\theta + i[\rho_S, \eta] d\theta \,. \tag{4.61}$$

To represent unconditional MF in the weak limit, we can simply replace V_j with a Kraus operator K_j representing the measurement and in-loop unitary acting on the controller. Due to the linearity of the trace, we can sum over these Kraus operators to represent unconditional measurement and in this way we obtain the expression for a single iteration of unconditional MF in the weak interaction limit:

$$\rho_S \to \rho_S + i[\rho_S, \Phi(\eta)] d\theta + i[\rho_S, \eta] d\theta \,, \tag{4.62}$$

where $\Phi(\eta) = \sum_j K_j \eta K_j^\dagger$.

We can interpret the transformations (4.61) and (4.62) as unitary evolution of the system under simulated Hamiltonians given by $\hat{H}_{CF} = \eta + V_j \eta V_j^\dagger$

and $\hat{H}_{MF} = \eta + \Phi(\eta)$ for a simulated time period $d\theta$.

By iteratively applying CF in the weak limit, this process can be used to generate unitary dynamics on the system:

$$U_{sim} = e^{-i(\eta+V_1\eta V_1)d\theta}e^{-i(\eta+V_2\eta V_2)d\theta}\dots e^{-i(\eta+V_n\eta V_n)d\theta}. \tag{4.63}$$

We wish to find out whether any unitary dynamics can be implemented on the system in this way, by selecting the correct sequence of in-loop unitaries V_j. Whether or not this is possible depends on the set of possible values of $V_j\eta V_j$. The requirement for CF to be able to simulate any unitary dynamics, generated by an arbitrary Hamiltonian, is that the set $\{\eta + V_j\eta V_j^\dagger\}$ must generate the entire space of Hermitian matrices by commutation. This is true for all pairs of Hermitian matrices except a set of measure zero [123], so it is exceedingly likely that any non-trivial set $\{\eta + V_j\eta V_j^\dagger\}$ will be able to simulate any unitary dynamics on the system. An important exception, however, is the case where η is the maximally mixed state. In this case, the set $\{\eta + V_j\eta V_j^\dagger\}$ will only contain one element, and coherent feedback will be unable to simulate any non-trivial unitary dynamics.

The same argument can be used to show that MF can be used to simulate any unitary dynamics, provided that set of possible in-loop CP-maps Φ is non-trivial. If the set of in-loop CP-maps is given by $\{\Phi_j\}$, then the condition for MF to be able to simulate any unitary dynamics would be that the set $\{\eta + \Phi_j(\eta)\}$ can generate the complete set of Hermitian matrices by commutation. This is again true for any non-trivial set $\{\eta + \Phi_j(\eta)\}$. An advantage that MF has over CF in this case is the fact that it can generate non-trivial system dynamics even when the controller state η is maximally mixed, since $\eta + \Phi_j(\eta)$ will not be proportional to the identity for all Φ_j.

4.4 Coherent Feedback in the Continuous Limit

In the previous sections of this chapter, we have considered coherent feedback as a discrete process. Now, we will look at what happens when we consider our general model of CF in continuous limit. This means we will investigate what happens when the interaction time between system and controller becomes instantaneous, as was the case in the optical coherent feedback loops in previous chapters modelled using the input-output formalism. However, the investigation contained here will be more general, as we are not limiting ourselves to Gaussian states.

Our model will be as follows. First, the system in state ρ and controller, in state η, will interact through the unitary U_1, which captures the dynamics arising from the the Hamiltonian H_S, which acts only on the system, and the coupling Hamiltonian V_1. This first interaction lasts for a time period $\Delta t/2$. Then, a unitary U acts on the controller only, representing the coherent in-loop process. We assume that this unitary is instantaneous. Finally, the system and controller interact again through another unitary U_2, which is generated by the coupling Hamiltonian V_2 and the system Hamiltonian H_S and lasts for a time period of $\Delta t/2$. The controller is then traced out, and the entire process takes time Δt. For simplicity, we have not included system noise from inaccessible dynamics separately, but we note that this noise could easily be incorporated into the definition of U_1 if necessary.

To ensure that the interaction unitaries are not trivial in the limit $\Delta t \to 0$, we now make the assumption that V_1 and V_2 are proportional to $1/\sqrt{\Delta t/2}$. This assumption is common in collision models [64] and is implicitly present (and physically justified) in the input-output formalism [71]. This is discussed in the introduction, in Section 1.4.3, in the context of the input-output formalism. Informally, this assumption can be justified by assuming that the interaction Hamiltonians V_1 and V_2 are much stronger than the system Hamiltonian. More thorough and mathematically formal discussion of this issue

can be found in [124]. This assumption means that, when Δt is small, and we expand U_1 and U_2, we can expand to second-order in V_1 and V_2, since $V_1^2(\Delta t)^2$ will be proportional to Δt. However, we will assume that the system Hamiltonian H_S does not grow with Δt. Therefore, we can expand U_1 and U_2 as:

$$U_1 = e^{-i(H_S+V_1)\frac{\Delta t}{2}} \approx \mathbb{1} - i(H_S+V_1)\frac{\Delta t}{2} - \frac{1}{2}V_1^2(\frac{\Delta t}{2})^2\,, \tag{4.64}$$

$$U_2 = e^{-i(V_2+H_S)\frac{\Delta t}{2}} \approx \mathbb{1} - i(V_2+H_S)\frac{\Delta t}{2} - \frac{1}{2}V_2^2(\frac{\Delta t}{2})^2\,. \tag{4.65}$$

Throughout one iteration of the CF protocol, the total unitary which acts on the system and controller is given by $U_A = U_2 U U_1$. Keeping only terms that are first-order in Δt ,we can write this as:

$$\begin{aligned} U_A =& U - iU(H_S+V_1)\frac{\Delta t}{2} - \frac{1}{2}UV_1^2(\frac{\Delta t}{2})^2 - i(V_2+H_S)U\frac{\Delta t}{2} \\ & - V_2UV_1(\frac{\Delta t}{2})^2 - \frac{1}{2}V_2^2U(\frac{\Delta t}{2})^2\,. \end{aligned} \tag{4.66}$$

Recall that U and H_S are independent of Δt and V_1 and V_2 are implicitly proportional to $1/\sqrt{\Delta t/2}$, explaining the presence of the higher-order terms. The change in the system state ρ after one iteration of the CF loop is given by:

$$\Delta\rho = \rho(t+\Delta t) - \rho(t) = \mathrm{Tr}_C[U_A\rho(t)\otimes\eta U_A^\dagger] - \rho(t)\,. \tag{4.67}$$

By plugging in the expansion of U_A from (4.66) into (4.67) and again only keeping the terms first order in Δt, we obtain the following expression which, leads to a master equation in the limit $\Delta t \to 0$:

$$\Delta\rho = -i[H_S+H_S^{(1)}+H_S^{(1)},\rho]\Delta t + \mathcal{D}_1[\rho]\Delta t + \mathcal{D}_2[\rho]\Delta t + \mathcal{C}[\rho]\Delta t + \mathcal{C}[\rho]\Delta t\,, \tag{4.68}$$

where $H_S^{(1)}$ are the Lamb shift Hamiltonians $H_S^{(1)}$ generated by the interaction with the controller. They are given by:

$$H_S^{(1)} = \frac{1}{2}\mathrm{Tr}_C[V_1\eta], \quad H_S^{(2)} = \frac{1}{2}\mathrm{Tr}_C[V_2U\eta U^\dagger]\,. \tag{4.69}$$

$\mathcal{D}_1$ is the normal Lindblad dissipator for a system interacting with an environmental state η through a coupling Hamiltonian V_1. $\mathcal{D}_2$ is the Lindblad dissipator for a system interacting with an environmental state $U\eta U^\dagger$ through a coupling Hamiltonian V_2. These are given by:

$$\mathcal{D}_1[\rho] = \frac{1}{2}\mathrm{Tr}_C[V_1\rho\otimes\eta V_1 - \frac{1}{2}\{V_1^2, \rho\otimes\eta\}]\frac{\Delta t}{2}\,, \tag{4.70}$$

$$\mathcal{D}_2[\rho] = \frac{1}{2}\mathrm{Tr}_C[V_2\rho\otimes U\eta U^\dagger V_2 - \frac{1}{2}\{V_2^2, \rho\otimes U\eta U^\dagger\}]\frac{\Delta t}{2}\,. \tag{4.71}$$

Recall that we are assuming that V_1 and V_2 are proportional to $1/\sqrt{\Delta t}$, which is why we are able to bring the extra Δt term as part of the definitions of $\mathcal{D}_{1,2}$ without the terms vanishing. The rest of the interaction terms are captured by the superoperator $\mathcal{C}$:

$$\mathcal{C}[\rho] = \frac{1}{2}\mathrm{Tr}_C[V_2U\rho\otimes\eta V_1U^\dagger + UV_1\rho\otimes\eta U^\dagger V_2 - U\rho\otimes\eta V_1U^\dagger V_2 - V_2UV_1\rho\otimes\eta U^\dagger]\frac{\Delta t}{2}\,.$$

Equation (4.68) is a master equation which characterises the evolution of a system subject to coherent feedback in the collisional framework. This equation is similar to those which describe 'cascaded collision models' which describe systems which undergo multiple collisions with an environment, though here we explicitly include an instantaneous 'in-loop' operation which occurs between the two interactions [69]. Since the input-output formalism can be framed as a collision model [71], we expect this master equation to completely subsume the dynamics of the Gaussian CF loops presented in chapters 2 and 3, and also allow for modelling of more complex, non-Gaussian CF loops constructed through the input-output formalism.

4.5 Measurement-based Feedback in the Continuous Limit

A master equation for collisional measurement-based feedback can be derived in the same way as the coherent feedback master equation (4.68) with a few

adjustments. First, we replace the instantaneous in-loop unitary with a Kraus operator, representing the action of the in-loop projective measurement, followed by the action of a unitary acting only on the controller. Again, we will assume that this in-loop process is instantaneous. We will denote these Kraus operators using L_j. Secondly, we will represent the stochasticity of the conditional measurement act using Poisson processes dN_j for each measurement outcome. This approach, using stochastic processes and discontinuous evolution of the system is similar to the 'quantum jumps' formalisms used elsewhere [125, 126, 127]. For each iteration, dN_j takes the value 1 for value of j corresponding to the measurement outcome, and 0 for the outcomes that are not realised. They therefore have the following properties [125]:

$$[dN_i(t)]^2 = dN_i(t), \quad dN_i(t)dN_j(t) = \delta_{ij}dN_j(t)\,. \tag{4.72}$$

The expectation value for each process depends on the likelihood of the outcome. Since the measurement process takes place after the system state ρ and controller state η have interacted through U_1, the expectation value of the measurement outcome corresponding to POVM operator L_j will be:

$$\langle dN_i(t)\rangle = \mathrm{Tr}[L_j U_1 \rho \otimes \eta U_1^\dagger L_j] = p_j\,. \tag{4.73}$$

By repeating the process used to obtain the CF master equation, and keeping only terms which are overall first-order in Δt, we obtain the following evolution

equation for a system subject to MF in the continuous limit:

$$\begin{aligned}\rho(t+\Delta t) = \sum_j \frac{1}{p_j} dN_j \Bigg[& q_j \big[\rho(t) - i[H_S,\rho]\Delta t)\big] + i\frac{\Delta t}{2}\mathrm{Tr}_C\big(L_j[\sigma,V_1]L_j^\dagger\big) \\ & + i\frac{\Delta t}{2}\mathrm{Tr}_C\big([L_j\sigma L_j^\dagger, V_2]\big) - \frac{1}{2}\mathrm{Tr}_C\big(L_j\{\sigma,V_1^2\}L_j^\dagger\big)(\frac{\Delta t}{2})^2 \\ & - \frac{1}{2}\mathrm{Tr}_C\big(\{L_j\sigma L_j^\dagger, V_2^2\}\big)(\frac{\Delta t}{2})^2 + \mathrm{Tr}_C\big(L_jV_1\sigma V_1 L_j^\dagger\big)(\frac{\Delta t}{2})^2 \\ & + \mathrm{Tr}_C\big(V_2L_j\sigma L_j^\dagger V_2\big)(\frac{\Delta t}{2})^2 + \mathrm{Tr}_C\big(L_jV_1\sigma L_j^\dagger V_2 + V_2L_j\sigma V_1L_j^\dagger \\ & - L_j\sigma V_1L_j^\dagger V_2 - V_2L_jV_1\sigma L_j^\dagger\big)(\frac{\Delta t}{2})^2\Bigg],\end{aligned} \tag{4.74}$$

where $q_j = \mathrm{Tr}[L_j\eta L_j^\dagger]$ and p_j is given by equation (4.73). The unconditional (and therefore deterministic) evolution is obtained from this equation by replacing the Poisson processes by their classical expectation values p_j, since this corresponds to averaging over all trajectories. We have not been able to identify an experimental implementation which allows for non-demolition measurements to be performed on a controller and fed back into the system in the continuous limit, so there may be no practical applications of this MF master equation. Nonetheless, we present it here for completeness.

4.6 Conclusion

In this section, we present a unified model of coherent and measurement-based feedback which allows the two to be compared on an equal footing. A key feature of this model is that, in MF, it allows for non-demolition measurements to be performed on the controller and fed back into the system. Both CF and MF in this model have access to the same ancilla states, in-loop unitaries, and system-controller interactions. The only difference between the two is that, in MF, a measurement is performed in-loop. This allows us to frame the question of comparing MF and CF as asking in what circumstances does performing a measurement act as a resource for a particular task, and in what circumstances is it a hindrance. We then investigated several control tasks using a toy model in our framework and compared the performance of MF and CF.

Investigating the task of generating low steady-state entropy states, we found that MF outperformed CF when the controller was noisy. When the controller was 'clean' (ie. free from noise, or low temperature), the comparison became more subtle. While MF still outperformed CF in many cases, there were some circumstances in which CF was better. This was due to the fact that performing measurements on the controller disrupted the coherent process of swapping the low entropy controller state with the system state (akin to the case investigated in [13]).

When we investigated operator control for the task of implementing a bit-flip, we showed that CF was superior to all possible MF protocols, due to the fact that measurement destroys information about the unknown input state. Performing weaker measurements in the loop leads to the performance of the MF protocol improving, but not to the point where it outperforms CF.

We then investigated a more general form of operator control, in the limit of weak interactions. We found that MF and CF had similar capabilities in most cases, though MF again had an advantage when the controller was noisy.

Finally, using the convention of continuous collision models, we derived master equations for both MF and CF in the continuous limit. We expect our CF master equation to be applicable to quantum optical setups with CF loops implemented through input-output interfaces, though we are unsure if any any setups exist to implement our MF protocols in the continuous limit. This is because they require non-demolition measurements to be performed at high speed and then fed back into the system with negligible delay, which is often not plausible. As a result, most continuous MF protocols assume destructive measurements, and involve the measurement signal being used to change the system Hamiltonian, rather than allowing a direct interaction between the system and the post-measurement state [12].

Chapter 5

Conclusions

First, we provide a summary of each chapter of the thesis (except the introduction and conclusion). Then, we suggest avenues for future work.

5.1 Summary of the Thesis

In Chapter 2, we introduced a general model of Gaussian coherent feedback through input-output interfaces. We derived a compact way of describing passive CF loops. Then, we showed that, for control of a single mode, passive CF can improve the steady state squeezing of a system quadrature for certain parameters, but cannot stabilise squeezing of any quadrature to below the 3dB bound. Then, we gave a simple example of such a CF loop, and showed that, under certain conditions, the 3dB bound could be beaten by homodyne monitoring of the output fields.

In Chapter 3, we applied our general model of Gaussian CF to a linearised optomechanical setup. We characterised the effect of three kinds of CF loops and investigated their ability to enhance the performance of the setup for cooling the mechanical oscillator, generating entanglement between the mechanical and optical modes, and generating optical and mechanical squeezing. Optimal CF setups for these tasks were found through analytical and numerical optimisation. We found that most of the benefits from CF came from the use of passive CF to tune the effective cavity loss rate. This allowed for the cooling of the mechanical oscillator to be greatly enhanced and the optomechanical en-

tanglement to be enhanced to a small degree. The presence of in-loop delays was also investigated and found to be slightly detrimental to the performance of the setup. Interestingly, active in-loop elements, such as squeezing were not found to be beneficial, except for the task of stabilising optical squeezing.

In Chapter 4, we introduced a general model of CF and MF, inspired by collision models and created a discrete toy model which we use to compare MF and CF for different tasks. We investigated the performance of MF and CF for the task of lowering the steady state entropy of a qudit and found that, in most cases, MF outperformed CF. In particular, MF proved to be more powerful when the controller was 'noisy' as measurements allowed for the controller to be purified, but in some circumstances, CF outperformed MF when the controller was 'clean'. This was due to the fact that the act of measurement disturbed the coherent process which transferred low entropy states from the controller to the system. For the task of implementing a bit-flip on a system qubit, CF proved to be superior, as measurements destroyed information about the unknown input state. In the limit of weak interactions, we found that in most cases, both MF and CF could be used to simulate any unitary dynamics on the system, but MF was able to do so even when the controller was maximally mixed, which CF could not. Finally, we took the continuous time limit of CF and MF to derive master equations for both.

5.2 Future Work

One extension to the work presented in Chapter 2 is to provide more comparisons between monitoring and CF for more complex, multimode setups, or different figures of merit, such as entanglement. Also, our general Gaussian model assumed that CF was instantaneous. Though we used a method for dealing with delays in a specific case in Chapter 3, we have not adapted our general model to take into account delays, so this would also be a logical extension of the work.

Building on Chapter 3, future work may include more investigation into

the transient dynamics of optomechanical systems, subject to CF, as we have mostly focused on steady state properties. In particular, we could consider dynamical modulation of κ_{eff}, which has already been found to be beneficial for mechanical cooling [128]. Dynamical modulation of the cavity loss rate can be achieved through tuning the free carrier plasma density [129, 130, 131] and using light absorbers or scatterers in deformable optical cavities [132], though we speculate that the implementation of the method presented here (using interferometric optical elements) may prove easier to implement. Also, all of our work took place in the linear, Gaussian regime, so an obvious extension would be to consider non-linear optomechanical systems, which would allow us to consider different CF loops, less approximated optomechanical dynamics, and a wider range of physical phenomena.

An obvious extension to Chapter 4 is to find concrete experimental setups and apply our model of feedback to find optimal control protocols for useful tasks. Of particular interest are experimental setups where collision models have already shown application. Collisional models of so-called 'giant atoms' [73, 74, 75, 76, 77] in circuit QED setups seem particularly promising as an experimental implementation of our model, as they allow for the 'atom' to be coupled to the same field at two different points. This suggests an analogy with coherent feedback, which requires a system to be coupled to a controller twice to form a feedback loop. Collision models have also been implemented in linear optics [78, 79]. The implementatation in [78] is particularly relevant, as it demonstrates the realisation of a partial swap interaction, which featured prominently in Chapter 4, using single-photon systems. Another extension would be further investigation of the relative benefits of CF and MF in more complex cases and a more thorough comparison of our model of MF with other previously established models.

Appendix A

Gaussian Operations

A.1 Symplectic Transformations in Quantum Optics

Here, we present several symplectic transformations, which correspond to physical transformations often found in quantum optics. Recall that a transformation characterised by a symplectic matrix S will transform the system modes and covariance matrix in the following way:

$$\hat{\boldsymbol{r}} \to S\hat{\boldsymbol{r}} \quad \boldsymbol{\sigma} \to S\boldsymbol{\sigma}S^{\mathsf{T}} \,. \tag{A.1}$$

A.1.1 Phase Shifter

Phase shifters are an example of a single-mode passive transformation. They correspond to local rotations in phase space, by an angle ϕ characterised by a matrix [38, 41]:

$$S_\phi = \begin{pmatrix} \cos\phi & \sin\phi \\ -\sin\phi & \cos\phi \end{pmatrix} \,. \tag{A.2}$$

A.1.2 Beam Splitter

Beam splitters are passive transformations which mix two modes together, characterised by an angle θ. When $\theta = 0$, the modes are not mixed at all, and when $\theta = \frac{\pi}{2}$, the modes are completely swapped (and a local phase shift is added to one mode). Physically, beam splitters to semi-reflective mirrors,

which mix two travelling modes. They are characterised by the symplectic matrix [41]:

$$S_\theta = \begin{pmatrix} \cos\theta & 0 & \sin\theta & 0 \\ 0 & \cos\theta & 0 & \sin\theta \\ -\sin\theta & 0 & \cos\theta & 0 \\ 0 & -\sin\theta & 0 & \cos\theta \end{pmatrix} . \tag{A.3}$$

A.1.3 Single-mode Squeezing

Squeezing is an active transformation on a single mode which reduces the variance of one quadrature, while increasing the variance of the other. It is characterised by a parameter $z > 0$, which specifies which quadrature is being squeezed and the degree of squeezing. The symplectic matrix for squeezing is [41]:

$$S_z = \begin{pmatrix} z & 0 \\ 0 & \frac{1}{z} \end{pmatrix} . \tag{A.4}$$

A.1.4 Two-mode Squeezing

Two-mode squeezing is an active transformation which entangles two modes and can be generated experimentally using optical parametric amplifiers [133]. The symplectic matrix for two-mode squeezing is characterised by a parameter r and reads [41]:

$$S_r = \begin{pmatrix} \cosh r & 0 & \sinh r & 0 \\ 0 & \cosh r & 0 & -\sinh r \\ \sinh r & 0 & \cosh r & 0 \\ 0 & -\sinh r & 0 & \cosh r \end{pmatrix} . \tag{A.5}$$

When this operation is performed inside a CF loop with one feedback mode and one ancilla as in Section 3.2.3, the E and F matrices are given by the top 2×2 submatrices, (as specified in Section 2.2). Therefore $E = \cosh r \mathbb{1}$ and $F = \sigma_z \sinh r$, as stated in equations (3.12).

In Section 3.2.3, we also consider a case where phase shifters act on the feedback mode after two-mode squeezing. Note that, in equation (A.2), when

$\phi = \pi$, $S_\phi = -\mathbb{1}$. If a phase shifter with this phase acts on feedback mode after a two-mode squeezer has acted, the net effect will be captured by the matrix:

$$S_{Tot} = ((-\mathbb{1}) \oplus \mathbb{1})S_r = \begin{pmatrix} -\cosh r\mathbb{1} & -\sinh r\sigma_z \\ \sinh r\sigma_z & \cosh r\mathbb{1} \end{pmatrix} . \tag{A.6}$$

If this operation is performed inside the feedback loop, the E and F matrices are again given by the top 2×2 submatrices, which in this case are $E_s = -\cosh r\mathbb{1}$ and $F_s = -\sinh r\sigma_z$ and are used to derived the expressions found in (3.16).

A.1.5 Losses Followed by Squeezing

In Section 3.2.2, we explored cases where the feedback mode was subject losses followed by squeezing. We will now derive the symplectic transformation corresponding to this operation, and use this to obtain the matrices given in (3.8).

The term 'losses' corresponds physically to leakage ie. interactions of the mode with some white noise environment. This interaction can be modelled by a beam splitter, whose symplectic matrix is given by (A.3). Squeezing on a single mode, while leaving the other unchanged is represented by the symplectic matrix $S_z \oplus \mathbb{1}$, where S_z is given by (A.4). The effect of losses, followed by squeezing is captured by multiplying these matrices:

$$S_{Tot} = (S_z \oplus \mathbb{1})S_\theta = \begin{pmatrix} \cos\theta S_z & \sin\theta S_z \\ -\sin\theta\mathbb{1} & \cos\theta\mathbb{1} \end{pmatrix} . \tag{A.7}$$

Recall that, in Section 2.2, the E and F matrices were derived from the top two blocks of the in-loop symplectic matrix. If the in-loop symplectic is given by (A.7) then these matrices will be given by $E = \cos\theta S_z$ and $F = \sin\theta S_z$. Writing these equations in terms of the effiency $\eta = \cos\theta$ and $\sqrt{1-\eta^2} = \sin\theta$ yields the E and F matrices given in (3.8).

A.2 Gaussian Measurements

As discussed in Section 1.2.10, general-dyne measurements are characterised by a covariance matrix $\boldsymbol{\sigma}_m$. Here we will introduce the expressions for $\boldsymbol{\sigma}_m$ for cases that are used in this thesis.

A.2.1 Homodyne Measurements

Homodyne measurements correspond to measurement of a single quadrature. Ideal homodyning, with unit efficiency is captured by a $\boldsymbol{\sigma}_m$ corresponding to a state in the limit of 'infinite squeezing', the squeezed quadrature corresponding to the one being measured [38, 134]. The expressions for homodyne measurements of the $\hat{x}$ and $\hat{p}$ quadratures are, respectively:

$$\boldsymbol{\sigma}_m^{hom,x} = \lim_{z\longrightarrow\infty} \begin{pmatrix} \frac{1}{z} & 0 \\ 0 & z \end{pmatrix} , \quad \boldsymbol{\sigma}_m^{hom,p} = \lim_{z\longrightarrow\infty} \begin{pmatrix} z & 0 \\ 0 & \frac{1}{z} \end{pmatrix} . \tag{A.8}$$

Homodyne measurements with an efficiency of less than 1 can be modelled as unit efficiency homodyne measurements on output modes subjected to mixing with a vacuum at a beam splitter. For an efficiency η the resulting $\boldsymbol{\sigma}_m$ expression for measurements of the $\hat{x}$ and $\hat{p}$ quadratures are, respectively [38]:

$$\boldsymbol{\sigma}_m^{x,\eta} = \lim_{z\longrightarrow\infty} \frac{1}{\eta} \begin{pmatrix} \frac{1}{z} + 1 - \eta & 0 \\ 0 & z + 1 - \eta \end{pmatrix} , \tag{A.9}$$

$$\boldsymbol{\sigma}_m^{p,\eta} = \lim_{z\longrightarrow\infty} \frac{1}{\eta} \begin{pmatrix} z + 1 - \eta & 0 \\ 0 & \frac{1}{z} + 1 - \eta \end{pmatrix} . \tag{A.10}$$

Appendix B

Coherent Feedback Setups which beat the 3dB Bound

First, we consider a *passive* coherent feedback setup for a two-mode system, as described by our model in chapter 2. We show that, for this example, there exists a passive coherent feedback setup which generates steady state whose eigenvalues beat the 3dB bound. Recall that a passive coherent feedback setup will generate a drift matrix given by $A = \Omega H - \frac{1}{2}D_0$, where D_0 is the diffusion matrix at zero temperature. For a setup with $D_0 = \mathbb{1}$ and a system Hamiltonian given by:

$$H = \frac{1}{3}\begin{pmatrix} 1 & 0 & 1 & 0 \\ 0 & 1 & 0 & -1 \\ 1 & 0 & -1 & 0 \\ 0 & -1 & 0 & 1 \end{pmatrix}, \tag{B.1}$$

the drift matrix is Hurwitz and the steady state covariance matrix has a steady state eigenvalue of 0.48, which is less than the value of 1/2 specified by the 3dB bound.

Next, we consider a single system mode subject to an *active* CF setup involving in-loop squeezing and show that it can beat the 3dB bound. Consider

a loop characterised by:

$$E = \begin{pmatrix} 0 & 0 \\ 0 & 0 \end{pmatrix} \quad F = \begin{pmatrix} z & 0 \\ 0 & 1/z \end{pmatrix} . \tag{B.2}$$

Note that (minus the extra mechanical mode), this setup can be generated using loops of the same form as section 3.2.2, containing squeezing and losses, with $\eta = 0$. The system is also subject to a squeezing Hamiltonian with strength $\chi = \gamma$. The eigenvalues of the drift matrix in this case are $-\frac{\gamma}{2}$ and $-\frac{3\gamma}{2}$, meaning it is Hurwitz and the system is stable. The steady state for this setup is:

$$\boldsymbol{\sigma}_\infty = \begin{pmatrix} \frac{1}{3}N(1+z^2) & 0 \\ 0 & N(1+\frac{1}{z}) \end{pmatrix} . \tag{B.3}$$

The smallest eigenvalue is squeezed below $N/2$ when $z < 1/\sqrt{2}$ and below $1/2$ when $z^2 < \frac{3}{2N} - 1$.

Appendix C

Appendix to Chapter 3

C.1 Numerically Solving the Drift-diffusion Equation

To find the transient behaviour of the optomechanical system and generate figures 3.2b and 3.2c, we solved the drift-diffusion equation (1.38) discretely. The drift-diffusion equation is:

$$\frac{d\boldsymbol{\sigma}}{dt} = A\boldsymbol{\sigma} + \boldsymbol{\sigma}A^{\mathsf{T}} + D\,. \tag{C.1}$$

This can be written discretely by replacing the infinitesmals $d\boldsymbol{\sigma}$ and dt with their discrete counterparts: Δt and $\Delta\boldsymbol{\sigma} = \boldsymbol{\sigma}(t+\Delta t) - \boldsymbol{\sigma}(t)$. Given an initial covariance matrix $\boldsymbol{\sigma}(t)$, the discrete version of the drift-diffusion equation then gives the covariance matrix at a later time $t + \Delta t$:

$$\boldsymbol{\sigma}(t+\Delta t) = \boldsymbol{\sigma}(t) + \Delta t\big[A\boldsymbol{\sigma}(t) + \boldsymbol{\sigma}(t)A^{\mathsf{T}} + D\big]\,. \tag{C.2}$$

This equation was implemented in Python to find the covariance matrix (and thus the average mechanical excitations) at each timestep. This discrete approximation is valid if the timestep Δt is much smaller than the characteristic timescales of the system at hand. In our optomechanical systems, the highest frequencies involved were either the cavity loss rate κ or the mechanical frequency ω_m, meaning that the smallest characteristic timescale of the system

was either $\frac{1}{\kappa}$ or $\frac{1}{\omega_m}$. When numerically solving equation (C.2), we ensured that the timesteps involved were smaller than $\frac{1}{\kappa}$ and $\frac{1}{\omega_m}$ by at least a factor of ten.

C.2 Active Coherent Feedback for Cooling

The steady state optomechanical covariance matrix resulting from the dynamics described in Section 3.3.3 is given by:

$$\boldsymbol{\sigma} = \begin{pmatrix} \sigma_{11} & 0 & 0 & \sigma_{14} \\ 0 & \sigma_{22} & \sigma_{24} & 0 \\ 0 & \sigma_{24} & \sigma_{33} & 0 \\ \sigma_{14} & 0 & 0 & \sigma_{44} \end{pmatrix} \tag{C.3}$$

where

$$\sigma_{11} = -\frac{z\left(\kappa N_l \alpha\left(4G^2 z + \kappa\Gamma_m\beta + z\Gamma_m^2\right) + 4G^2 z\Gamma_m N_m\right)}{\left(-z\Gamma_m + \kappa\eta\left(3z^2-1\right) - 2\kappa z\right)\left(4G^2 z + \kappa\Gamma_m\beta\right)}, \tag{C.4}$$

$$\sigma_{14} = \frac{2G\kappa z\Gamma_m\left(zN_l\alpha + N_m\left(\eta\left(3z^2-1\right) - 2z\right)\right)}{\left(-z\Gamma_m + \kappa\eta\left(3z^2-1\right) - 2\kappa z\right)\left(4G^2 z + \kappa\Gamma_m\beta\right)}, \tag{C.5}$$

$$\sigma_{22} = \frac{\kappa N_l\alpha\left(4G^2 z + \Gamma_m\left(z\Gamma_m + \kappa\eta\left(z^2-3\right) + 2\kappa z\right)\right) + 4G^2 z^3\Gamma_m N_m}{z\left(z\Gamma_m + \kappa\eta\left(z^2-3\right) + 2\kappa z\right)\left(4G^2 z + \kappa\Gamma_m\gamma\right)}, \tag{C.6}$$

$$\sigma_{33} = \frac{4G^2\kappa N_l\alpha + \Gamma_m N_m\left(4G^2 z^2 + \kappa z\Gamma_m\gamma + \kappa^2\gamma^2\right)}{\left(z\Gamma_m + \kappa\eta\left(z^2-3\right) + 2\kappa z\right)\left(4G^2 z + \kappa\Gamma_m\left(\eta\left(z^2-3\right) + 2z\right)\right)}, \tag{C.7}$$

$$\sigma_{44} = -\frac{4G^2\kappa z^2 N_l\alpha + \Gamma_m N_m\left(4G^2 z^2 + \kappa z\Gamma_m\beta + \kappa^2\beta^2\right)}{\left(-z\Gamma_m + \kappa\eta\left(3z^2-1\right) - 2\kappa z\right)\left(4G^2 z + \kappa\Gamma_m\beta\right)}, \tag{C.8}$$

$$\alpha = \left(-2\eta z + z^2 + 1\right), \quad \beta = \left(-3\eta z^2 + \eta + 2z\right), \tag{C.9}$$

$$\gamma = \left(\eta\left(z^2-3\right) + 2z\right). \tag{C.10}$$

The symplectic eigenvalue of the mechanical covariance matrix is:

$$\nu = \sqrt{\frac{\delta\left(4G^2\left(\kappa N_l\alpha + z^2\Gamma_m N_m\right) + \kappa\Gamma_m N_m\gamma\left(z\Gamma_m + \kappa\eta\left(z^2-3\right) + 2\kappa z\right)\right)}{\left(z\Gamma_m + \kappa\eta\left(z^2-3\right) + 2\kappa z\right)\left(z\Gamma_m + \kappa\beta\right)\left(4G^2 z + \kappa\Gamma_m\beta\right)\left(4G^2 z + \kappa\Gamma_m\gamma\right)}} \tag{C.11}$$

$$\delta = \left(4G^2\kappa z^2 N_l\alpha + \Gamma_m N_m\left(4G^2 z^2 + \kappa z\Gamma_m\beta + \kappa^2\beta^2\right)\right). \tag{C.12}$$

Appendix D

Appendix to Chapter 4

D.1 Performing a bit-flip using Projective Measurement-based Feedback

This Section contains details to supplement Section 4.3.2. The fidelity of the output state of our MF protocol to the desired state is given by $F_{MF} = \langle \phi_X \rho^{out}_{S,MF} | \, |\psi_X\rangle$. When an input state given by (4.45) is used in MF, this fidelity is:

$$
\begin{aligned}
F_{MF} =& \frac{1}{8} e^{-2i\phi} \bigg(\frac{1}{2} s^2 \sin(3\phi)(\cot(3\phi) + i) \left(2\sin(\chi)\sin\left(2\theta_v\right) \left(\left(2c^2 - ics - s^2\right)\cos(\chi)\right.\right. \\
&+ 2c^2 + ics + s^2 + s(s+ic)(2\sin(\chi) + \sin(2\chi))\sin\left(2\theta_u\right) \\
&+ s^2 e^{i\phi}\sin(\chi)\sin\left(2\theta_v\right)\left(\left(2c^2 + ics - s^2\right)\cos(\chi) + 2c^2 - ics + s^2\right) \\
&+ 2c^2(c+is)\sin^2(\chi)\left(c + is\cos\left(2\theta_v\right)\right) + 2c^2 e^{4i\phi}(c-is)\sin^2(\chi)\left(c - is\cos\left(2\theta_v\right)\right) \\
&- 2e^{2i\phi}\left(c^4\cos(2\chi) - c^4 + s^2\cos(\chi)\left(s^2\left(2\cos^2\left(\frac{\chi}{2}\right)\cos\left(2\theta_u\right) + (\cos(\chi) - 1)\cos\left(2\theta_v\right)\right)\right.\right. \\
&- 4c^2\cos^2\left(\theta_v\right) - 4c^2s^2 - 2s^4 + 4s^3 e^{i\phi}(s - ic)\sin\left(\frac{\chi}{2}\right)\cos^3\left(\frac{\chi}{2}\right)\sin\left(2\theta_u\right) \\
&+ 2c\eta_0 s\left(\sin(\chi)\left(c\sin(\chi)\left(ic\left(-1 + e^{4i\phi}\right)\left(\cos\left(2\theta_u\right) + \cos\left(2\theta_v\right) + 2\right)\right.\right.\right. \\
&- s\left(1 + e^{4i\phi}\right)\left(\cos\left(2\theta_u\right) - \cos\left(2\theta_v\right)\right) + 2se^{2i\phi}\left(\sin\left(2\theta_u\right)\left(c\cos(\phi) + s\sin(\phi)\right)\right. \\
&+ \sin\left(2\theta_v\right)\left(s\sin(\phi) - c\cos(\phi)\right) + se^{i\phi}\cos(\chi)\left(-\left((c - is)\sin(\chi)\sin\left(2\theta_u\right)\right)\right. \\
&- e^{2i\phi}(c+is)\sin(\chi)\sin\left(2\theta_u\right) - 2e^{i\phi}\left(\sin(\chi)\sin\left(2\theta_v\right)\left(c\cos(\phi) + s\sin(\phi)\right)\right. \\
&+ c\left(\cos\left(2\theta_u\right) + \cos\left(2\theta_v\right) + 2\right).
\end{aligned}
$$

D.2 Measurement-based feedback with General POVMs

This Section supplements Section 4.3.3. In the MF protocol described in this Section, the fidelity of the output state to the desired state, before it is averaged over the Haar measure is given by:

$$
\begin{aligned}
F_{MF} =& e^{i\phi}\sin(\frac{\chi}{2})(\cos(\frac{\chi}{2})(c(c-is)(\frac{1}{2}ce^{i\phi}(c+is)u_{10}\eta_{00}u_{10}^{*}\sin(\chi)a^{2} \\
&+\frac{1}{2}(1-a^{2})ce^{i\phi}(c+is)v_{10}\eta_{00}v_{10}^{*}\sin(\chi) \\
&+u_{11}^{*}(-\frac{1}{2}ce^{i\phi}(c-is)u_{11}(\eta_{00}-1)\sin(\chi)b^{2} \\
&-\frac{1}{2}iacsu_{10}(-2\eta_{00}+\cos(\chi)+1)b) \\
&+v_{11}^{*}(-\frac{1}{2}i\sqrt{1-a^{2}}\sqrt{1-b^{2}}csv_{10}(-2\eta_{00}+\cos(\chi)+1) \\
&-\frac{1}{2}(1-b^{2})ce^{i\phi}(c-is)v_{11}(\eta_{00}-1)\sin(\chi))) \\
&+i(c-is)s(u_{00}^{*}(a^{2}u_{10}(c^{2}\eta_{00}\sin^{2}(\frac{\chi}{2}) \\
&-\frac{1}{2}s^{2}(\eta_{00}-1)(\cos(\chi)+1)) \\
&-\frac{1}{2}iabe^{i\phi}(c-is)su_{11}(\eta_{00}-1)\sin(\chi))+v_{00}^{*}((1-a^{2})v_{10}(c^{2}\eta_{00}\sin^{2}(\frac{\chi}{2}) \\
&-\frac{1}{2}s^{2}(\eta_{00}-1)(\cos(\chi)+1)) \\
&-\frac{1}{2}i\sqrt{1-a^{2}}\sqrt{1-b^{2}}e^{i\phi}(c-is)sv_{11}(\eta_{00}-1)\sin(\chi)) \\
&+u_{01}^{*}(\frac{1}{2}u_{11}(\eta_{00}-1)(\cos(\chi)-1)b^{2} \\
&+\frac{1}{2}a(c+is)su_{10}(\eta_{00}-1)(i\cos(\phi)+\sin(\phi))\sin(\chi)b) \\
&+v_{01}^{*}(\frac{1}{2}(1-b^{2})v_{11}(\eta_{00}-1)(\cos(\chi)-1) \\
&+\frac{1}{2}\sqrt{1-a^{2}}\sqrt{1-b^{2}}(c+is)sv_{10}(\eta_{00}-1)(i\cos(\phi)+\sin(\phi))\sin(\chi))) \\
&+(c+is)(c(\frac{1}{2}ce^{i\phi}(c+is)u_{00}\eta_{00}u_{00}^{*}\sin(\chi)a^{2} \\
&+\frac{1}{2}(1-a^{2})ce^{i\phi}(c+is)v_{00}\eta_{00}v_{00}^{*}\sin(\chi) \\
&+u_{01}^{*}(-\frac{1}{2}ce^{i\phi}(c-is)u_{01}(\eta_{00}-1)\sin(\chi)b^{2}
\end{aligned}
$$

$$
\begin{aligned}
&- \frac{1}{2} iacsu_{00}(-2\eta_{00} + \cos(\chi) + 1)b) \\
&+ v_{01}^*(-\frac{1}{2} i\sqrt{1-a^2}\sqrt{1-b^2}csv_{00}(-2\eta_{00} + \cos(\chi) + 1) \\
&- \frac{1}{2}(1-b^2)ce^{i\phi}(c - is)v_{01}(\eta_{00} - 1)\sin(\chi))) \\
&- is(u_{01}^*(u_{11}(s^2\eta_{00}\sin^2(\frac{\chi}{2}) \\
&- \frac{1}{2}c^2(\eta_{00} - 1)(\cos(\chi) + 1))b^2 + \frac{1}{2}ae^{-i\phi}s(ic + s)u_{10}\eta_{00}\sin(\chi)b) \\
&+ u_{00}^*(\frac{1}{2}u_{10}\eta_{00}(\cos(\chi) + 1)a^2 + \frac{1}{2}be^{i\phi}s(s - ic)u_{11}\eta_{00}\sin(\chi)a) \\
&+ v_{01}^*((1-b^2)v_{11}(s^2\eta_{00}\sin^2(\frac{\chi}{2}) \\
&- \frac{1}{2}c^2(\eta_{00} - 1)(\cos(\chi) + 1)) \\
&+ \frac{1}{2}\sqrt{1-a^2}\sqrt{1-b^2}e^{-i\phi}s(ic + s)v_{10}\eta_{00}\sin(\chi)) \\
&+ v_{00}^*(\frac{1}{2}(1-a^2)v_{10}\eta_{00}(\cos(\chi) + 1) \\
&+ \frac{1}{2}\sqrt{1-a^2}\sqrt{1-b^2}e^{i\phi}s(s - ic)v_{11}\eta_{00}\sin(\chi))))) \\
&+ e^{-i\phi}\sin(\frac{\chi}{2})((c - is)(c + is)(u_{01}^*(u_{01}(s^2\eta_{00}\sin^2(\frac{\chi}{2}) \\
&- \frac{1}{2}c^2(\eta_{00} - 1)(\cos(\chi) + 1))b^2 \\
&+ \frac{1}{2}ae^{-i\phi}s(ic + s)u_{00}\eta_{00}\sin(\chi)b) + u_{00}^*(\frac{1}{2}u_{00}\eta_{00}(\cos(\chi) + 1)a^2 \\
&+ \frac{1}{2}be^{i\phi}s(s - ic)u_{01}\eta_{00}\sin(\chi)a) + v_{01}^*((1-b^2)v_{01}(s^2\eta_{00}\sin^2(\frac{\chi}{2}) \\
&- \frac{1}{2}c^2(\eta_{00} - 1)(\cos(\chi) + 1)) \\
&+ \frac{1}{2}\sqrt{1-a^2}\sqrt{1-b^2}e^{-i\phi}s(ic + s)v_{00}\eta_{00}\sin(\chi)) \\
&+ v_{00}^*(\frac{1}{2}(1-a^2)v_{00}\eta_{00}(\cos(\chi) + 1) \\
&+ \frac{1}{2}\sqrt{1-a^2}\sqrt{1-b^2}e^{i\phi}s(s - ic)v_{01}\eta_{00}\sin(\chi))) \\
&+ c(c(u_{11}^*(u_{11}(s^2\eta_{00}\sin^2(\frac{\chi}{2}) \\
&- \frac{1}{2}c^2(\eta_{00} - 1)(\cos(\chi) + 1))b^2 + \frac{1}{2}ae^{-i\phi}s(ic + s)u_{10}\eta_{00}\sin(\chi)b) \\
&+ u_{10}^*(\frac{1}{2}u_{10}\eta_{00}(\cos(\chi) + 1)a^2 + \frac{1}{2}be^{i\phi}s(s - ic)u_{11}\eta_{00}\sin(\chi)a) \\
&+ v_{11}^*((1-b^2)v_{11}(s^2\eta_{00}\sin^2(\frac{\chi}{2}) - \frac{1}{2}c^2(\eta_{00} - 1)(\cos(\chi) + 1))
\end{aligned}
$$

$$
\begin{aligned}
&+ \frac{1}{2}\sqrt{1-a^2}\sqrt{1-b^2}e^{-i\phi}s(ic+s)v_{10}\eta_{00}\sin(\chi))\\
&+ v_{10}^*(\frac{1}{2}(1-a^2)v_{10}\eta_{00}(\cos(\chi)+1)\\
&+ \frac{1}{2}\sqrt{1-a^2}\sqrt{1-b^2}e^{i\phi}s(s-ic)v_{11}\eta_{00}\sin(\chi)))\\
&- is(\frac{1}{2}ce^{i\phi}(c+is)u_{00}\eta_{00}u_{10}^*\sin(\chi)a^2\\
&+ \frac{1}{2}(1-a^2)ce^{i\phi}(c+is)v_{00}\eta_{00}v_{10}^*\sin(\chi)\\
&+ u_{11}^*(-\frac{1}{2}ce^{i\phi}(c-is)u_{01}(\eta_{00}-1)\sin(\chi)b^2\\
&- \frac{1}{2}iacsu_{00}(-2\eta_{00}+\cos(\chi)+1)b)\\
&+ v_{11}^*(-\frac{1}{2}i\sqrt{1-a^2}\sqrt{1-b^2}csv_{00}(-2\eta_{00}+\cos(\chi)+1)\\
&- \frac{1}{2}(1-b^2)ce^{i\phi}(c-is)v_{01}(\eta_{00}-1)\sin(\chi))))\\
&+ is(c(-\frac{1}{2}ce^{-i\phi}(c+is)u_{11}(\eta_{00}-1)u_{01}^*\sin(\chi)b^2\\
&- \frac{1}{2}(1-b^2)ce^{-i\phi}(c+is)v_{11}(\eta_{00}-1)v_{01}^*\sin(\chi)\\
&+ u_{00}^*(\frac{1}{2}ce^{-i\phi}(c-is)u_{10}\eta_{00}\sin(\chi)a^2\\
&+ \frac{1}{2}ibcsu_{11}(-2\eta_{00}+\cos(\chi)+1)a)\\
&+ v_{00}^*(\frac{1}{2}i\sqrt{1-a^2}\sqrt{1-b^2}csv_{11}(-2\eta_{00}+\cos(\chi)+1)\\
&+ \frac{1}{2}(1-a^2)ce^{-i\phi}(c-is)v_{10}\eta_{00}\sin(\chi))) - is(u_{00}^*(a^2u_{00}(c^2\eta_{00}\sin^2(\frac{\chi}{2})\\
&- \frac{1}{2}s^2(\eta_{00}-1)(\cos(\chi)+1))\\
&- \frac{1}{2}iabe^{i\phi}(c-is)su_{01}(\eta_{00}-1)\sin(\chi))\\
&+ v_{00}^*((1-a^2)v_{00}(c^2\eta_{00}\sin^2(\frac{\chi}{2}) - \frac{1}{2}s^2(\eta_{00}-1)(\cos(\chi)+1))\\
&- \frac{1}{2}i\sqrt{1-a^2}\sqrt{1-b^2}e^{i\phi}(c-is)sv_{01}(\eta_{00}-1)\sin(\chi))\\
&+ u_{01}^*(\frac{1}{2}u_{01}(\eta_{00}-1)(\cos(\chi)-1)b^2\\
&+ \frac{1}{2}a(c+is)su_{00}(\eta_{00}-1)(i\cos(\phi)\\
&+ \sin(\phi))\sin(\chi)b) + v_{01}^*(\frac{1}{2}(1-b^2)v_{01}(\eta_{00}-1)(\cos(\chi)-1)\\
&+ \frac{1}{2}\sqrt{1-a^2}\sqrt{1-b^2}(c+is)sv_{00}(\eta_{00}-1)(i\cos(\phi)+\sin(\phi))\sin(\chi))))))
\end{aligned}
$$

$$
\begin{aligned}
&+ \cos(\frac{\chi}{2})(\cos(\frac{\chi}{2})((c-is)(c+is)(u_{10}^{*}(a^2u_{10}(c^2\eta_{00}\sin^2(\frac{\chi}{2})\\
&- \frac{1}{2}s^2(\eta_{00}-1)(\cos(\chi)+1)) - \frac{1}{2}iabe^{i\phi}(c-is)su_{11}(\eta_{00}-1)\sin(\chi))\\
&+ v_{10}^{*}((1-a^2)v_{10}(c^2\eta_{00}\sin^2(\frac{\chi}{2}) - \frac{1}{2}s^2(\eta_{00}-1)(\cos(\chi)+1))\\
&- \frac{1}{2}i\sqrt{1-a^2}\sqrt{1-b^2}e^{i\phi}(c-is)sv_{11}(\eta_{00}-1)\sin(\chi))\\
&+ u_{11}^{*}(\frac{1}{2}u_{11}(\eta_{00}-1)(\cos(\chi)-1)b^2\\
&+ \frac{1}{2}a(c+is)su_{10}(\eta_{00}-1)(i\cos(\phi)+\sin(\phi))\sin(\chi)b)\\
&+ v_{11}^{*}(\frac{1}{2}(1-b^2)v_{11}(\eta_{00}-1)(\cos(\chi)-1)\\
&+ \frac{1}{2}\sqrt{1-a^2}\sqrt{1-b^2}(c+is)sv_{10}(\eta_{00}-1)(i\cos(\phi)+\sin(\phi))\sin(\chi)))\\
&+ is(c(\frac{1}{2}ce^{i\phi}(c+is)u_{00}\eta_{00}u_{10}^{*}\sin(\chi)a^2\\
&+ \frac{1}{2}(1-a^2)ce^{i\phi}(c+is)v_{00}\eta_{00}v_{10}^{*}\sin(\chi)\\
&+ u_{11}^{*}(-\frac{1}{2}ce^{i\phi}(c-is)u_{01}(\eta_{00}-1)\sin(\chi)b^2\\
&- \frac{1}{2}iacsu_{00}(-2\eta_{00}+\cos(\chi)+1)b)\\
&+ v_{11}^{*}(-\frac{1}{2}i\sqrt{1-a^2}\sqrt{1-b^2}csv_{00}(-2\eta_{00}+\cos(\chi)+1)\\
&- \frac{1}{2}(1-b^2)ce^{i\phi}(c-is)v_{01}(\eta_{00}-1)\sin(\chi)))\\
&- is(u_{11}^{*}(u_{11}(s^2\eta_{00}\sin^2(\frac{\chi}{2}) - \frac{1}{2}c^2(\eta_{00}-1)(\cos(\chi)+1))b^2\\
&+ \frac{1}{2}ae^{-i\phi}s(ic+s)u_{10}\eta_{00}\sin(\chi)b)\\
&+ u_{10}^{*}(\frac{1}{2}u_{10}\eta_{00}(\cos(\chi)+1)a^2\\
&+ \frac{1}{2}be^{i\phi}s(s-ic)u_{11}\eta_{00}\sin(\chi)a) + v_{11}^{*}((1-b^2)v_{11}(s^2\eta_{00}\sin^2(\frac{\chi}{2})\\
&- \frac{1}{2}c^2(\eta_{00}-1)(\cos(\chi)+1))\\
&+ \frac{1}{2}\sqrt{1-a^2}\sqrt{1-b^2}e^{-i\phi}s(ic+s)v_{10}\eta_{00}\sin(\chi))\\
&+ v_{10}^{*}(\frac{1}{2}(1-a^2)v_{10}\eta_{00}(\cos(\chi)+1)\\
&+ \frac{1}{2}\sqrt{1-a^2}\sqrt{1-b^2}e^{i\phi}s(s-ic)v_{11}\eta_{00}\sin(\chi))))\\
&+ c(c(u_{00}^{*}(a^2u_{00}(c^2\eta_{00}\sin^2(\frac{\chi}{2}) - \frac{1}{2}s^2(\eta_{00}-1)(\cos(\chi)+1))
\end{aligned}
$$

$$
\begin{aligned}
&- \frac{1}{2} iabe^{i\phi}(c - is)su_{01}(\eta_{00} - 1)\sin(\chi)) + v_{00}^*((1 - a^2)v_{00}(c^2\eta_{00}\sin^2(\frac{\chi}{2}) \\
&- \frac{1}{2} s^2(\eta_{00} - 1)(\cos(\chi) + 1)) \\
&- \frac{1}{2} i\sqrt{1 - a^2}\sqrt{1 - b^2}e^{i\phi}(c - is)sv_{01}(\eta_{00} - 1)\sin(\chi)) \\
&+ u_{01}^*(\frac{1}{2} u_{01}(\eta_{00} - 1)(\cos(\chi) - 1)b^2 \\
&+ \frac{1}{2} a(c + is)su_{00}(\eta_{00} - 1)(i\cos(\phi) + \sin(\phi))\sin(\chi)b) \\
&+ v_{01}^*(\frac{1}{2}(1 - b^2)v_{01}(\eta_{00} - 1)(\cos(\chi) - 1) \\
&+ \frac{1}{2}\sqrt{1 - a^2}\sqrt{1 - b^2}(c + is)sv_{00}(\eta_{00} - 1)(i\cos(\phi) + \sin(\phi))\sin(\chi))) \\
&- is(-\frac{1}{2} ce^{-i\phi}(c + is)u_{11}(\eta_{00} - 1)u_{01}^*\sin(\chi)b^2 \\
&- \frac{1}{2}(1 - b^2)ce^{-i\phi}(c + is)v_{11}(\eta_{00} - 1)v_{01}^*\sin(\chi) \\
&+ u_{00}^*(\frac{1}{2} ce^{-i\phi}(c - is)u_{10}\eta_{00}\sin(\chi)a^2 \\
&+ \frac{1}{2} ibcsu_{11}(-2\eta_{00} + \cos(\chi) + 1)a) \\
&+ v_{00}^*(\frac{1}{2} i\sqrt{1 - a^2}\sqrt{1 - b^2}csv_{11}(-2\eta_{00} + \cos(\chi) + 1) \\
&+ \frac{1}{2}(1 - a^2)ce^{-i\phi}(c - is)v_{10}\eta_{00}\sin(\chi))))) \\
&+ e^{-i\phi}\sin(\frac{\chi}{2})(c(c - is)(-\frac{1}{2} ce^{-i\phi}(c + is)u_{01}(\eta_{00} - 1)u_{01}^*\sin(\chi)b^2 \\
&- \frac{1}{2}(1 - b^2)ce^{-i\phi}(c + is)v_{01}(\eta_{00} - 1)v_{01}^*\sin(\chi) \\
&+ u_{00}^*(\frac{1}{2} ce^{-i\phi}(c - is)u_{00}\eta_{00}\sin(\chi)a^2 \\
&+ \frac{1}{2} ibcsu_{01}(-2\eta_{00} + \cos(\chi) + 1)a) \\
&+ v_{00}^*(\frac{1}{2} i\sqrt{1 - a^2}\sqrt{1 - b^2}csv_{01}(-2\eta_{00} + \cos(\chi) + 1) \\
&+ \frac{1}{2}(1 - a^2)ce^{-i\phi}(c - is)v_{00}\eta_{00}\sin(\chi))) \\
&+ i(c - is)s(u_{11}^*(u_{01}(s^2\eta_{00}\sin^2(\frac{\chi}{2}) - \frac{1}{2} c^2(\eta_{00} - 1)(\cos(\chi) + 1))b^2 \\
&+ \frac{1}{2} ae^{-i\phi}s(ic + s)u_{00}\eta_{00}\sin(\chi)b) \\
&+ u_{10}^*(\frac{1}{2} u_{00}\eta_{00}(\cos(\chi) + 1)a^2 \\
&+ \frac{1}{2} be^{i\phi}s(s - ic)u_{01}\eta_{00}\sin(\chi)a)
\end{aligned}
$$

$$
\begin{aligned}
&+ v_{11}^*((1-b^2)v_{01}(s^2\eta_{00}\sin^2(\frac{\chi}{2}) - \frac{1}{2}c^2(\eta_{00}-1)(\cos(\chi)+1)) \\
&+ \frac{1}{2}\sqrt{1-a^2}\sqrt{1-b^2}e^{-i\phi}s(ic+s)v_{00}\eta_{00}\sin(\chi)) \\
&+ v_{10}^*(\frac{1}{2}(1-a^2)v_{00}\eta_{00}(\cos(\chi)+1) \\
&+ \frac{1}{2}\sqrt{1-a^2}\sqrt{1-b^2}e^{i\phi}s(s-ic)v_{01}\eta_{00}\sin(\chi))) \\
&+ (c+is)(c(-\frac{1}{2}ce^{-i\phi}(c+is)u_{11}(\eta_{00}-1)u_{11}^*\sin(\chi)b^2 \\
&- \frac{1}{2}(1-b^2)ce^{-i\phi}(c+is)v_{11}(\eta_{00}-1)v_{11}^*\sin(\chi) \\
&+ u_{10}^*(\frac{1}{2}ce^{-i\phi}(c-is)u_{10}\eta_{00}\sin(\chi)a^2 \\
&+ \frac{1}{2}ibcsu_{11}(-2\eta_{00}+\cos(\chi)+1)a) \\
&+ v_{10}^*(\frac{1}{2}i\sqrt{1-a^2}\sqrt{1-b^2}csv_{11}(-2\eta_{00}+\cos(\chi)+1) \\
&+ \frac{1}{2}(1-a^2)ce^{-i\phi}(c-is)v_{10}\eta_{00}\sin(\chi))) \\
&- is(u_{10}^*(a^2u_{00}(c^2\eta_{00}\sin^2(\frac{\chi}{2}) - \frac{1}{2}s^2(\eta_{00}-1)(\cos(\chi)+1)) \\
&- \frac{1}{2}iabe^{i\phi}(c-is)su_{01}(\eta_{00}-1)\sin(\chi)) + v_{10}^*((1-a^2)v_{00}(c^2\eta_{00}\sin^2(\frac{\chi}{2}) \\
&- \frac{1}{2}s^2(\eta_{00}-1)(\cos(\chi)+1)) \\
&- \frac{1}{2}i\sqrt{1-a^2}\sqrt{1-b^2}e^{i\phi}(c-is)sv_{01}(\eta_{00}-1)\sin(\chi)) \\
&+ u_{11}^*(\frac{1}{2}u_{01}(\eta_{00}-1)(\cos(\chi)-1)b^2 \\
&+ \frac{1}{2}a(c+is)su_{00}(\eta_{00}-1)(i\cos(\phi)+\sin(\phi))\sin(\chi)b) \\
&+ v_{11}^*(\frac{1}{2}(1-b^2)v_{01}(\eta_{00}-1)(\cos(\chi)-1) \\
&+ \frac{1}{2}\sqrt{1-a^2}\sqrt{1-b^2}(c+is)sv_{00}(\eta_{00}-1)(i\cos(\phi)+\sin(\phi))\sin(\chi))))))\,.
\end{aligned}
$$

Averaging over the Haar measure, this yields:

$$
\begin{aligned}
A_{MF} =& \frac{1}{6}\Big(\sqrt{1-a^2}\sqrt{1-b^2}c^2s^2v_{11}v_{00}^* + \sqrt{1-a^2}\sqrt{1-b^2}c^2s^2v_{00}v_{11}^* \\
&+ \sqrt{1-a^2}\sqrt{1-b^2}c^2s^2v_{10}v_{01}^* + \sqrt{1-a^2}\sqrt{1-b^2}c^2s^2v_{01}v_{10}^* \\
&+ \sqrt{1-a^2}\sqrt{1-b^2}s^4v_{10}v_{01}^* + \sqrt{1-a^2}\sqrt{1-b^2}s^4v_{01}v_{10}^* \\
&- 2a^2c^4\eta_{00}|v_{00}|^2 - 2a^2c^4\eta_{00}|v_{10}|^2 - 2a^2c^2\eta_{00}s^2|v_{00}|^2 - 2a^2c^2s^2|v_{00}|^2 - 2a^2c^2\eta_{00}s^2|v_{10}|^2 \\
&- 2a^2c^2s^2|v_{10}|^2 - a^2s^4|v_{00}|^2 - 2a^2s^4|v_{10}|^2 - bu_{01}^*\left(-as^2u_{10} - 2bu_{01}\left(-\eta_{00}c^2+1\right)\right) \\
&+ au_{10}^*\left(2au_{10}\left(c^2\eta_{00}+s^2\right) + bs^2u_{01}\right) + au_{00}^*\left(au_{00}\left(2c^4\eta_{00} + 2c^2(\eta_{00}+1)s^2 + s^4\right) + bc^2s^2u_{11}\right) \\
&+ bu_{11}^*\left(ac^2s^2u_{00} + bu_{11}\left(-2c^4(\eta_{00}-1) - 2c^2(\eta_{00}-2)s^2 + s^4\right)\right) \\
&+ 2b^2c^4\eta_{00}|v_{01}|^2 - 2b^2c^4|v_{01}|^2 + 2b^2c^4\eta_{00}|v_{11}|^2 - 2b^2c^4|v_{11}|^2 + 2b^2c^2\eta_{00}s^2|v_{01}|^2 \\
&- 4b^2c^2s^2|v_{01}|^2 + 2b^2c^2\eta_{00}s^2|v_{11}|^2 - 4b^2c^2s^2v_{11}v_{11}^* - 2b^2s^4|v_{01}|^2 - b^2s^4v_{11}v_{11}^* + 2c^4\eta_{00}|v_{00}|^2 \\
&- 2c^4\eta_{00}v_{01}v_{01}^* + 2c^4|v_{01}|^2 + 2c^4\eta_{00}v_{10}v_{10}^* - 2c^4\eta_{00}|v_{11}|^2 + 2c^4v_{11}v_{11}^* + 2c^2\eta_{00}s^2|v_{00}|^2 \\
&+ 2c^2s^2v_{00}v_{00}^* - 2c^2\eta_{00}s^2|v_{01}|^2 + 4c^2s^2v_{01}v_{01}^* + 2c^2\eta_{00}s^2|v_{10}|^2 + 2c^2s^2v_{10}v_{10}^* - 2c^2\eta_{0000}s^2|v_{11}|^2 \\
&+ 4c^2s^2v_{11}v_{11}^* + s^4|v_{00}|^2 + 2s^4|v_{01}|^2 + 2s^4|v_{10}|^2 + s^4|v_{11}|^2\,,
\end{aligned}
$$

(this averaging was done using Mathematica's inbuilt Integrate function). To analyse this equation, we use the decomposition of the unitary matrices U and V:

$$
U = \begin{pmatrix} e^{i\phi_{1u}}\cos\theta_u & e^{i\phi_{2u}}\sin\theta_u \\ -e^{-i\phi_{2u}}\sin\theta_u & e^{-i\phi_{1u}}\cos\theta_u \end{pmatrix}, \quad V = \begin{pmatrix} e^{i\phi_{1v}}\cos\theta_v & e^{i\phi_{2v}}\sin\theta_v \\ -e^{-i\phi_{2v}}\sin\theta_v & e^{-i\phi_{1v}}\cos\theta_v \end{pmatrix}. \tag{D.1}
$$

When this substitution is made, the Haar-measure averaged fidelity simplifies to:

$$\begin{aligned}A_{MF} = \frac{1}{6}\Big(&\left(c^2-2\right)\left(a^2+b^2-2\right)\sin^2(\theta_v) - \sin^2(\theta_u)\left(\left(c^2-2\right)\left(a^2+b^2\right)\right.\\
&-2ab\left(c^2-1\right)\cos(2\phi_{2u}) \qquad + \qquad 2\sqrt{1-a^2}\sqrt{1-b^2}c^2\sin^2(\theta_v)\cos(2\phi_{2v})\\
&+\cos^2(\theta_u)\left(-\left(c^4-c^2-1\right)\left(a^2+b^2\right)-2ab\left(c^2-1\right)c^2\cos(2\phi_{1u})\right)\\
&+\cos^2(\theta_v)\left(\left(c^4-c^2-1\right)\left(a^2+b^2-2\right)-2\sqrt{1-a^2}\sqrt{1-b^2}c^2\left(c^2-1\right)\cos(2\phi_{1v})\right)\\
&-2\sqrt{1-a^2}\sqrt{1-b^2}\sin^2(\theta_v)\cos(2\phi_{2v})\,.\end{aligned} \tag{D.2}$$

This fidelity was analysed numerically for different values of c from $c = 0.1$ to $c = 0.9$ in steps of 0.1. For each value of c, Mathematica's inbuilt 'NMaximise' function was used to maximise this fidelity with respect to the feedback parameters a, b, θ_u, θ_v, ϕ_{1u}, ϕ_{2u}, ϕ_{1v}, ϕ_{2v}. It was found that, in each case, the fidelity was maximised when $a = b$ (for any value of a and b), $\theta_u = \theta_v = \phi_{2u} = \phi_{2v} = \frac{\pi}{2}$ and any value of ϕ_{1u} and ϕ_{1v}. Recall that, when $a = b$, the measurement is 'infinitely weak', so that the MF protocol becomes coherent feedback. Also note that, these optimal values of the parameters correspond to the case where $U = V = \sigma_x$. Thus, for the values of c considered, we conclude that CF outperforms all possible MF protocols.

When we substitute in $\theta_u = \theta_v = \phi_{2u} = \phi_{2v} = \frac{\pi}{2}$ into equation (D.2), we obtain the following equation:

$$A = \frac{1}{3}\left(-\left(c^2\left(\sqrt{1-a^2}\sqrt{1-b^2}+1\right)\right)+\sqrt{1-a^2}\sqrt{1-b^2}+a\left(b-bc^2\right)+2\right), \tag{D.3}$$

which gives the output fidelity of the protocol for any POVM with feedback unitaries $U = V = \sigma_x$, which, as we have seen, is optimal in both the case of projective measurements, and the case of fully coherent feedback. Substituting $a = b$ into (D.3) recovers the CF fidelity derived in Section 4.3.1: $A_{CF} = 1-\frac{2}{3}c^2$. Substituing $a = 1$, $b = 0$ recovers the case of projective measurement covered in Section 4.3.2: $A_{MF} = \frac{2}{3} - \frac{1}{3}c^2$.

Bibliography

[1] A. Harwood and A. Serafini, "Ultimate squeezing through coherent quantum feedback," *Physical Review Research*, vol. 2, no. 4, p. 043103, 2020.

[2] A. Harwood, M. Brunelli, and A. Serafini, "Cavity optomechanics assisted by optical coherent feedback," *Physical Review A*, vol. 103, no. 2, p. 023509, 2021.

[3] A. Harwood, M. Brunelli, and A. Serafini, "Unified collision model of coherent and measurement-based quantum feedback
for optimal state and operator control," *(Unpublished Manuscript, in preparation)*, 2022.

[4] T. Kailath, *Linear systems*, vol. 156. Prentice-Hall Englewood Cliffs, NJ, 1980.

[5] A. Sinha, *Linear systems: optimal and robust control*. CRC Press, 2007.

[6] V. P. Belavkin, "On the theory of controlling observable quantum systems," *Avtomatika i Telemekhanika*, no. 2, pp. 50–63, 1983.

[7] V. Belavkin, "Towards the theory of control in observable quantum systems," *arXiv preprint quant-ph/0408003*, 2004.

[8] H. M. Wiseman and G. J. Milburn, "All-optical versus electro-optical quantum-limited feedback," *Physical Review A*, vol. 49, no. 5, p. 4110, 1994.

[9] H. M. Wiseman, "Quantum theory of continuous feedback," *Physical Review A*, vol. 49, no. 3, p. 2133, 1994.

[10] H. J. Carmichael, "Quantum trajectory theory for cascaded open systems," *Physical Review Letters*, vol. 70, pp. 2273–2276, Apr. 1993.

[11] S. Lloyd, "Coherent quantum feedback," *Physical Review A*, vol. 62, no. 2, p. 022108, 2000.

[12] H. M. Wiseman and G. J. Milburn, *Quantum measurement and control*. Cambridge University Press, 2009.

[13] K. Jacobs, X. Wang, and H. M. Wiseman, "Coherent feedback that beats all measurement-based feedback protocols," *New Journal of Physics*, vol. 16, no. 7, p. 073036, 2014.

[14] C. W. Gardiner and M. J. Collett, "Input and output in damped quantum systems: Quantum stochastic differential equations and the master equation," *Physical Review A*, vol. 31, no. 6, p. 3761, 1985.

[15] H. I. Nurdin, M. R. James, and I. R. Petersen, "Coherent quantum LQG control," *Automatica*, vol. 45, no. 8, pp. 1837–1846, 2009.

[16] N. Yamamoto, "Coherent versus measurement feedback: Linear systems theory for quantum information," *Physical Review X*, vol. 4, no. 4, p. 041029, 2014.

[17] R. Hamerly and H. Mabuchi, "Advantages of coherent feedback for cooling quantum oscillators," *Physical Review Letters*, vol. 109, no. 17, p. 173602, 2012.

[18] J. Combes, J. Kerckhoff, and M. Sarovar, "The SLH framework for modeling quantum input-output networks," *Advances in Physics: X*, vol. 2, no. 3, pp. 784–888, 2017.

[19] J. Gough, R. Gohm, and M. Yanagisawa, "Linear quantum feedback networks," *Physical Review A*, vol. 78, no. 6, p. 062104, 2008.

[20] J. Gough and M. R. James, "The series product and its application to quantum feedforward and feedback networks," *IEEE Transactions on Automatic Control*, vol. 54, no. 11, pp. 2530–2544, 2009.

[21] M. Rossi, D. Mason, J. Chen, Y. Tsaturyan, and A. Schliesser, "Measurement-based quantum control of mechanical motion," *Nature*, vol. 563, pp. 53–58, Nov. 2018.

[22] M. Koch, C. Sames, A. Kubanek, M. Apel, M. Balbach, A. Ourjoumtsev, P. W. H. Pinkse, and G. Rempe, "Feedback Cooling of a Single Neutral Atom," *Physical Review Letters*, vol. 105, p. 173003, Oct. 2010.

[23] K. C. Cox, G. P. Greve, J. M. Weiner, and J. K. Thompson, "Deterministic Squeezed States with Collective Measurements and Feedback," *Physical Review Letters*, vol. 116, p. 093602, Mar. 2016.

[24] P. Bushev, D. Rotter, A. Wilson, F. Dubin, C. Becher, J. Eschner, R. Blatt, V. Steixner, P. Rabl, and P. Zoller, "Feedback Cooling of a Single Trapped Ion," *Physical Review Letters*, vol. 96, p. 043003, Feb. 2006.

[25] R. Vijay, C. Macklin, D. H. Slichter, S. J. Weber, K. W. Murch, R. Naik, A. N. Korotkov, and I. Siddiqi, "Stabilizing Rabi oscillations in a superconducting qubit using quantum feedback," *Nature*, vol. 490, pp. 77–80, Oct. 2012.

[26] D. Ristè, C. C. Bultink, K. W. Lehnert, and L. DiCarlo, "Feedback Control of a Solid-State Qubit Using High-Fidelity Projective Measurement," *Physical Review Letters*, vol. 109, p. 240502, Dec. 2012.

[27] C. Sayrin, I. Dotsenko, X. Zhou, B. Peaudecerf, T. Rybarczyk, S. Gleyzes, P. Rouchon, M. Mirrahimi, H. Amini, M. Brune, J.-M. Rai-

mond, and S. Haroche, "Real-time quantum feedback prepares and stabilizes photon number states," *Nature*, vol. 477, pp. 73–77, Sept. 2011.

[28] W. Smith, J. Reiner, L. Orozco, S. Kuhr, and H. M. Wiseman, "Capture and release of a conditional state of a cavity QED system by quantum feedback," *Physical Review Letters*, vol. 89, no. 13, p. 133601, 2002.

[29] S. Shankar, M. Hatridge, Z. Leghtas, K. M. Sliwa, A. Narla, U. Vool, S. M. Girvin, L. Frunzio, M. Mirrahimi, and M. H. Devoret, "Autonomously stabilized entanglement between two superconducting quantum bits," *Nature*, vol. 504, pp. 419–422, Dec. 2013.

[30] J. Zhang, R. Wu, Y. Liu, C. Li, and T. Tarn *IEEE Transactions on Automatic Control*, vol. 57, p. 1997, 2012.

[31] W.-L. Ma, S. Puri, R. J. Schoelkopf, M. H. Devoret, S. M. Girvin, and L. Jiang *Science Bulletin*, vol. 66, p. 1789, 2021.

[32] S. Iida, M. Yukawa, H. Yonezawa, N. Yamamoto, and A. Furusawa, "Experimental Demonstration of Coherent Feedback Control on Optical Field Squeezing," *IEEE Transactions on Automatic Control*, vol. 57, pp. 2045–2050, Aug. 2012.

[33] M. Hirose and P. Cappellaro, "Coherent feedback control of a single qubit in diamond," *Nature*, vol. 532, pp. 77–80, Apr. 2016.

[34] H. Mabuchi, "Coherent-feedback quantum control with a dynamic compensator," *Physical Review A*, vol. 78, p. 032323, Sept. 2008.

[35] G.-L. Schmid, C. T. Ngai, M. Ernzer, M. B. Aguilera, T. M. Karg, and P. Treutlein, "Coherent feedback cooling of a nanomechanical membrane with atomic spins," *Physical Review X*, vol. 12, no. 1, p. 011020, 2022.

[36] M. Woolley and A. Clerk, "Two-mode squeezed states in cavity optomechanics via engineering of a single reservoir," *Physical Review A*, vol. 89, no. 6, p. 063805, 2014.

[37] J. S. Bennett, L. S. Madsen, M. Baker, H. Rubinsztein-Dunlop, and W. P. Bowen, "Coherent control and feedback cooling in a remotely coupled hybrid atom–optomechanical system," *New Journal of Physics*, vol. 16, no. 8, p. 083036, 2014.

[38] A. Serafini, *Quantum continuous variables: a primer of theoretical methods*. CRC Press, 2017.

[39] A. Ferraro, S. Olivares, and M. G. Paris, "Gaussian states in continuous variable quantum information," *arXiv preprint quant-ph/0503237*, 2005.

[40] B. Dutta, N. Mukunda, R. Simon, *et al.*, "The real symplectic groups in quantum mechanics and optics," *Pramana*, vol. 45, no. 6, pp. 471–497, 1995.

[41] G. Adesso, S. Ragy, and A. R. Lee, "Continuous variable quantum information: Gaussian states and beyond," *Open Systems & Information Dynamics*, vol. 21, no. 01n02, p. 1440001, 2014.

[42] G. Vidal and R. F. Werner, "Computable measure of entanglement," *Physical Review A*, vol. 65, no. 3, p. 032314, 2002.

[43] M. B. Plenio, "Logarithmic negativity: a full entanglement monotone that is not convex," *Physical Review Letters*, vol. 95, no. 9, p. 090503, 2005.

[44] D. Walls and G. Milburn, *Quantum Optics*. Springer study edition, Springer, 1994.

[45] P. C. Parks, "A.M. Lyapunov's stability theory—100 years on," *IMA journal of Mathematical Control and Information*, vol. 9, no. 4, pp. 275–303, 1992.

[46] A. M. Lyapunov, "The general problem of the stability of motion," *International journal of control*, vol. 55, no. 3, pp. 531–534, 1992.

[47] S. V. Raković and M. Lazar, "The Minkowski–Lyapunov equation for linear dynamics: Theoretical foundations," *Automatica*, vol. 50, no. 8, pp. 2015–2024, 2014.

[48] J. Fiurášek, "Gaussian transformations and distillation of entangled Gaussian states," *Physical Review Letters*, vol. 89, no. 13, p. 137904, 2002.

[49] J. Eisert, S. Scheel, and M. B. Plenio, "Distilling Gaussian states with Gaussian operations is impossible," *Physical Review Letters*, vol. 89, no. 13, p. 137903, 2002.

[50] M. Aspelmeyer, T. J. Kippenberg, and F. Marquardt, "Cavity optomechanics," *Reviews of Modern Physics*, vol. 86, no. 4, p. 1391, 2014.

[51] W. P. Bowen and G. J. Milburn, *Quantum optomechanics*. CRC Press, 2015.

[52] M. Paternostro, S. Gigan, M. S. Kim, F. Blaser, H. R. Böhm, and M. Aspelmeyer, "Reconstructing the dynamics of a movable mirror in a detuned optical cavity," *New Journal of Physics*, vol. 8, pp. 107–107, jun 2006.

[53] I. Wilson-Rae, N. Nooshi, W. Zwerger, and T. J. Kippenberg, "Theory of ground state cooling of a mechanical oscillator using dynamical backaction," *Physical Review Letters*, vol. 99, p. 093901, Aug 2007.

[54] F. Marquardt, J. P. Chen, A. A. Clerk, and S. M. Girvin, "Quantum theory of cavity-assisted sideband cooling of mechanical motion," *Physical Review Letters*, vol. 99, p. 093902, Aug 2007.

[55] K. Hammerer, K. Stannigel, C. Genes, P. Zoller, P. Treutlein, S. Camerer, D. Hunger, and T. W. Hänsch, "Optical lattices with micromechanical mirrors," *Physical Review A*, vol. 82, p. 021803, Aug 2010.

[56] S. Camerer, M. Korppi, A. Jöckel, D. Hunger, T. W. Hänsch, and P. Treutlein, "Realization of an optomechanical interface between ultracold atoms and a membrane," *Physical Review Letters*, vol. 107, p. 223001, Nov 2011.

[57] S. Mancini, D. Vitali, and P. Tombesi, "Optomechanical cooling of a macroscopic oscillator by homodyne feedback," *Physical Review Letters*, vol. 80, pp. 688–691, Jan 1998.

[58] D. Vitali, S. Mancini, L. Ribichini, and P. Tombesi, "Mirror quiescence and high-sensitivity position measurements with feedback," *Physical Review A*, vol. 65, p. 063803, May 2002.

[59] A. Hopkins, K. Jacobs, S. Habib, and K. Schwab, "Feedback cooling of a nanomechanical resonator," *Physical Review B*, vol. 68, p. 235328, Dec 2003.

[60] J. Guo, R. Norte, and S. Gröblacher, "Feedback cooling of a room temperature mechanical oscillator close to its motional ground state," *Physical Review Letters*, vol. 123, p. 223602, Nov 2019.

[61] S. Gröblacher, K. Hammerer, M. R. Vanner, and M. Aspelmeyer, "Observation of strong coupling between a micromechanical resonator and an optical cavity field," *Nature*, vol. 460, no. 7256, pp. 724–727, 2009.

[62] J. D. Teufel, D. Li, M. Allman, K. Cicak, A. Sirois, J. Whittaker, and R. Simmonds, "Circuit cavity electromechanics in the strong-coupling regime," *Nature*, vol. 471, no. 7337, pp. 204–208, 2011.

[63] F. Brennecke, S. Ritter, T. Donner, and T. Esslinger, "Cavity optomechanics with a Bose-Einstein condensate," *Science*, vol. 322, no. 5899, pp. 235–238, 2008.

[64] F. Ciccarello, S. Lorenzo, V. Giovannetti, and G. M. Palma, "Quantum collision models: open system dynamics from repeated interactions," *arXiv preprint arXiv:2106.11974*, 2021.

[65] J. Rau, "Relaxation phenomena in spin and harmonic oscillator systems," *Physical Review*, vol. 129, no. 4, p. 1880, 1963.

[66] C. M. Caves, "Quantum mechanics of measurements distributed in time. a path-integral formulation," *Physical Review D*, vol. 33, no. 6, p. 1643, 1986.

[67] C. M. Caves and G. J. Milburn, "Quantum-mechanical model for continuous position measurements," *Physical Review A*, vol. 36, no. 12, p. 5543, 1987.

[68] T. Rybár, S. N. Filippov, M. Ziman, and V. Bužek, "Simulation of indivisible qubit channels in collision models," *Journal of Physics B: Atomic, Molecular and Optical Physics*, vol. 45, no. 15, p. 154006, 2012.

[69] V. Giovannetti and G. Palma, "Master equation for cascade quantum channels: a collisional approach," *Journal of Physics B: Atomic, Molecular and Optical Physics*, vol. 45, no. 15, p. 154003, 2012.

[70] F. Ciccarello, G. Palma, and V. Giovannetti, "Collision-model-based approach to non-Markovian quantum dynamics," *Physical Review A*, vol. 87, no. 4, p. 040103, 2013.

[71] F. Ciccarello, "Collision models in quantum optics," *Quantum Measurements and Quantum Metrology*, vol. 4, no. 1, pp. 53–63, 2017.

[72] P. Strasberg, G. Schaller, T. Brandes, and M. Esposito, "Quantum and information thermodynamics: a unifying framework based on repeated interactions," *Physical Review X*, vol. 7, no. 2, p. 021003, 2017.

[73] D. Cilluffo, A. Carollo, S. Lorenzo, J. A. Gross, G. M. Palma, and F. Ciccarello, "Collisional picture of quantum optics with giant emitters," *Physical Review Research*, vol. 2, no. 4, p. 043070, 2020.

[74] A. Carollo, D. Cilluffo, and F. Ciccarello, "Mechanism of decoherence-free coupling between giant atoms," *Physical Review Research*, vol. 2, no. 4, p. 043184, 2020.

[75] M. V. Gustafsson, T. Aref, A. F. Kockum, M. K. Ekström, G. Johansson, and P. Delsing, "Propagating phonons coupled to an artificial atom," *Science*, vol. 346, no. 6206, pp. 207–211, 2014.

[76] B. Kannan, M. J. Ruckriegel, D. L. Campbell, A. Frisk Kockum, J. Braumüller, D. K. Kim, M. Kjaergaard, P. Krantz, A. Melville, B. M. Niedzielski, *et al.*, "Waveguide quantum electrodynamics with superconducting artificial giant atoms," *Nature*, vol. 583, no. 7818, pp. 775–779, 2020.

[77] A. F. Kockum, "Quantum optics with giant atoms—the first five years," in *International Symposium on Mathematics, Quantum Theory, and Cryptography*, pp. 125–146, Springer Singapore, 2021.

[78] C. Marletto, V. Vedral, L. T. Knoll, F. Piacentini, E. Bernardi, E. Rebufello, A. Avella, M. Gramegna, I. P. Degiovanni, and M. Genovese, "Emergence of constructor-based irreversibility in quantum systems: Theory and experiment," *Physical Review Letters*, vol. 128, no. 8, p. 080401, 2022.

[79] N. K. Bernardes, A. Cuevas, A. Orieux, C. H. Monken, P. Mataloni, F. Sciarrino, and M. F. Santos *Scientific Reports*, vol. 5, p. 17520, 2015.

[80] W. R. Inc., "Mathematica, Version 12.1." Champaign, IL, 2022.

[81] S. Boyd, S. P. Boyd, and L. Vandenberghe, *Convex optimization*. Cambridge University Press, 2004.

[82] W. R. Inc., "Some notes on internal implementation." https://reference.wolfram.com/language/tutorial/SomeNotesOnInternalImplementation.html#10453.

[83] M. Avriel, *Nonlinear programming: analysis and methods*. Courier Corporation, 2003.

[84] C. M. Caves, "Quantum limits on noise in linear amplifiers," *Physical Review D*, vol. 26, no. 8, p. 1817, 1982.

[85] M. G. Genoni, S. Mancini, and A. Serafini, "Optimal feedback control of linear quantum systems in the presence of thermal noise," *Physical Review A*, vol. 87, no. 4, p. 042333, 2013.

[86] M. G. Genoni, S. Mancini, H. M. Wiseman, and A. Serafini, "Quantum filtering of a thermal master equation with a purified reservoir," *Physical Review A*, vol. 90, no. 6, p. 063826, 2014.

[87] J. Gough, M. R. James, and H. I. Nurdin, "Squeezing components in linear quantum feedback networks," *Physical Review A*, vol. 81, no. 2, p. 023804, 2010.

[88] H. Vahlbruch, M. Mehmet, K. Danzmann, and R. Schnabel, "Detection of 15 dB squeezed states of light and their application for the absolute calibration of photoelectric quantum efficiency," *Physical Review Letters*, vol. 117, no. 11, p. 110801, 2016.

[89] J. Chan, T. P. M. Alegre, A. H. Safavi-Naeini, J. T. Hill, A. Krause, S. Gröblacher, M. Aspelmeyer, and O. Painter, "Laser cooling of a nanomechanical oscillator into its quantum ground state," *Nature*, vol. 478, no. 7367, pp. 89–92, 2011.

[90] J. D. Teufel, T. Donner, D. Li, J. W. Harlow, M. S. Allman, K. Cicak, A. J. Sirois, J. D. Whittaker, K. W. Lehnert, and R. W. Simmonds,

"Sideband cooling of micromechanical motion to the quantum ground state," *Nature*, vol. 475, no. 7356, pp. 359–363, 2011.

[91] R. W. Peterson, T. P. Purdy, N. S. Kampel, R. W. Andrews, P.-L. Yu, K. W. Lehnert, and C. A. Regal, "Laser cooling of a micromechanical membrane to the quantum backaction limit," *Physical Review Letters*, vol. 116, p. 063601, Feb 2016.

[92] L. Qiu, I. Shomroni, P. Seidler, and T. J. Kippenberg, "Laser cooling of a nanomechanical oscillator to its zero-point energy," *Physical Review Letters*, vol. 124, p. 173601, Apr 2020.

[93] U. Delić, M. Reisenbauer, K. Dare, D. Grass, V. Vuletić, N. Kiesel, and M. Aspelmeyer, "Cooling of a levitated nanoparticle to the motional quantum ground state," *Science*, 2020.

[94] T. A. Palomaki, J. D. Teufel, R. W. Simmonds, and K. W. Lehnert, "Entangling mechanical motion with microwave fields," *Science*, vol. 342, no. 6159, pp. 710–713, 2013.

[95] R. Riedinger, S. Hong, R. A. Norte, J. A. Slater, J. Shang, A. G. Krause, V. Anant, M. Aspelmeyer, and S. Gröblacher, "Non-classical correlations between single photons and phonons from a mechanical oscillator," *Nature*, vol. 530, no. 7590, pp. 313–316, 2016.

[96] C. Gut, K. Winkler, J. Hoelscher-Obermaier, S. G. Hofer, R. M. Nia, N. Walk, A. Steffens, J. Eisert, W. Wieczorek, J. A. Slater, M. Aspelmeyer, and K. Hammerer, "Stationary optomechanical entanglement between a mechanical oscillator and its measurement apparatus," *Physical Review Research*, vol. 2, p. 033244, Aug 2020.

[97] J.-M. Pirkkalainen, E. Damskägg, M. Brandt, F. Massel, and M. A. Sillanpää, "Squeezing of quantum noise of motion in a micromechanical resonator," *Physical Review Letters*, vol. 115, p. 243601, Dec 2015.

[98] F. Lecocq, J. B. Clark, R. W. Simmonds, J. Aumentado, and J. D. Teufel, "Quantum nondemolition measurement of a nonclassical state of a massive object," *Physical Review X*, vol. 5, p. 041037, Dec 2015.

[99] K. Jacobs, H. I. Nurdin, F. W. Strauch, and M. James, "Comparing resolved-sideband cooling and measurement-based feedback cooling on an equal footing: Analytical results in the regime of ground-state cooling," *Physical Review A*, vol. 91, no. 4, p. 043812, 2015.

[100] S. Huang and A. Chen, "Cooling of a mechanical oscillator and normal mode splitting in optomechanical systems with coherent feedback," *Applied Sciences*, vol. 9, no. 16, p. 3402, 2019.

[101] X. You, Z. Li, and Y. Li, "Strong quantum squeezing of mechanical resonator via parametric amplification and coherent feedback," *Physical Review A*, vol. 96, no. 6, p. 063811, 2017.

[102] C. Joshi, U. Akram, and G. J. Milburn, "An all-optical feedback assisted steady state of an optomechanical array," *New Journal of Physics*, vol. 16, p. 023009, feb 2014.

[103] J. Li, G. Li, S. Zippilli, D. Vitali, and T. Zhang, "Enhanced entanglement of two different mechanical resonators via coherent feedback," *Physical Review A*, vol. 95, p. 043819, Apr 2017.

[104] Z. Wang and A. H. Safavi-Naeini, "Enhancing a slow and weak optomechanical nonlinearity with delayed quantum feedback," *Nature Communications*, vol. 8, no. 1, p. 15886, 2017.

[105] M. Brunelli, D. Malz, and A. Nunnenkamp, "Conditional dynamics of optomechanical two-tone backaction-evading measurements," *Physical Review Letters*, vol. 123, p. 093602, Aug 2019.

[106] S. Huang and G. S. Agarwal, "Enhancement of cavity cooling of a micromechanical mirror using parametric interactions," *Physical Review A*, vol. 79, p. 013821, Jan 2009.

[107] S. Huang and G. S. Agarwal, "Normal-mode splitting in a coupled system of a nanomechanical oscillator and a parametric amplifier cavity," *Physical Review A*, vol. 80, p. 033807, Sep 2009.

[108] K. Jähne, C. Genes, K. Hammerer, M. Wallquist, E. S. Polzik, and P. Zoller, "Cavity-assisted squeezing of a mechanical oscillator," *Physical Review A*, vol. 79, p. 063819, Jun 2009.

[109] J. B. Clark, F. Lecocq, R. W. Simmonds, J. Aumentado, and J. D. Teufel, "Sideband cooling beyond the quantum backaction limit with squeezed light," *Nature*, vol. 541, no. 7636, pp. 191–195, 2017.

[110] M. Asjad, S. Zippilli, and D. Vitali, "Suppression of stokes scattering and improved optomechanical cooling with squeezed light," *Physical Review A*, vol. 94, p. 051801, Nov 2016.

[111] X.-Y. Lü, Y. Wu, J. R. Johansson, H. Jing, J. Zhang, and F. Nori, "Squeezed optomechanics with phase-matched amplification and dissipation," *Physical Review Letters*, vol. 114, p. 093602, Mar 2015.

[112] J. Williamson, "On the algebraic problem concerning the normal forms of linear dynamical systems," *American Journal of Mathematics*, vol. 58, no. 1, pp. 141–163, 1936.

[113] R. Simon, S. Chaturvedi, and V. Srinivasan, "Congruences and canonical forms for a positive matrix: Application to the Schweinler–Wigner extremum principle," *Journal of Mathematical Physics*, vol. 40, no. 7, pp. 3632–3642, 1999.

[114] A. L. Grimsmo, "Time-delayed quantum feedback control," *Physical Review Letters*, vol. 115, no. 6, p. 060402, 2015.

[115] M. R. Vanner, I. Pikovski, G. D. Cole, M. S. Kim, Č. Brukner, K. Hammerer, G. J. Milburn, and M. Aspelmeyer, "Pulsed quantum optomechanics," *Proceedings of the National Academy of Sciences*, 2011.

[116] A. A. Clerk, F. Marquardt, and K. Jacobs, "Back-action evasion and squeezing of a mechanical resonator using a cavity detector," *New Journal of Physics*, vol. 10, no. 9, p. 095010, 2008.

[117] M. G. Genoni, J. Zhang, J. Millen, P. F. Barker, and A. Serafini, "Quantum cooling and squeezing of a levitating nanosphere via time-continuous measurements," *New Journal of Physics*, vol. 17, p. 073019, jul 2015.

[118] M. Brunelli, D. Malz, A. Schliesser, and A. Nunnenkamp, "Stroboscopic quantum optomechanics," *Physical Review Research*, vol. 2, p. 023241, May 2020.

[119] M. A. Nielsen and I. Chuang, "Quantum computation and quantum information," 2002.

[120] K. Audenaert, N. Datta, and M. Ozols, "Entropy power inequalities for qudits," *Journal of Mathematical Physics*, vol. 57, no. 5, p. 052202, 2016.

[121] E. A. Carlen, E. H. Lieb, and M. Loss, "A sharp analog of Young's inequality on SN and related entropy inequalities," *The Journal of Geometric Analysis*, vol. 14, no. 3, pp. 487–520, 2004.

[122] T. Tilma and E. Sudarshan, "Generalized Euler angle parametrization for SU (N)," *Journal of Physics A: Mathematical and General*, vol. 35, no. 48, p. 10467, 2002.

[123] S. Lloyd, "Almost any quantum logic gate is universal," *Physical Review Letters*, vol. 75, no. 2, p. 346, 1995.

[124] D. Grimmer, D. Layden, R. B. Mann, and E. Martín-Martínez, "Open dynamics under rapid repeated interaction," *Physical Review A*, vol. 94, no. 3, p. 032126, 2016.

[125] H.-P. Breuer, F. Petruccione, *et al.*, *The theory of open quantum systems*. Oxford University Press on Demand, 2002.

[126] M. B. Plenio and P. L. Knight, "The quantum-jump approach to dissipative dynamics in quantum optics," *Reviews of Modern Physics*, vol. 70, no. 1, p. 101, 1998.

[127] C. Gardiner, P. Zoller, and P. Zoller, *Quantum noise: a handbook of Markovian and non-Markovian quantum stochastic methods with applications to quantum optics*. Springer Science & Business Media, 2004.

[128] Y.-C. Liu, Y.-F. Xiao, X. Luan, and C. W. Wong, "Dynamic dissipative cooling of a mechanical resonator in strong coupling optomechanics," *Physical Review Letters*, vol. 110, p. 153606, Apr 2013.

[129] Q. Xu, P. Dong, and M. Lipson, "Breaking the delay-bandwidth limit in a photonic structure," *Nature Physics*, vol. 3, no. 6, pp. 406–410, 2007.

[130] K. Kondo, M. Shinkawa, Y. Hamachi, Y. Saito, Y. Arita, and T. Baba, "Ultrafast slow-light tuning beyond the carrier lifetime using photonic crystal waveguides," *Physical Review Letters*, vol. 110, no. 5, p. 053902, 2013.

[131] R. A. Soref and B. R. Bennett, "Electrooptical effects in silicon," *IEEE Journal of Quantum Electronics*, vol. 23, no. 1, pp. 123–129, 1987.

[132] I. Favero and K. Karrai, "Optomechanics of deformable optical cavities," *Nature Photonics*, vol. 3, no. 4, pp. 201–205, 2009.

[133] J. Laurat, G. Keller, J. A. Oliveira-Huguenin, C. Fabre, T. Coudreau, A. Serafini, G. Adesso, and F. Illuminati, "Entanglement of two-mode Gaussian states: characterization and experimental production and manipulation," *Journal of Optics B: Quantum and Semiclassical Optics*, vol. 7, no. 12, p. S577, 2005.

[134] W. Vogel and D.-G. Welsch, *Quantum optics*. John Wiley & Sons, 2006.